Chapter-5

Results and Discussions

5.1 Preformulation studies

5.1.1 UV spectrophotometric analytical method for ATR

Standard calibration plots of ATR concentrations versus absorbance at 247 nm (λ_{max}) in different buffer solutions were established by using UV-Visible spectrophotometer. Concentration range of ATR was taken between 2-25 µg/ml. Standard calibration plots of ATR in distilled water (DW), phosphate buffer pH 7.4, pH 6.8 and pH 4.5 are depicted in **Fig. 5.1, Fig. 5.2, Fig. 5.3** and **Fig. 5.4;** respectively. All the calibration plots were obtained as straight line with high regression coefficients (>0.99).

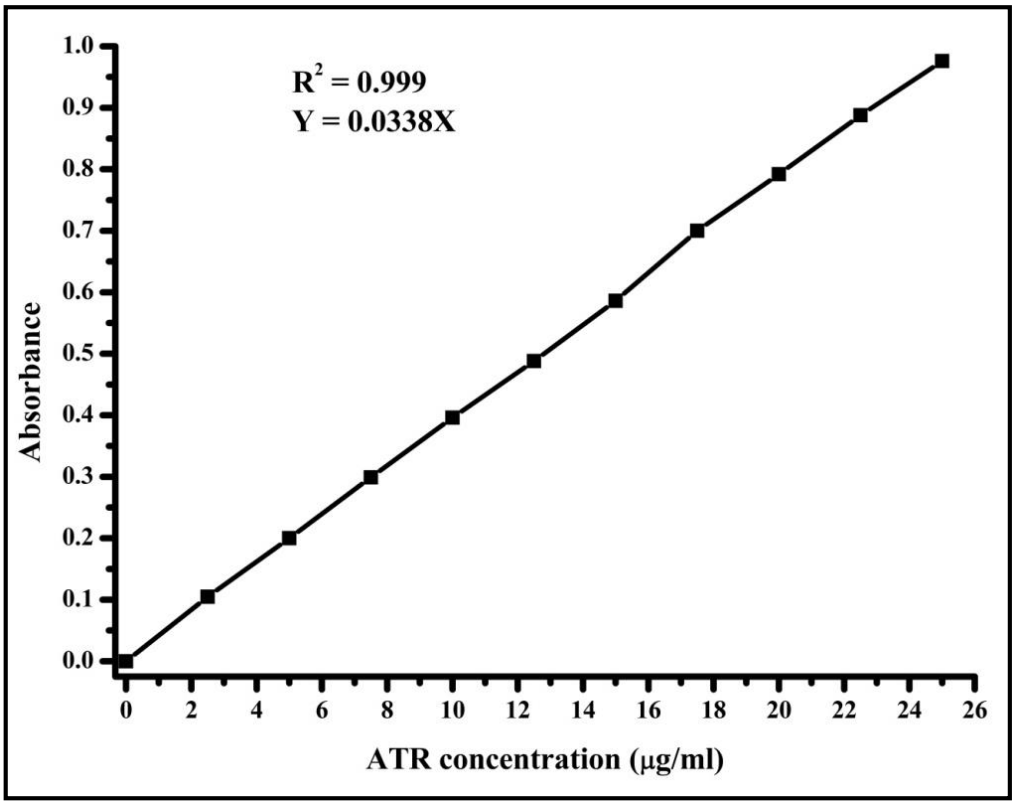

Fig. 5.1 Standard calibration plot of ATR in DW

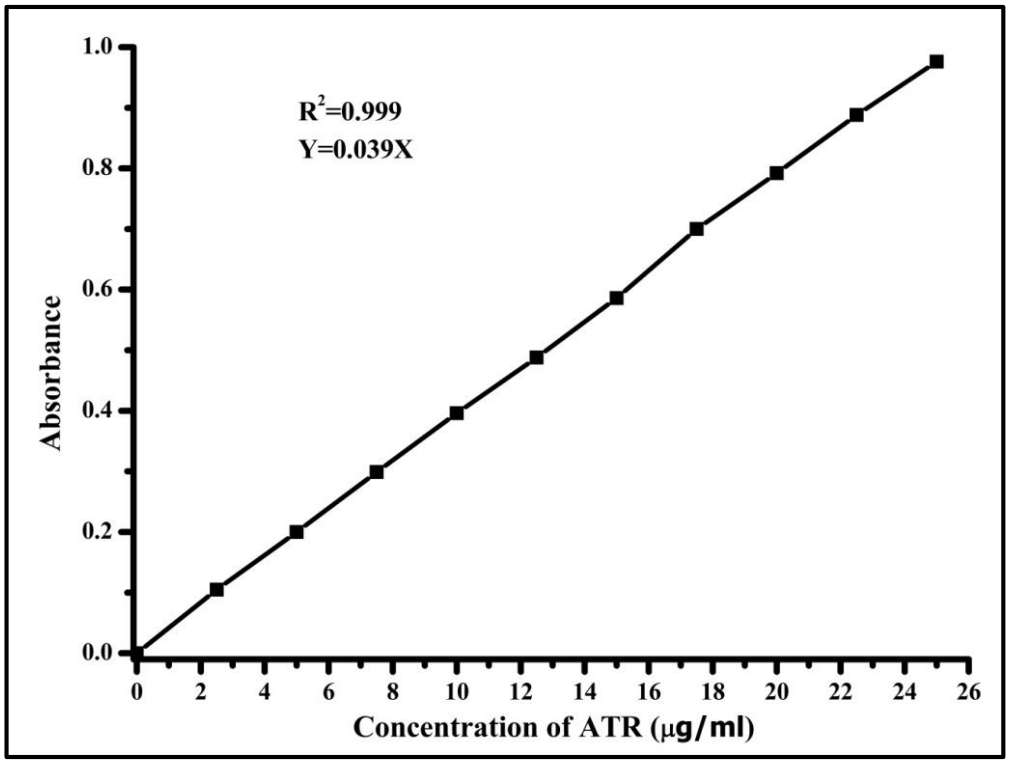

Fig. 5.2 Standard calibration plot of ATR in phosphate buffer pH 7.4

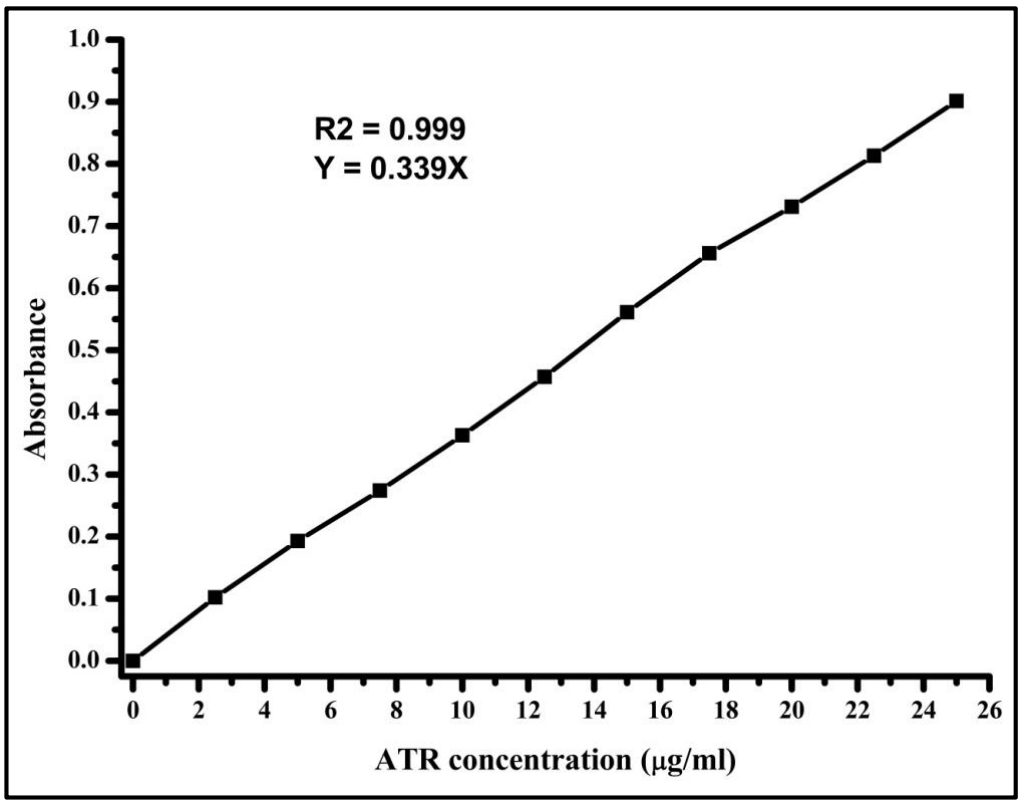

Fig. 5.3 Standard calibration plot of ATR in phosphate buffer pH 6.8

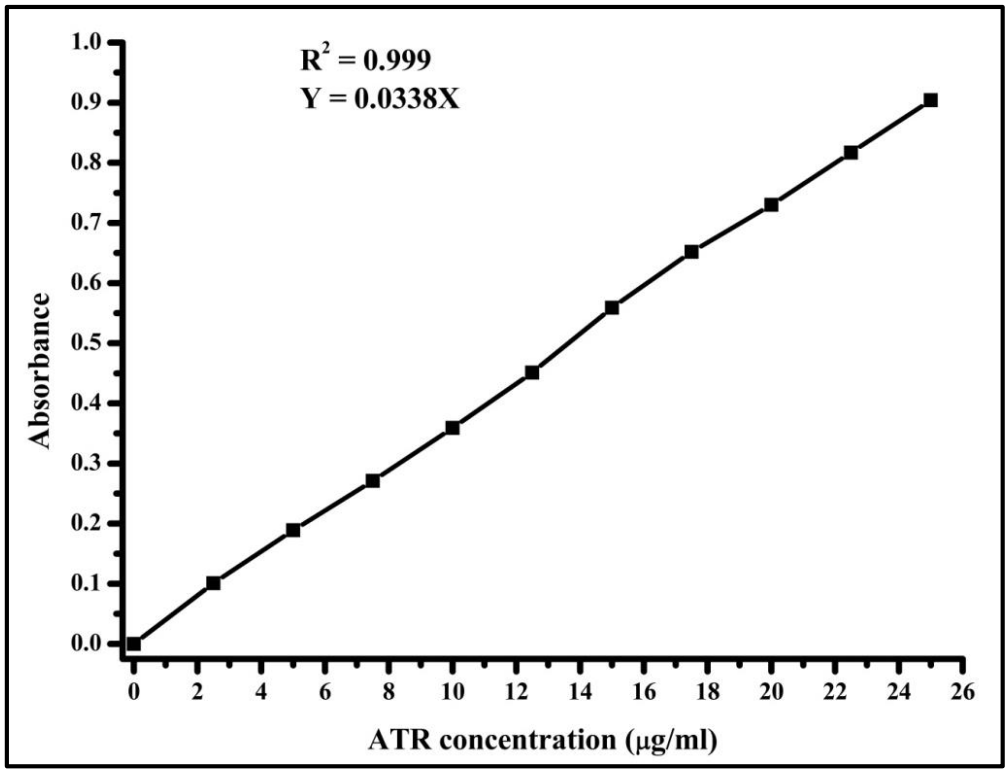

Fig. 5.4 Standard calibration plot of ATR in phosphate buffer pH 4.5

5.1.2 Analytical method development and validation of ATR by HPLC in mobile phase and plasma samples

Assay validation must demonstrate that the analytical procedure is able to predict accurately and precisely the concentrations of unknown samples. The C-18 column, mobile phase system, flow rate, liquid extraction procedure and other operating conditions were found to be optimal to get better accurate and precise response. Methanol was selected for standard stock solution due to higher solubility of ATR in methanol. The chromatograms of ATR (200 ng/ml) spiked in each of mobile phase and in plasma are demonstrated in **Fig. 5.5.** ATR and RST peaks were found to be well resolved and separated. The retention times of ATR and RST were observed at 5.63 min and 3.61 min respectively in mobile phase. The retention times of ATR and RST was slightly delayed in plasma samples as shown in **Fig. 5.5** and Table 5.1. Plasma/mobile phase interference with RST/ATR were found to be absent in chromatograms. Peaks were observed to be nearly symmetrical. The optimal RP-HPLC assay conditions were observed at 3:1 aqueous to organic phase ratio mobile phase (pH 4.5 adjusted with the use

of ortho-phosphoric acid), flow rate 1.2 ml/minute at 37°C column temperature and 247 nm wavelength. The calibration curves of ATR in mobile phase and in plasma are shown in **Fig. 5.6** which is found to be straight line with higher correlation coefficient (R^2). The validation parameters of calibration plots are enlisted in Table 5.1.

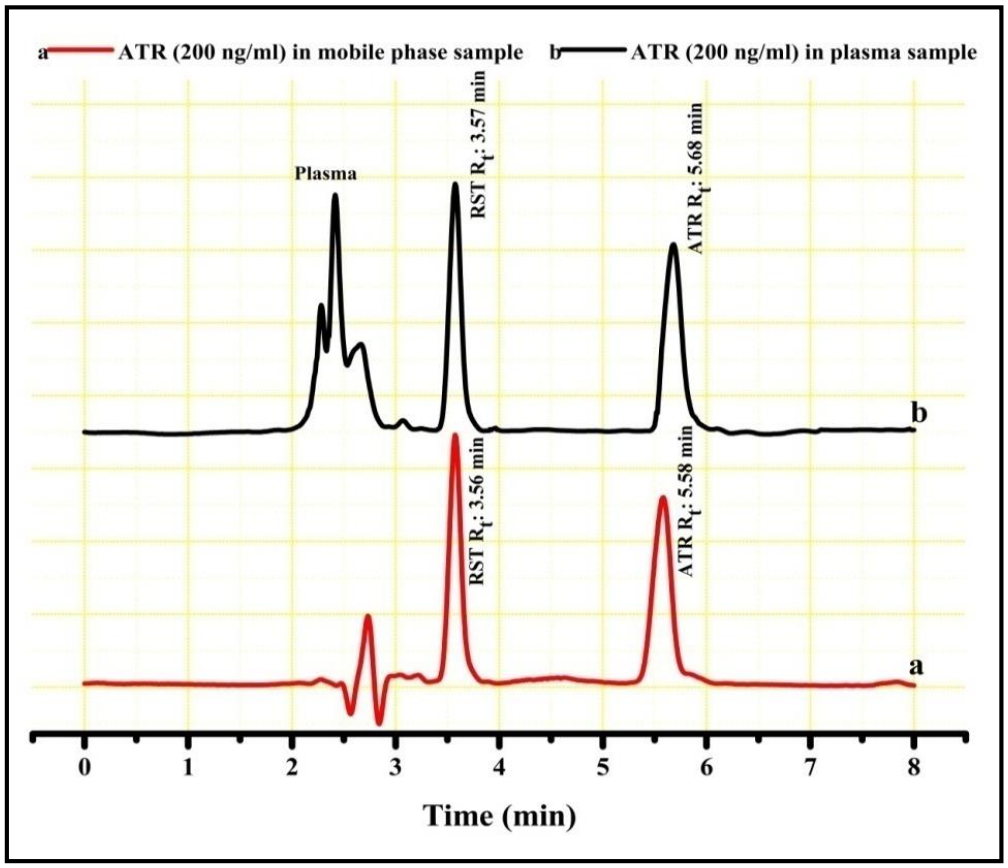

Fig. 5. HPLC chromatograms of ATR (200 ng/ml) spiked in plasma as well as in mobile phase samples (RST as internal standard)

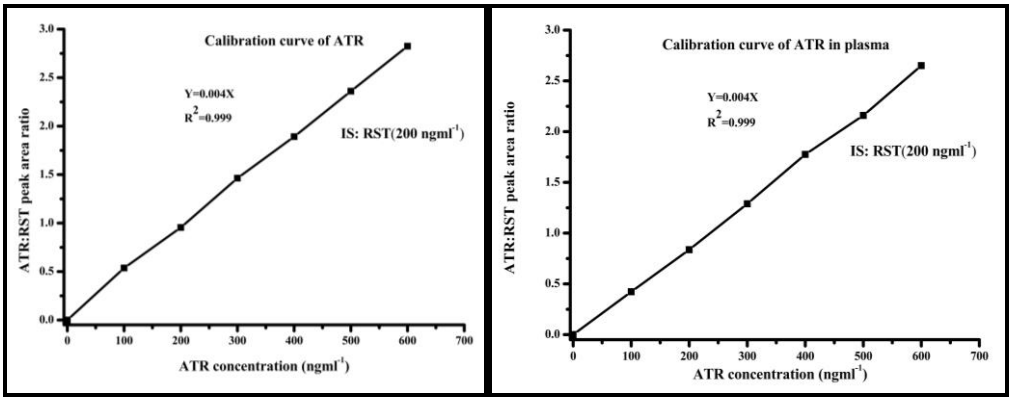

Fig. 5.6 Calibration plots of ATR in mobile phase and in plasma samples at 247 nm wavelength

Table 5.1 Validation parameters of calibration plot developed by HPLC method

Sample medium	Linearity range (ng/ml)	R^2	Equation	LOD (ng/ml)	LOQ (ng/ml)	Retention time (min)	
						ATR	RST
Mobile phase	25-1000	0.999	Y = 0.004X	7	22	5.627±0.023	3.611±0.014
Plasma	25-1000	0.999	Y = 0.004X	7	23	5.733±0.055	3.632±0.017

Extraction ratio of ATR from plasma was determined at three concentration levels (50, 300 and 1000 ng/ml) by comparing the response from drug spiked plasma samples to that of standard sample in mobile phase. The extraction ratio obtained at above mentioned concentrations is shown in Table 5.2. The data supported the authenticity of this extraction method for the analysis of plasma sample.

Table 5.2 Extraction ratio of ATR from rat plasma

S. No.	Concentration (ng/ml)	Extraction ratio (%) (Mean±S.D.: n=3)	RSD (%)
1	50	87.34±2.03	2.32
2	300	88.72±1.62	1.83
3	1000	89.35±1.54	1.72

Accuracy of an analytical method is the closeness of observed results by the method to that of the true result. Accuracy is primarily assessed by bias measurement. The intra-day and inter-day accuracy and precision of the ATR in mobile phase and rat plasma are enlisted in Table 5.3. The data showed that the RP-HPLC method is reproducible, accurate and henceforth suitable to the pharmacokinetic study of ATR in rats.

LOD and LOQ of ATR by this RP-HPLC analytical method were found to be 7 ng/ml and 22-23 ng/ml respectively as mentioned in Table 5.1. The stock solutions of ATR and RST were found to be stable for at least 4 week stored at 4°C. Plasma samples spiked with ATR were also stable for month stored at -40°C.

Table 5.3 The intra-day and inter-day precision of the RP-HPLC method

Standard concentration (ng/ml)		Intra-day variation (n=6)			Inter-day variation (n=6)		
		Recovery (mean±SD)	Bias (%)	RSD (%)	Recovery (mean±SD)	Bias (%)	RSD (%)
Mobile phase sample	30	29.53±0.49	-1.43	1.66	29.47±0.55	-1.77	1.87
	300	304.33±3.51	1.44	1.15	291.67±5.68	-2.78	1.95
	1000	991.7±7.73	-0.83	0.63	984.67±9.03	-1.53	0.92
Plasma samples	30	29.13±0.94	-2.9	3.27	28.05±1.01	-6.5	3.6
	300	287±4.19	-4.33	1.46	285.21±6.72	-4.93	2.36
	1000	983.51±8.53	-1.65	0.87	978.24±11.53	2.18	1.18

The aforementioned RP-HPLC analytical method is highly specific, sensitive and reproducible for the quantitative analysis of ATR in mobile phase as well as rat plasma samples. All the peaks of RST and ATR are sharp and well separated without any interference. Fine linearity, precision and accuracy of ATR quantitative estimation established the feasibility of this assay method in the pharmacokinetic study.

5.1.3 Assessment of solubility studies of ATR in different buffer solutions with various surfactants

Solubility and gastrointestinal permeability of drugs are two crucial determining factors of their biopharmaceutical classification system (BCS), oral absorption and quality of *in vitro* - *in vivo* correlation (Amidon et al., 1995). More than 40% of the new chemical entities are reported to be lipophilic and show poor aqueous solubility (Beig et al., 2012). Drug solubility in various dissolution media plays a crucial role in dissolution study of its formulation. Several approaches are being employed to maintain sink condition (drug concentration in dissolution media is always kept lesser than one tenth of its saturation concentration to maintain optimal concentration gradient) in dissolution study of insoluble drugs (BCS class II and IV) (USP, 2005; Mooney et al., 1981). Use of surfactants is very popular method to maintain sink condition by wetting and miceller solubilization of insoluble drugs. Surfactants provide the simulation of

the gastrointestinal environment where bio-surfactant like bile salts are released to emulsify and help in absorption of lipophilic substrates (McClements & Gumus, 2016). Surfactant above critical micelle concentration in aqueous media aggregates to form a hydrophobic (hydrocarbon skeleton) core and hydrophilic shell like colloidal structure called micelle to encapsulate hydrophobic solute, which enhance its solubility and reduce interfacial surface tension (**Fig. 5.7**). Mostly drugs are ionisable molecule containing at least one acidic or basic functional group and pH of media also substantially influences their solubility.

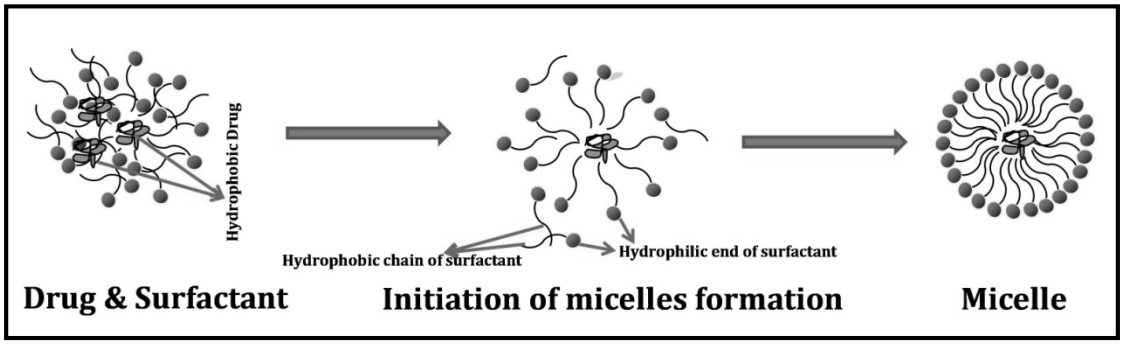

Fig. 5.7 Depiction of micelle formation

5.1.3.1 Solubility study in water and buffer without surfactants

The solubility study of ATR in water and buffer solutions were carried out to evaluate the behaviour of drug solubility with respect to pH of media and ionic strength. The ATR was found to be very slightly soluble (124±10 µM) in water. ATR was found to be practically insoluble in pH 1.2 (17±2 µM), pH 3 (27±2 µM) and pH 4.5 (45±4 µM); while very slightly soluble in pH 5.8 (214±21 µM), pH 6.8 (281±32 µM), pH 7.2 (327±33 µM) and pH 7.4 (352±36 µM). ATR exhibited pH dependent solubility and increased solubility with the increasing order of pH of media. ATR, a salt of weak acid having pK_a 4.5, showed enhanced solubility at pH>4.5. Solubility profile in acidic media (pH<4.5) strongly suggested the need of solubility improvement of ATR in dissolution study to maintain sink condition. Even, in phosphate buffer of intestinal pH require solubility enhancement for the dissolution study of higher strength (80 mg). Surfactant addition to dissolution media has been implemented to improve solubility and maintain sink condition, subsequently.

5.1.3.2 Solubility study in water and buffer with surfactants

The effect of surfactant on the solubility of ATR has been assessed by dividing media in deionized water, acidic media (pH 1.2, pH 3 and pH 4.5 buffer) and phosphate buffer (pH 5.8, pH 6.8, pH 7.2 and pH 7.4).

Effect of sodium lauryl sulphate (SLS)

The influence of SLS on ATR solubility behaviour in different media is depicted in **Fig. 5.8**. The solubility increased gradually with the increment of surfactant concentration in all the media. The pH of the media played an important role in ionization and solubilization of surfactant as well as drug. At lower pH (1.2 and 3.0), drug as well as SLS did not ionize much due to acidic nature of drug and SLS both. The ionization of surfactant is essential for exhibiting greater surface active property. At lower pH, the solubilization property of SLS was attenuated due to lack of ionization of molecule. At higher pH, SLS showed enhanced solubilization property due to ionization of SLS along with ATR. The rise in solubility of ATR was observed at all concentration of SLS. Surfactant at lower concentration (<10 mM) only imparted in wetting property and contributed in slow rise of solubility whereas, at higher concentration (>10 mM) contributed in micelle formation and sudden rise in solubility.

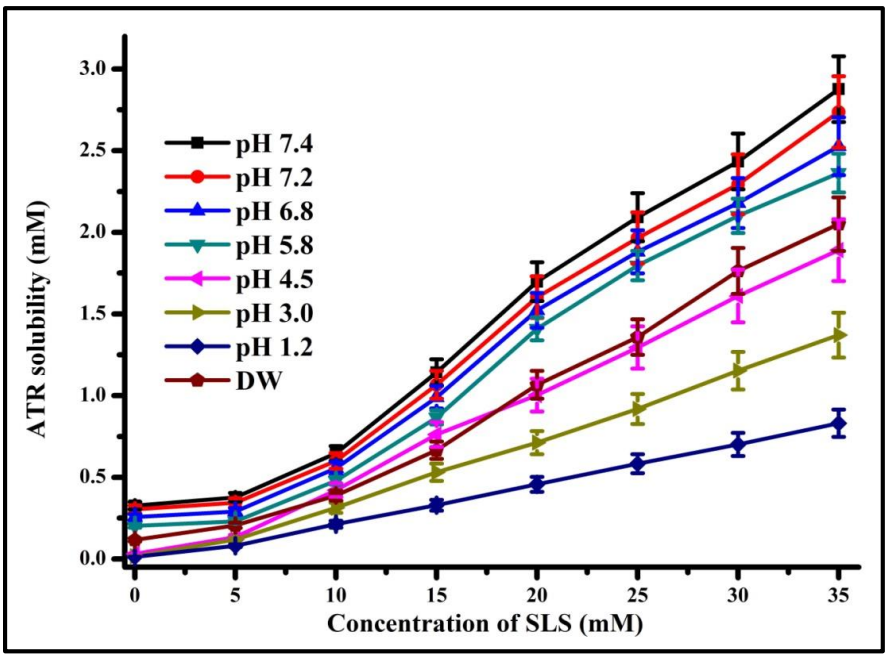

Fig. 5.8 Effect of concentration of SLS on the solubility of ATR in different solutions (vertical bars indicate SD)

Effect of sodium taurocholate (STC)

The effect of STC concentration on solubility of ATR in different media has been exhibited in **Fig. 5.9.** ATR showed low solubility in acidic buffer media (pH 1.2 & 3.0) with all the concentration of STC. Ionization of STC did not occur at lower acidic media or in deionized water due to its anionic nature and this lead to limited solubility enhancement in acidic buffer. STC itself did not get dissolved in acidic buffer (pH≤3) and therefore, did not help at all in solubility enhancement. At higher pH buffer ionization of STC occurred, which lead to solubility enhancement by micelle formation with the drug. STC exhibited limited solubility enhancement at lower concentration (≤10mM) in higher pH buffer solution and marked enhancement at higher concentration as its critical micelle concentration lies in the range of 3-11 mM. STC showed substantial enhancement in solubility of ATR at concentration above 10 mM.

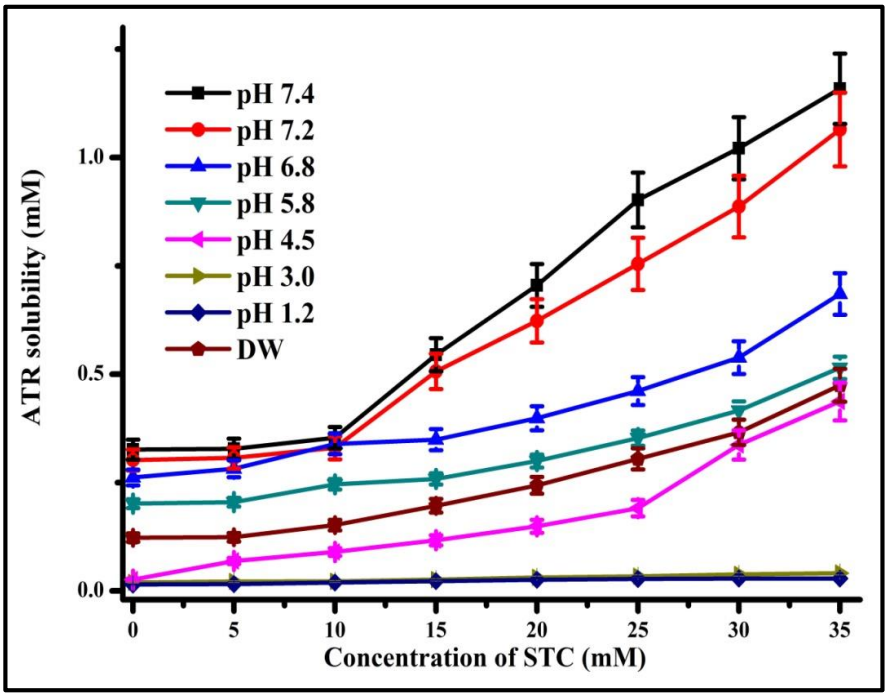

Fig. 5.9 Effect of concentration of STC on the solubility of ATR in different solutions (vertical bars indicate SD)

Effect of cetyl trimethyl ammonium bromide (CTAB)

Fig. 5.10 demonstrates the solubility pattern of ATR with respect to enhancement in CTAB concentration in different aqueous media. CTAB showed

anomalous behaviour in solubilization of ATR. CTAB beyond 15 mM concentration exhibited sudden reduction in solubility in ionic media possibly due to formation of insoluble ionic adduct between drug and surfactant. CTAB in ionic media possessed positive ionic charge and ATR negative ionic charge, which may results into ionic interaction between opposite charged molecules to form insoluble adducts. There is a reported case in which erythromycin and PG-300995 (an anti-HIV agent) solubility decreased with the addition of SLS due to insoluble estolate salt formation (Jain et al., 2004; Stubbs & Kanfer, 1990). CTAB helped in solubility enhancement at lower concentration (≤10mM) in all ionic aqueous media. Solubility enhancement of CTAB was found to be good in deionized water and CTAB concentration showed linear relationship with ATR solubility. Due to insoluble adduct formation of CTAB with ATR in buffer media, CTAB was not evaluated for further solubility parameters.

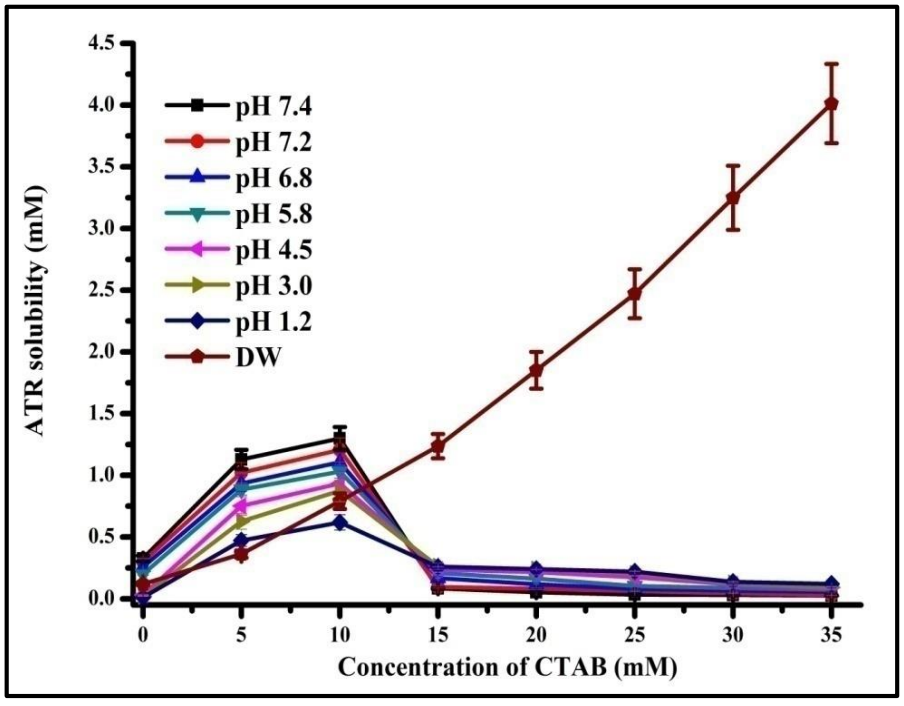

Fig. 5.10 Effect of concentration of CTAB on the solubility of ATR in different solutions (vertical bars indicate SD)

Effect of Tween 80

Tween 80 [polyoxyethylene (20) sorbitan mono-oleate, also known as polysorbate 80] is a mixture of polyoxyethylene ethers of mixed partial oleic acid

esters of sorbitol anhydrides (Ema et al., 2008). It has been widely used as non-ionic emulsifying and dispersing agents in pharmaceutical and food products. Solubility profile of ATR in various aqueous solutions with Tween 80 concentrations is shown in **Fig. 5.11**. ATR solubility was found to be continuously increasing from 5 to 35 mM of Tween 80 in all the solutions. It did not exhibit any ionic interaction with drug due to its non-ionic nature. It was observed that the solubilization effect is higher at high pH than at low pH indicating better surface activity in the basic pH. Availability of substantial molar fraction of Tween 80 in miceller form due to extremely low CMC is responsible for exhibiting higher solubility. Lower CMC value of Tween 80 is advantageous in fortifying the stability of the drug incorporated micelles for pharmacological point of view. When drug incorporated micelle administered intravenously, surfactants with very low CMC only maintain micelle integrity against dilution of surfactant offered by large volume of blood, while micelle of surfactant having higher CMC value may dissociate into monomers and their content may precipitate in the blood (Yokoyama, 1992).

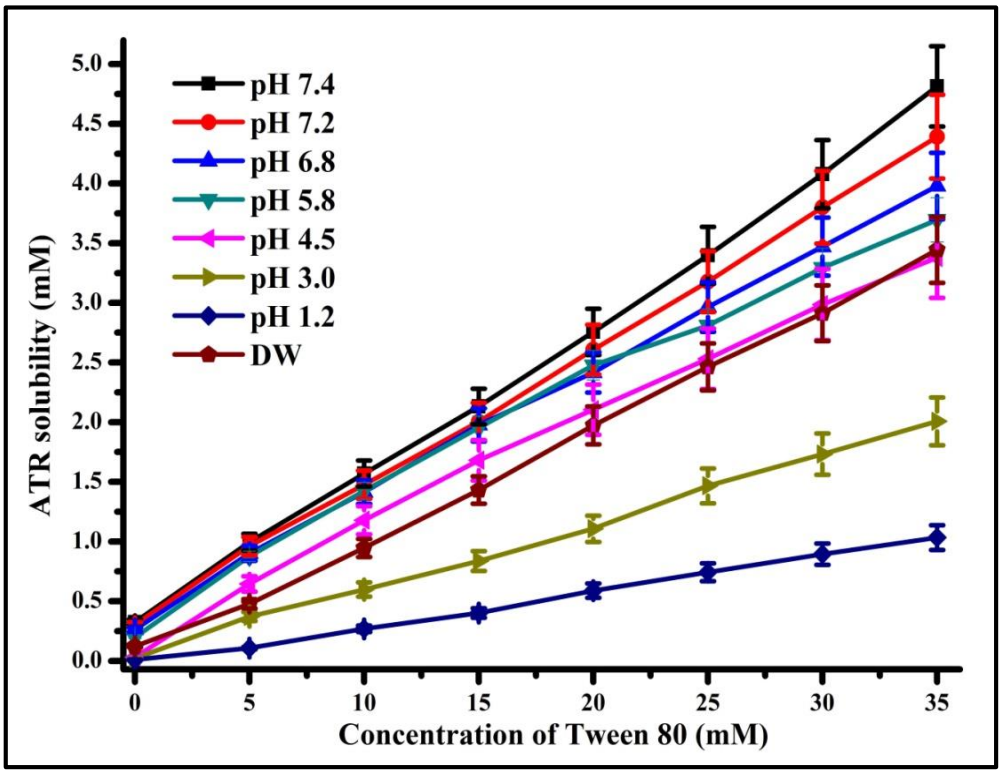

Fig. 5.11 Effect of concentration of Tween 80 on the solubility of ATR in different solutions (vertical bars indicate SD)

Effect of D-α-tocopheryl polyethylene glycol 1000 succinate (TPGS)

TPGS is water soluble derivative of a natural source of Vitamin E and predominantly used as a non-ionic emulsifying agent in pharmaceutical formulations (Zhang et al., 2012). Currently, it has been increasingly used as an adjunct in colloidal formulation developed for cancer pharmacotherapy (Guo et al., 2013). The solubility of ATR with concentration of TPGS as depicted in **Fig. 5.12**. The solubility of ATR increases gradually at all concentrations (1-10 mM) of TPGS, owing to micellar solubilization of the drug. As TPGS is non-ionic in nature, it does not offer any ionic interaction with ATR in any buffer solution. TPGS exhibited higher solubility enhancement in higher pH buffer solution as compared to low pH buffer solution and this may be attributed to better surface activity of TPGS at higher pH. Its major fraction exists in micelle form due to low CMC which lead to higher solubility enhancement. Highest solubility enhancement of ATR was observed with TPGS micelle formation.

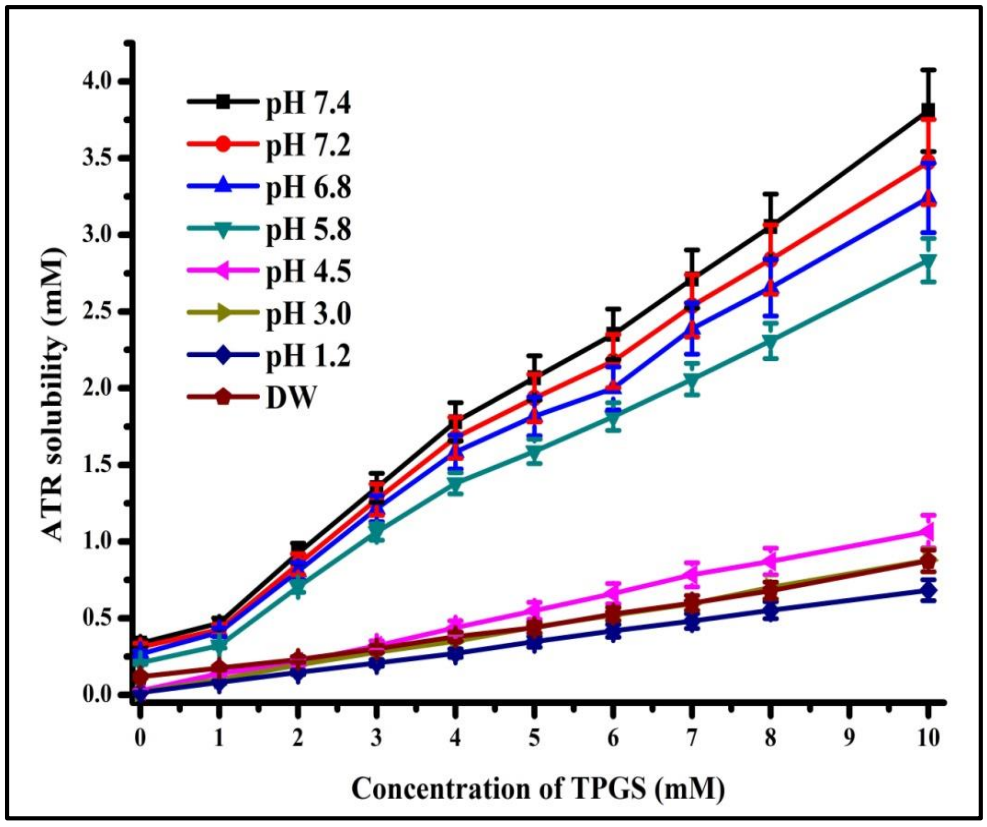

Fig. 5.12 Effect of concentration of TPGS on the solubility of ATR in different solutions (vertical bars indicate SD)

Solubility parameters of surfactants

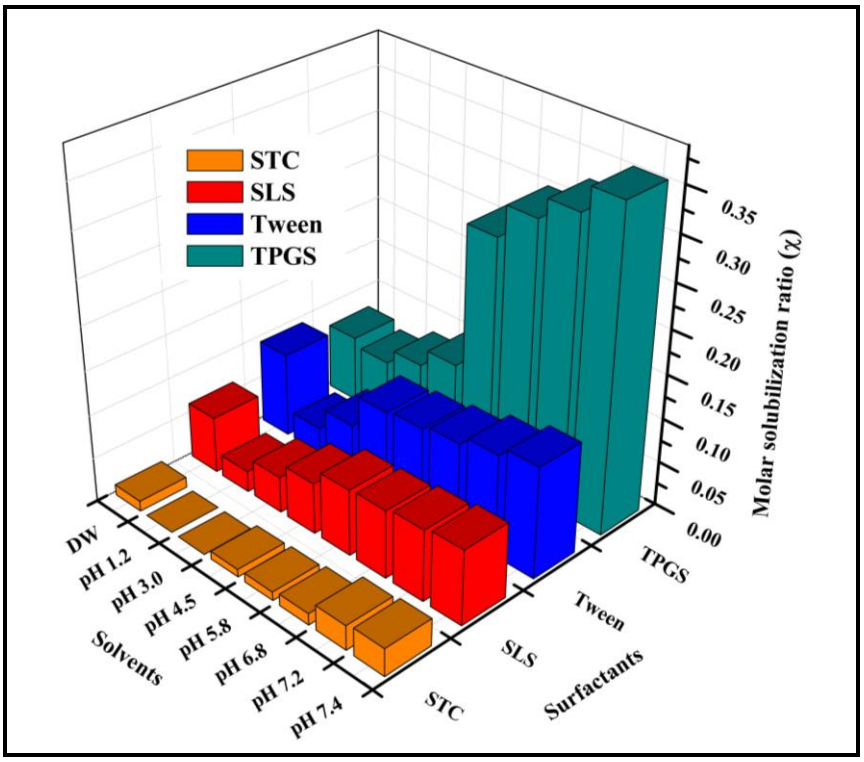

Fig. 5.13 Values of molar solubilization ratio (χ) of all four surfactants at different pH

The molar solubilization ratios (χ) of the different surfactants followed the following trend: TPGS > T80 > SDS > STC **(Fig. 5.13).** The low χ value of STC in comparison to others is probably because of limited solubility of the surfactants and electrostatic repulsion of ATR with similar negatively charged surfactant. The relatively low χ value of STC in comparison to SLS can be discussed on the basis of their solubility in media. STC solubility in different buffer media was found to be lower than that of SLS. Aggregation number (N) and size of surfactant and solute (molecular weight) also play role in solubilization property. Four molecules of STC cannot easily accommodate big molecule like ATR (1209 M_W) in its micelle but sixty molecules of SLS can easily accommodate ATR. Tween 80 showed highest value of χ in deionized water due to relatively lower CMC and higher solubility. Further, the χ value of TPGS was obtained highest in all four surfactants in phosphate buffer (pH≥4.5).

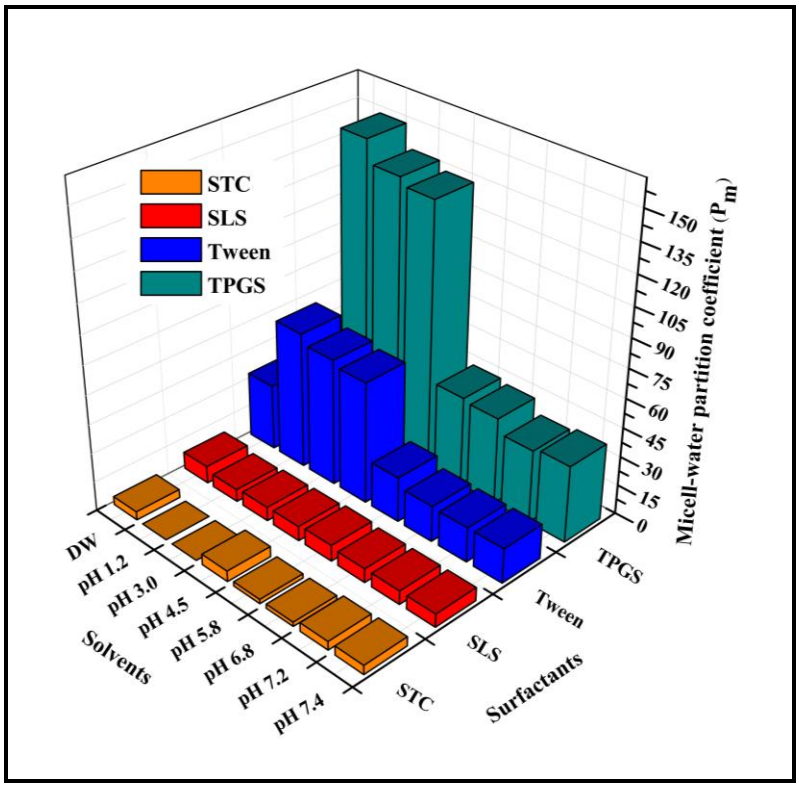

Fig. 5.14 Values of micelle-water partition coefficient (P_m) of all four surfactants at different pH

The micelle-water partition coefficient (P_m) of various surfactants has been exhibited in **Fig. 5.14**. TPGS showed highest value of P_m in all four surfactants in all the solutions. Anionic surfactants (STC and SLS) exhibited smaller value of P_m due to electrostatic repulsion with anionic ATR. Higher aggregation number (N=62) of SLS favored in micelle formation with ATR in comparison to STC (N=4). Highest P_m value was found in acidic buffer with anionic surfactants. In acidic buffer, solubilized ATR substantially partitioned into micelle due to low solubility and non-ionic character of ATR in acidic buffer (pH≤4.5) which may possibly cause higher value of P_m.

The standard free energy of solubilization (ΔG_s^o) is measurement of energy utilized in the formation of micelles and incorporation of the solute molecules within them. The higher negative value of ΔG_s^o indicates more favorable condition to uptake the solute within micelles. **Fig. 5.15** enlisted the ΔG_s^o value of all surfactants. All the ΔG_s^o values are negative (except STC value at

pH 1.2 & pH 3.0) which indicates spontaneous miceller solubilization. The value of $|\Delta G_s^o|$ followed the similar trend of P_m.

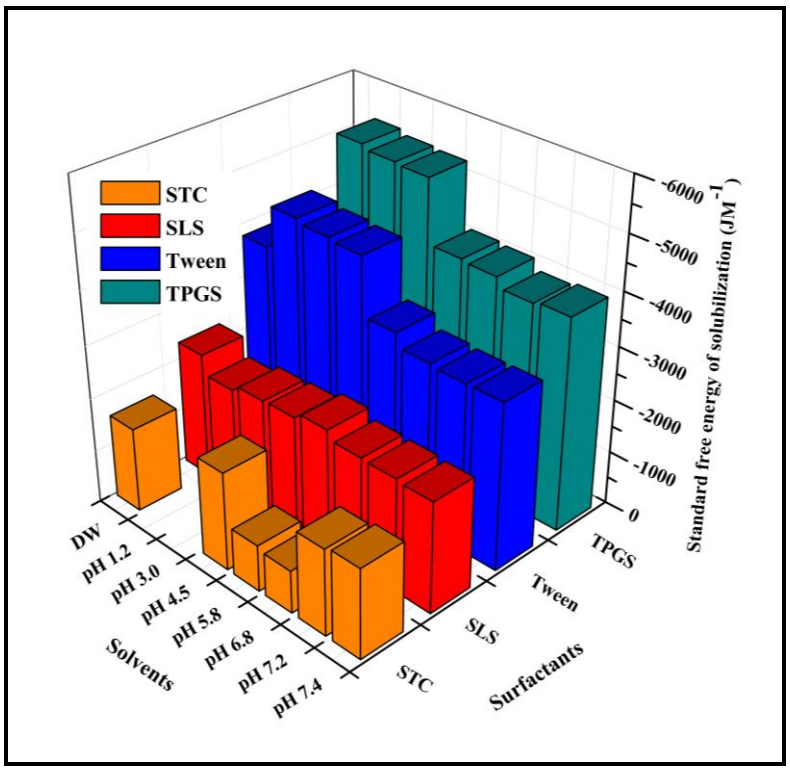

Fig. 5.15 Values of standard free energy of solubilization (ΔG_s^o) of all four surfactants at different pH

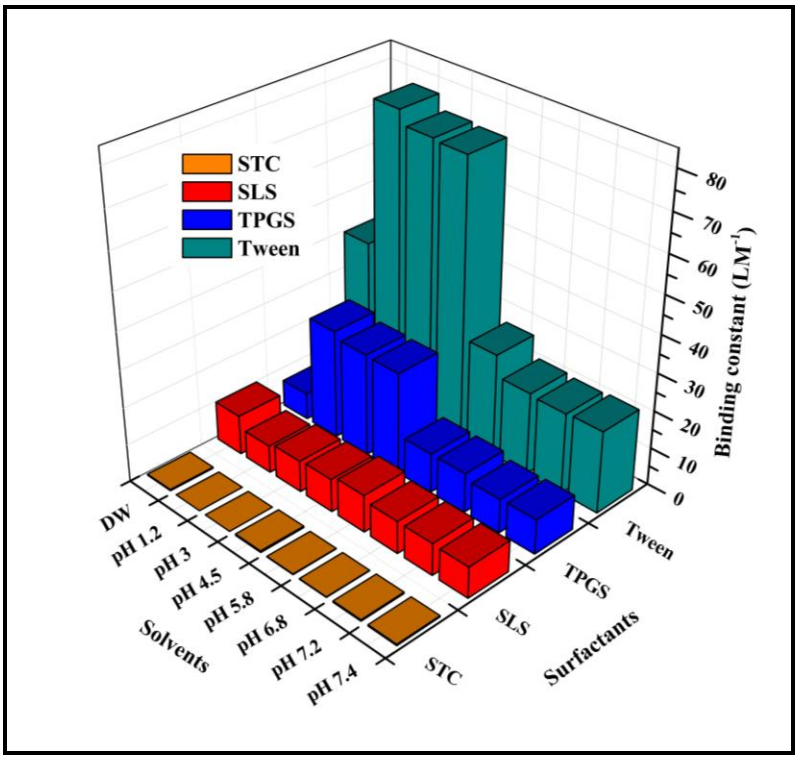

Fig. 5.16 Values of binding constant (K) of all four surfactants at different pH

Irrespective of pH of the media, STC exhibited lowest binding constant (K) as shown in **Fig. 5.16**. Anionic surfactants exhibited lowest binding constant due to electrostatic repulsion between ATR and surfactants. SLS showed relatively higher value of K due to higher aggregation number (N=62) in micelle formation than the STC (N=4). Tween 80 showed highest value of K due to higher N value (60) than TPGS (N=10).

5.2 Formulation development, *in vitro* and *in vivo* characterizations

In the current research work, three novel drug delivery formulations were developed to improve bioavailability, efficacy and safety profile of ATR. ATR encapsulated Eudragit RSPO nanoparticles (AERSNs), ATR loaded PLGA nanoparticles (APLNs) and ATR loaded PCL nanoparticles (ALPNs) were developed and extensively evaluated for *in vitro* as well as *in vivo* characterizations. The study divided into three parts as stated below.

- Preparation, *in vitro* and *in vivo* characterization of ATR encapsulated Eudragit RSPO nanoparticles
- Preparation, *in vitro* and *in vivo* characterization of ATR loaded biodegradable PLGA nanoparticles
- Preparation, *in vitro* and *in vivo* characterization of ATR loaded biodegradable PCL nanoparticles

5.2.1 Preparation, *in vitro* and *in vivo* characterization of AERSNs

5.2.1.1 AERSNs preparation and optimization using CCD experimental design

Emulsification solvent evaporation technique is a simple and reproducible method for the preparation of PNs. Chloroform was used as oil phase since ATR is sparingly soluble in ethyl acetate and dichloromethane. PVA was selected as an emulsifier owing to its good stabilizing property and its ability to favor nanoparticles of relatively smaller size with uniform distribution[28]. Prepared AERSNs were obtained as translucent milky suspension.

30 batches of AERSNs were successfully prepared using four factors and five levels CCD experimental design as shown in Table 2. The value of dependent variables R_1 and R_2 were found to be in the range of 167 to 449 nm and 49.3 to 98.6%, respectively. Second order polynomial equations were established, expressing each dependent variable as a function of independent variables by response surface regression analysis using Design- Expert 7.0 software. A lower student t-test value (p<0.05) indicates significance of independent variables on dependent response and higher value of correlation co-efficient value indicates better fit of second order equation. Polynomial equations obtained are as follows:

Mean diameter particle size (R_1) = $250.8 + 45.8X_1 - 13.3X_2 - 27.3X_3 - 23X_4 + 7.5X_3X_4 + 26.6X_1^2$ equation (5.1)

Entrapment efficiency (R_2) = $71.7 + 10.8X_1 - 3.7X_2 – 4.5X_3 - 5.0X_4 + 1.4X_1^2$ equation (5.2)

Above mentioned equation (5.1) and equation (5.2) include only significant terms (p<0.05). Equation (5.1) represents the dependence of mean diameter particle size of AERSNs on all the independent factors with correlation coefficient (R^2) 0.99. The model (p<0.001) and lack of fit (p=0.495) indicated that the model was significant. The polymer content more significantly determined the particle size of AERSNs and its positive sign of cofficient factor indicated that the particle size increases with the increase in polymer content. All other independent factors like PVA concentration, volume of organic solvent and homogenization speed showed negative cofficient factor, which indicated that PS of AERSNs decreases with the increase of these variables, as depicted in 3D response surface plot in **Fig. 5.17A & B**.

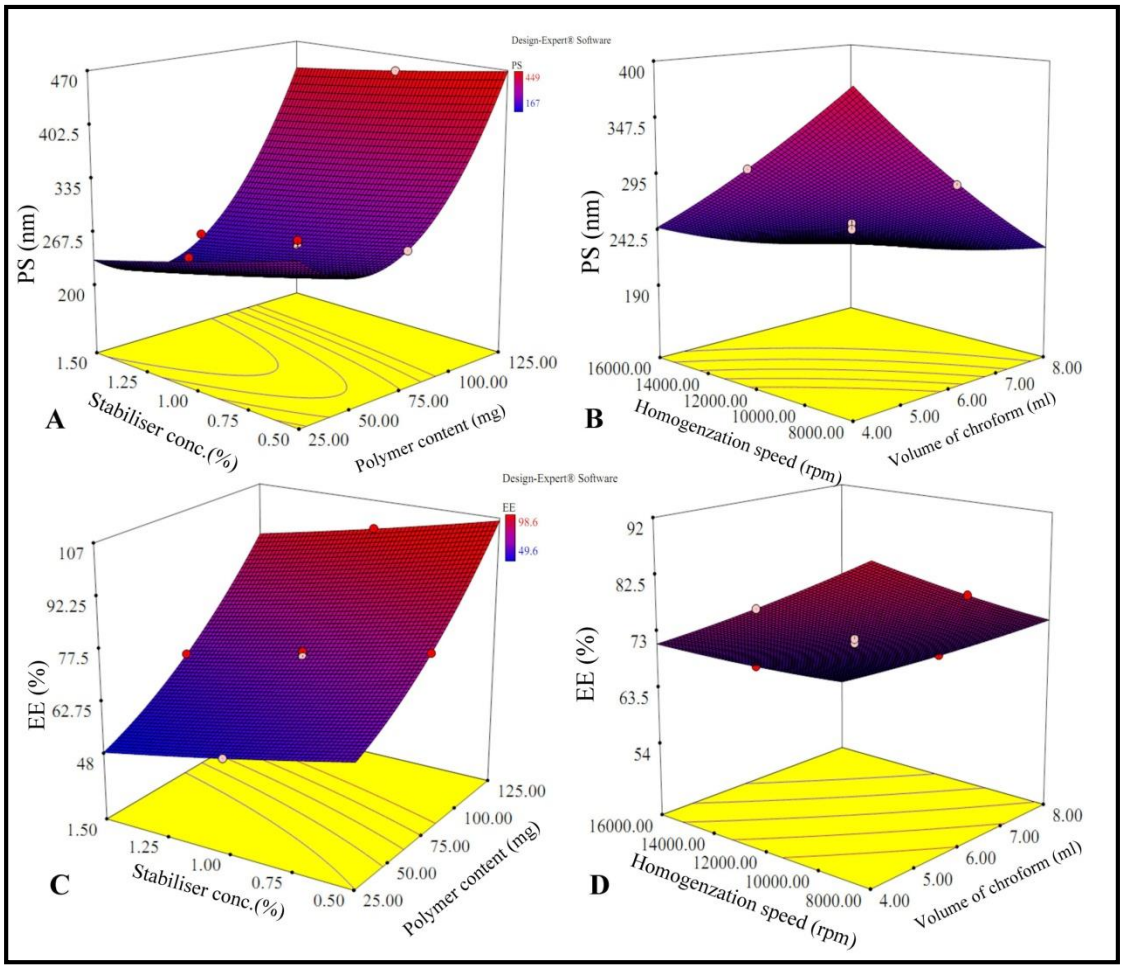

Fig. 5.17 Three-dimensional response surface plot showing the effect of polymer content, concentration of surfactant, volume of organic phase and homogenization speed on (A & B) Mean diameter particle size and (C & D) Mean entrapment efficiency

Equation (5.2) represents the expression of EE as a function of independent variables with correlation coefficient (R^2) of 0.995. EE model was significant (p<0.0001) and lack of fit was insignificant (p=0.805) which were desirable for the fitness of model. All the independent variables significantly influenced the EE of AERSNs. The polymer content predominantly determined the EE of AERSNs as its coefficient was found to be greater than the other independent variables. EE increased with the increase of ploymer content while decreased with the increase of other independent variables as exhibitted in **Fig. 5.17C & D** of 3D response surface plot. The central point batch was selected as optimized batch on the basis of smaller particle size and higher entrapment efficiency. The optimized batch of AERSNs was prepared by using 75 mg of

polymer, 1% (w/v) of PVA concentration, 6 ml of chloroform and 12000 rpm homogenization speed with 251±5 nm PS, 71.7±0.8% EE, 0.228±.009 PDI and +29.3±1.1 mV zeta potential.

5.2.1.2 Determination of PS, PDI, ZP and EE

Polymer content predominantly influenced the PS of AERSNs among all the significant factors. An increase in polymer content promoted the formation of larger size droplet probably due to increased organic phase viscosity, which eventually lead to hindered dispersion of organic phase in aqueous phase, resulting in increased particle size after evaporation of organic phase[29]. Increased stabilizer concentration favored smaller PS as stabilizer tends to form a boundary layer around droplets, which prevents impingement of droplets and consequently, favors the formation of non-aggregated dispersion[30]. Increased volume of chloroform resulted in reduction of mean PS due to decreased viscosity of organic phase and more dilution of polymer. As homogenization provides the shear force to reduce the particle size, higher homogenization speed favored lower PS.

PDI of AERSNs was found to be in the range of 0.195 to 0.587. Smaller PDI is desired for stable and better PNs as it indicated homogeneity of dispersion. A higher PDI favors the destabilization of dispersion due to Ostwald ripening[31]. Higher Zeta potential is expected for the stable colloidal system as it overcomes the particle aggregation due to repulsion forces. Zeta potential of the prepared PNs was observed in the range of +27 to +34 mV which indicated a stable formulation. Positive surface charge of AERSNs was attributed to the cationic nature of polymer.

The polymer content was found to be predominant among other significant independent variables in determination of EE of PNs. Raised polymer content caused increase in diffusion barrier, which hinders the diffusion of drug from the organic phase to aqueous phase and enhances the EE. Raised concentration of surfactant increased the miceller solubilization of drug with surfactant leading to lower EE. Raised volume of chloroform dilutes the diffusion

barriers, which facilitates the drug diffusion from the organic phase and resulted in lesser EE. Higher stirring speed also facilitates drug diffusion from organic phase to aqueous phase, resulting in lower EE.

5.2.1.3 Solid state characterization of AERSNs by FT-IR, DSC and PXRD

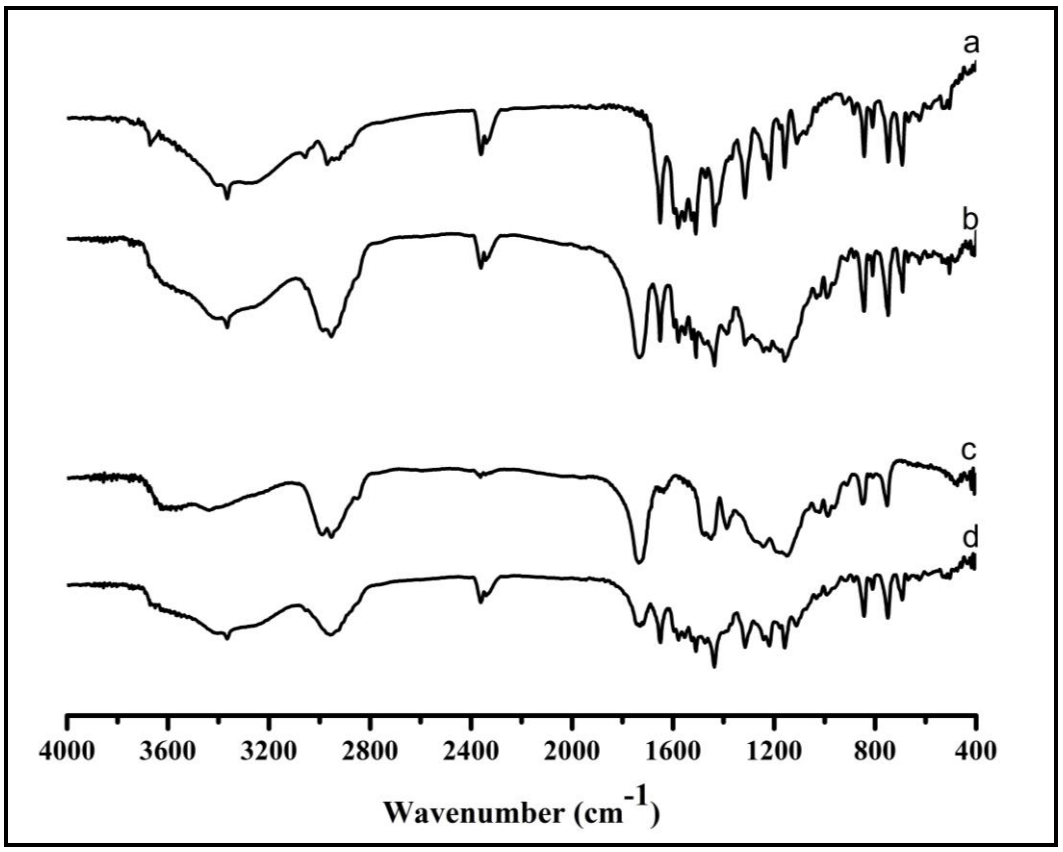

Fig. 5.18 FT-IR spectra of (a) ATR, (b) PM of ATR and PLGA, (c) Placebo nanoparticles and (d) Optimized batch of AERSNs

FT-IR spectra of ATR, placebo nano-formulation, physical mixture (PM) of ATR with eudragit RSPO and freeze dried batch AERSNs are depicted in **Fig. 5.18**. ATR displayed various characteristic peak at 3670 cm^{-1} (free O-H stretching of trihydrate functionality), 3367 cm^{-1} (N-H stretching), 3222 cm^{-1} (asymmetric O-H stretching), 3055 cm^{-1} (symmetric O-H stretching), 1649 (asymmetric C=O stretching), 1578 (symmetric C=O stretching), 1550–1468 (C–C ring stretching), 1317 (CH_3/CH_2 deformation), 1243 (C–N stretching) and 1213 cm^{-1} (C–N stretching/C–O stretching) (Kim et al., 2008). Most of the spectral peaks of ATR were preserved in PM and AERSNs, indicating chemical compatibility of ATR with polymer in AERSNs. O-H stretching peak of possible

trihydrate molecules at 3670 cm^{-1} was absent in AERSNs due to amorphous nature of ATR incorporated in nanoparticles. On the basis of FT-IR spectral investigation, no chemical interactions were observed between drug and polymer.

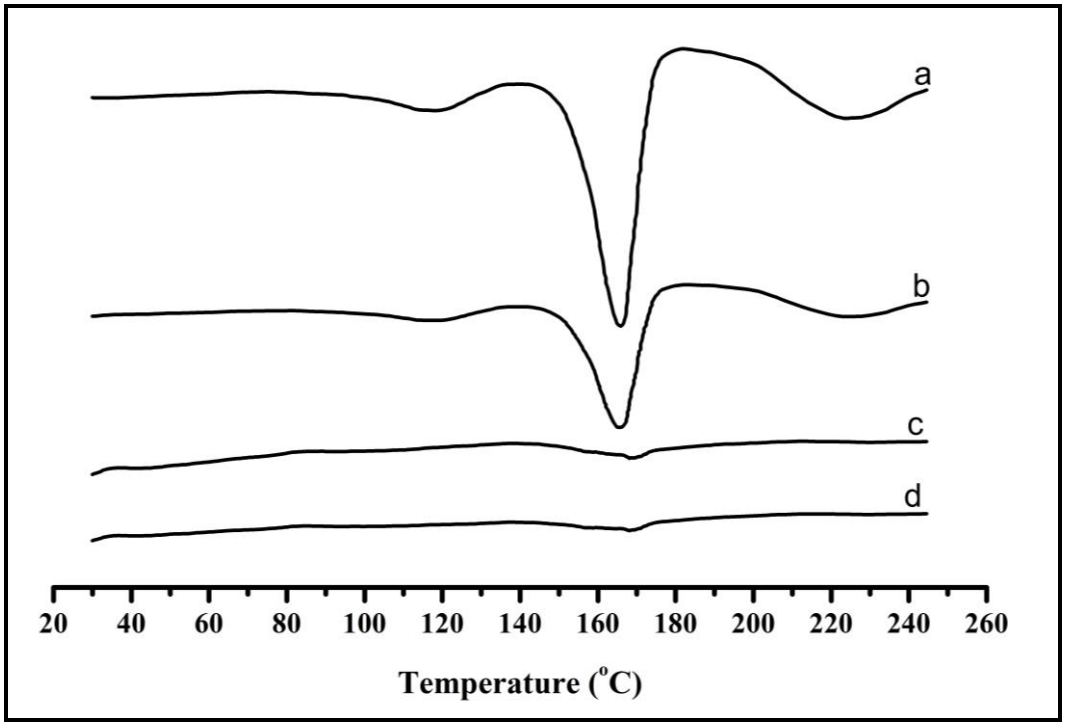

Fig. 5.19 DSC thermograms of (a) ATR, (b) PM of ATR and PLGA, (c) Placebo nanoparticles and (d) Optimized batch of AERSNs

DSC thermograms of ATR, PM, placebo nanoparticles and freeze dried batch of AERSNs are depicted in **Fig. 5.19**. A broad endotherm between 70-130°C and a sharp endotherm at 165°C were observed in thermogram of ATR. Broad endotherm range from 70 to 130°C pointed out the loss of 3 molecule of water while the sharp endotherm exhibited melting point of ATR. Sharp melting point of ATR indicated its crystalline nature. No shift of ATR endotherm was observed in PM, which suggested ATR compatibility with polymers. Absence of endotherm in placebo nanoparticle and AERSNs suggested the amorphous character of placebo as well as AERSNs. The amorphous nature of ATR in freeze dried batch AERSNs was attributed to particle size reduction and homogeneous dispersion of ATR inside polymer matrix.

PXRD diffraction pattern of ATR, PM, placebo nanoparticle and freeze dried AERSNs are represented in **Fig. 5.20**. Prominent diffraction peaks at diffraction angle (2θ) of 6.02, 9.06, 9.36, 10.16, 10.44, 11.76, 12.08, 16.92, 19.32, 21.50, 22.58, 23.18 and 23.56^{o} were observed for pure ATR (Kim et al., 2008). All the diffraction peak pattern of ATR was found to be retained in PM, confirming the good physical compatibility with polymer. The diffraction pattern of freeze dried placebo nanoparticles and AERSNs did not exhibit any peak thereby, confirming the amorphous nature of placebo nanoparticles and AERSNs.

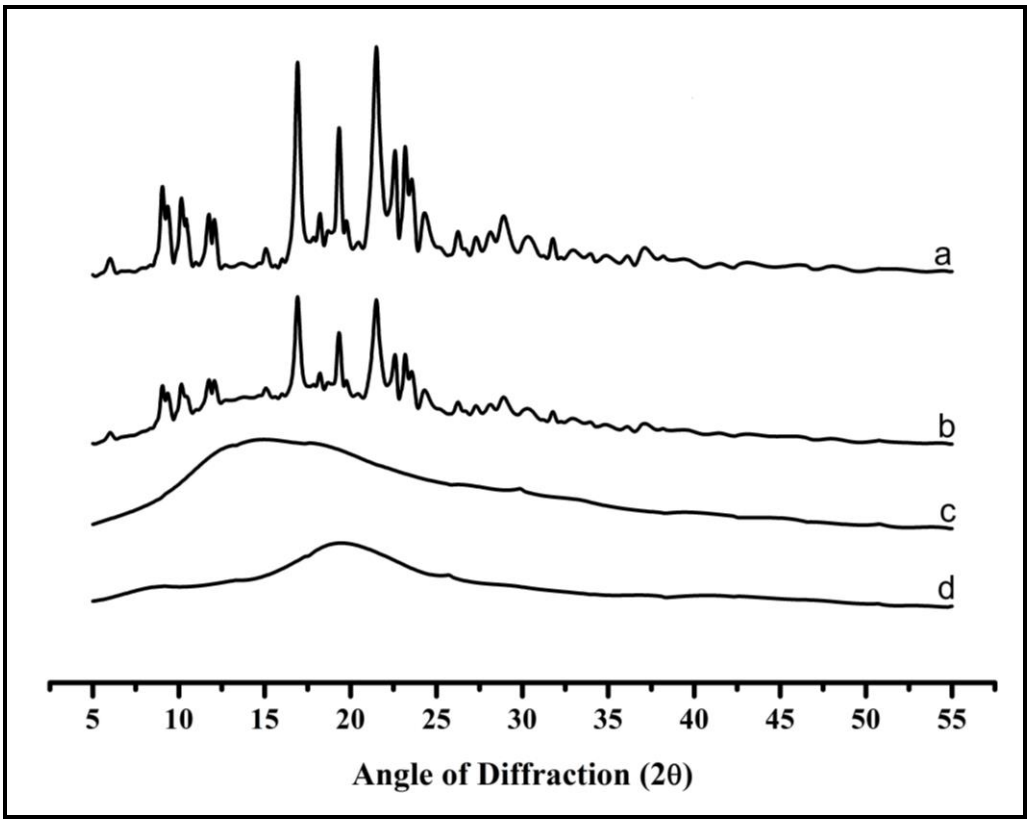

Fig. 5.20 PXRD diffractograms of (a) ATR, (b) PM of ATR and PLGA, (c) Placebo nanoparticles and (d) Optimized batch of AERSNs

5.2.1.4 Morphological study of AERSNs

The AFM image of AERSNs is represented in **Fig. 5.21A**, which exhibited the morphological characteristics of nanoparticles. Image demonstrated spherical shape and smooth surface of nanoparticles with uniform distribution. Observed PS was found comparable with the PS obtained from particle size analyzer.

TEM image of AERSNs is depicted in **Fig. 5.21B**. Image demonstrated spherical shape of nanoparticles with uniform distribution. Here, particle size was observed to be around 243 nm. Electron diffraction ring pattern of AERSNs was found to show smooth halo ring without any spotty pattern as shown in **Fig. 5.21C**, confirming the amorphous nature of AERSNs (Chaurasia et al., 2015).

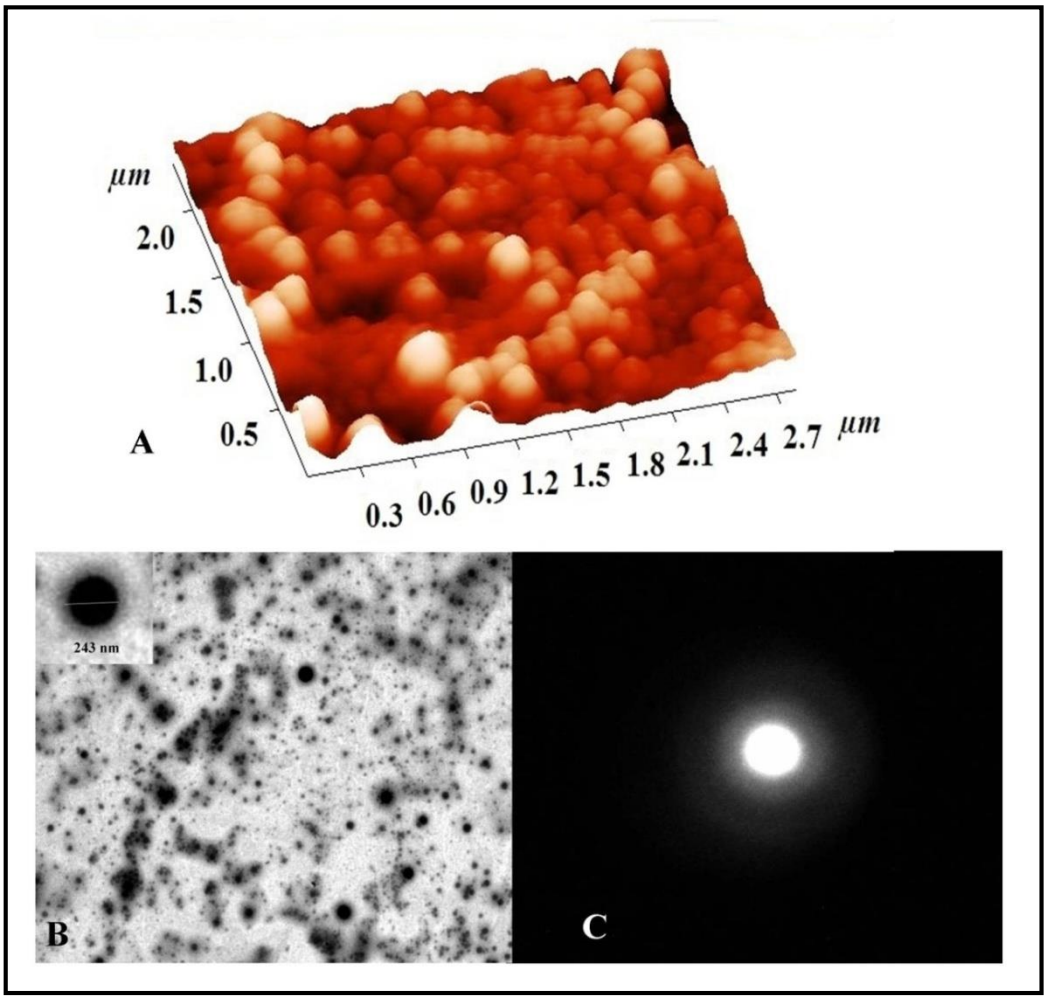

Fig. 5.21 (A) AFM image (B) TEM image and (C) TEM diffraction pattern of optimized batch of AERSNs

5.2.1.5 In vitro release study

The *in vitro* drug release profiles of AERSNs and pure drug suspension are shown in **Fig. 5.22A**. 50% of the drug was released in 6 h and 90% in 24 h from the AERSNs whereas 50% of drug was released in 1.5 h and 90% in 8 h from pure drug suspension. Various release kinetic models (zero order, first order, Higuchi, Hixson-Crowell and Korsmeyer-Peppas model) were fitted with the

release data of AERSNs and analyzed for release mechanism (Uskoković, 2013). Release kinetic parameters of AERSNs in various kinetic models are shown in Table 5.4. Based on higher R^2 value, the release kinetic best suited in Korsmeyer-Peppas model with n<0.45, confirming the Fickian diffusion controlled release mechanism.

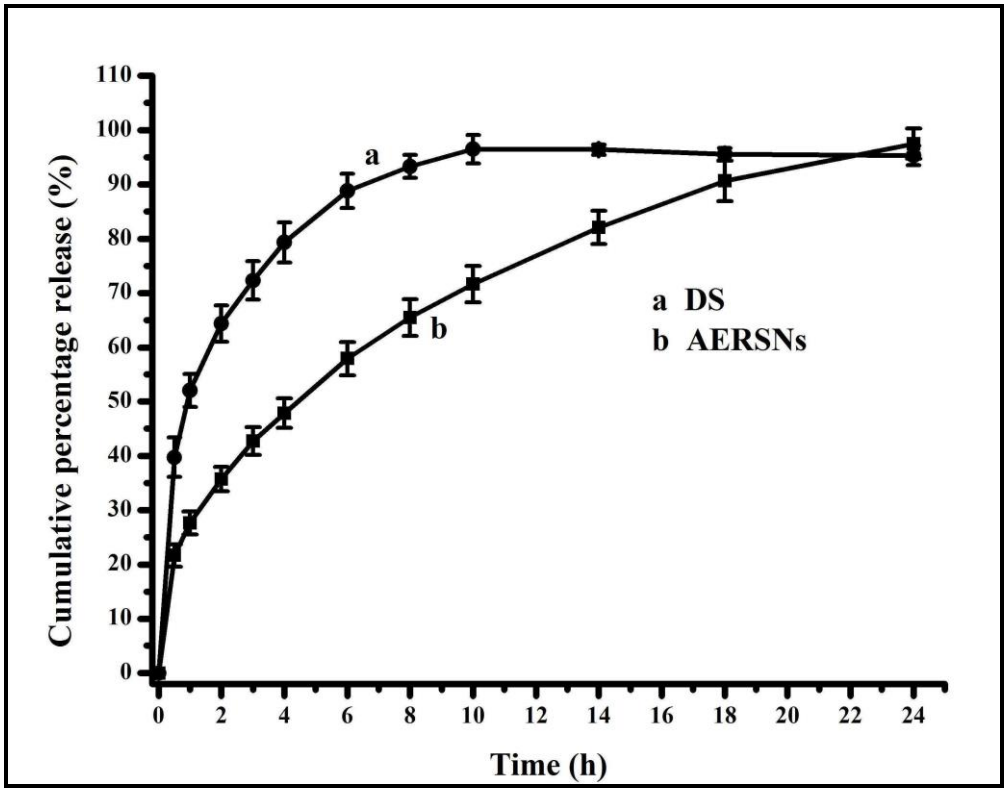

Fig. 5.22 Representing the *in vitro* drug release profile of optimized batch of AERSNs and drug suspension (DS) in phosphate buffer pH 7.4 (vertical bars reperesent the standard deviation)

Table 5.4 Release kinetic parameters of optimized AERSNs in PBS (pH 7.4)

Release kinetic model of AERSNs										
Zero order		**First order**		**Higuchi model**		**Korsmeyer-Peppas model**			**Hixson-Crowell model**	
R^2	K_0 (%/h)	R^2	K_1 (h^{-1})	R^2	K_H (%$h^{-1/2}$)	R^2	K_{kp}	n	R^2	K_{HC} (%$^{1/3}$h^{-1})
0.877	3.514	0.821	0.011	0.977	21.17	0.998	27.7	0.404	0.985	0.114

5.2.1.6 Storage stability study:

The stability of colloidal dispersion is crucial for its *in vivo* performance. The change in properties of AERSNs (PS, PDI and EE) during stability study over 6 months is depicted in **Fig. 5.23**. There was no any significant change in properties of AERSNs stored at refrigerated condition (4±1°C) as observed. However a marked change in particle size, EE and PDI of AERSNs stored at room temperature (25±2°C) was observed. Under accelerated stability condition (40±2°C/75±5% RH), a significant change in properties of AERSNs was observed due to instability of drug as well as colloidal system at higher temperature. Refrigerated condition was found to be best suited for storage condition of AERSNs.

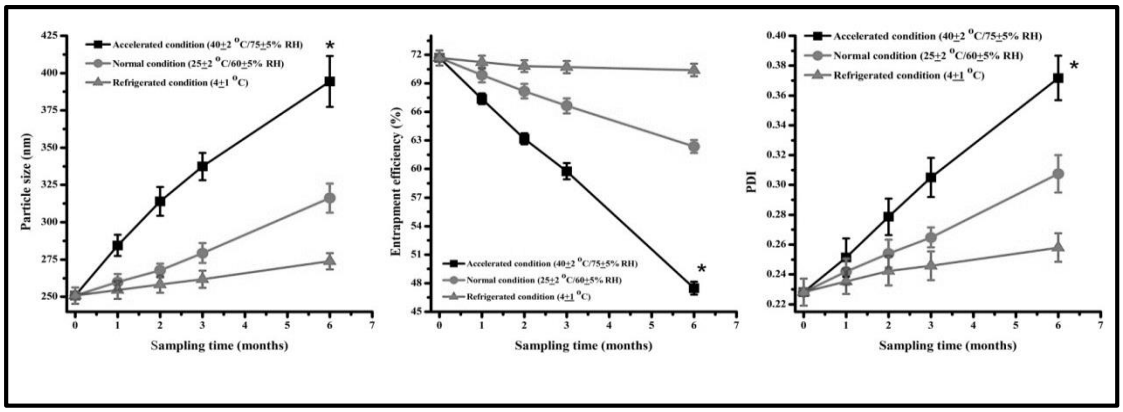

Fig. 5.23 The particle size, entrapment efficiency and polydispersity index (PDI) of optimized AERSNs during stability study of 6 months under different environmental conditions [* represents a significant change (p<0.05) compared to properties of AERSNs on 0 days]

5.2.1.7 Trace organic solvent (chloroform) estimation in formulation

Under the same gas chromatographic (GC) condition as discussed in chapter 4.2.2.8, various validation parameters were obtained and which suggested the sensitive, precise and accurate methodology of GC. The standard chromatograms of chloroform with internal standard (1-propanol) and freshly prepared AERSNs spiked with IS are shown in **Fig. 5.24**. There was absence of chloroform signals in AERSNs sample which concluded that the residual chloroform in AERSNs was either absent or may be present below detectable amount (LOD: 20 ppm).

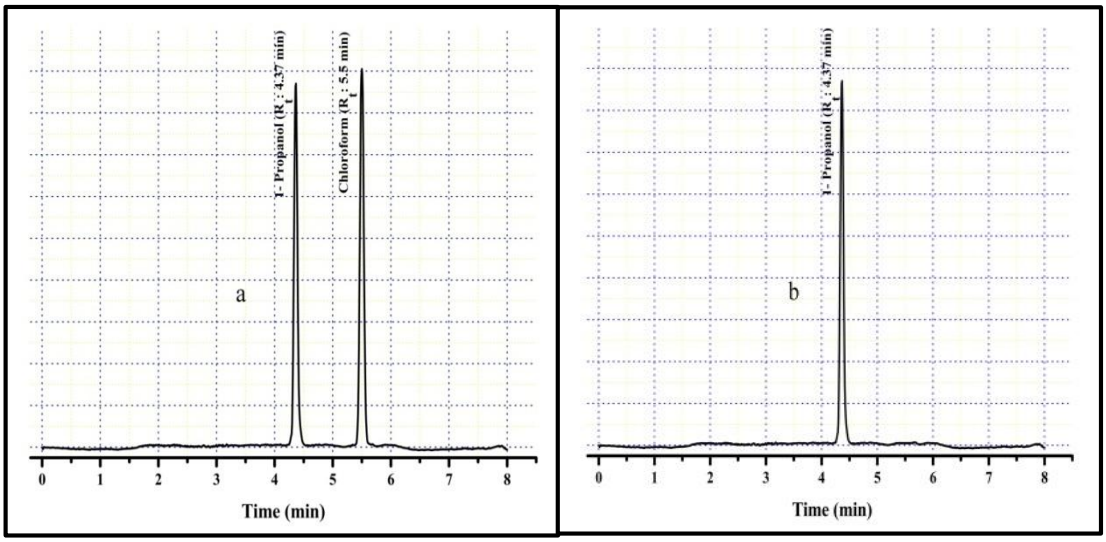

Fig. 5.24 Gas chromatogram of (a) Standard chloroform (1250 ppm) and internal standard 1-propanol (1000 ppm) in deionized water (b) Aqueous sample of AERSNs with internal standard 1-propanol (1000 ppm)

5.2.1.8 In vivo study

5.2.1.8.1 Pharmacokinetic study

ATR concentration was quantified in rat plasma by RP-HPLC method as reported by Kumar et al., 2014. After single oral dose administration, the plasma drug concentration time profiles of pure drug suspension and the AERSNs are depicted in **Fig. 5.25**. Pharmacokinetic parameters of AERSNs and pure drug suspension were calculated and compared statistically by using Kinetica and Graphpad Prism, respectively which are enlisted in Table 5.4. Significant enhancement in C_{max} (p<0.05) was observed for AERSNs as compared to ATR suspension which attributed to higher absorption of PNs through gastrointestinal tract. Tmax was higher for AERSNs than the drug suspension, confirming the sustained release characteristics of drug from AERSNs as found during *in vitro* release study. After 2 h post dose, AERSNs maintained higher plasma concentration till 24 h than that of drug suspension. Observed area under curve till 24 h (AUC0-24 h) and infinite time (AUC0-∞) of ATR from AERSNs were found to be significantly (p<0.05) higher, almost 1.81 and 2.37 times than that of pure drug suspension, indicating greater extent of drug availability in systemic circulation from AERSNs than drug suspension. This significant enhancement is attributed to enhanced systemic absorption of PNs and released

drug at the absorption site due to nano range particle size and bio-adhesive property offered by eudragit as well as PVA (Patel et al., 2015; Lopedota et al., 2009; Elshafeey et al., 2010; Tabata & Ikada, 1990). Intact nanoparticles might be absorbed through paracellular, transcellular and lymphatic (via M cell of Payer's patches) uptake pathways and transferred to systemic circulation (des Rieux et al., 2006). Mean residence time (MRT) of drug from AERSNs was also observed to be significantly higher (p<0.05) than drug suspension. Positive surface charge and surface absorbed hydrophilic PVA on AERSNs possibly enhanced its systemic residence time (Xu et al., 2009; Lee et al., 1999).

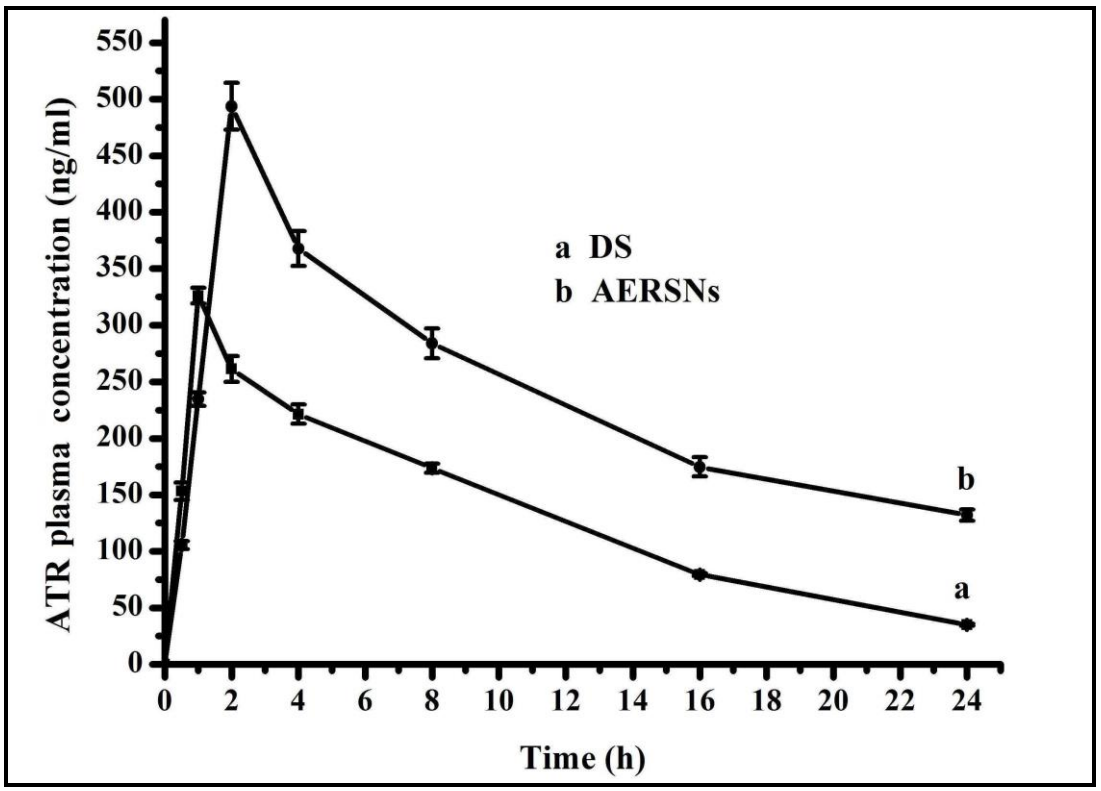

Fig. 5.25 Pharmacokinetic profiles of AERSNs and drug suspension (DS) (vertical bars indicate SD and dose was equivalent to 20mg/kg of ATR)

Table 5.5 Pharmacokinetic parameters of AERSNs and drug suspension after single oral dose administration (dose: 20 mg/kg) and all values are expressed as mean±SEM (n=6))

Pharmacokinetic Parameter	AERSNs	Drug suspension
$AUC_{0\text{-}24h}$(ng h ml^{-1})	5643.7±219.4**	3113.0±55.8
$AUC_{0\text{-}\infty}$(ng h ml^{-1})	8239.4±306.9**	3470.9±58.7
T_{max} (h)	2.0	1.0
C_{max} (ng ml^{-1})	493.7±20.9*	326.2±6.9
F_{rel}	2.37±0.11	1.0
MRT (h)	20.6±0.5*	11.1±0.1

*P < 0.05, **P < 0.01, ***P < 0.001 as compared to drug suspension

5.2.1.8.2 Efficacy study

At the end of fourth week, HFD fed rats exhibited significant elevation in plasma levels of different biochemical parameters such as PTC, PTG, LDL_C, glucose and $VLDL_C$, whereas decrease in HDL_C level than the NDC group. As demonstrated in **Fig. 5.26**, After 4 weeks, a 75-80% elevation in PTC, 75-85% elevation in PTG and 200-300% elevation in LDL_C was observed; whereas a decline by 28-33% of HDL_C level was observed in all HFD fed groups compared to the NDC group. HFPET, HFAST and HFAET groups were treated as aforementioned during 4^{th}-6^{th} weeks (Table 4.10, Chapter 4.2.2.9.3). As ATR is a competitive HMG CoA reductase inhibitor, it suppresses intracellular cholesterol synthesis. Subsequently, the decreased plasma level of cholesterol up-regulates LDL receptor which enhances the plasma LDL_C clearance leading to lowering of LDL_C level in plasma (Funatsu et al., 2011). Prolonged treatment with ATR significantly reduces the PTG level due to decreased assembly and secretion of VLDL caused by down-regulation of microsomal triglyceride transfer protein mRNA and up-regulation of LDL receptors (Mohammadi et al., 1998). Statins increase the plasma HDL_C level possibly by producing ApoAI to increase functional HDL_C that can activate reverse cholesterol transport and by inhibiting cholesterol ester transfer proteins, which produce dysfunctional HDL_C with pro-inflammatory and atherogenic properties (Yamashita et al., 2010; Francis et al.,

2003). Statins therapy indicated an activation of peroxisome proliferator-activated receptor-γ, a pleiotropic effect in several experimental models which assist in insulin sensitization and reduction in glucose levels, subsequently (Grip et al., 2002). A significant decrement in elevated levels of PTC, PTG, LDL_C and PGL whereas, considerable enhancement in HDL_C level were observed in HFAST and HFAET groups than HFC and HFPET groups at the end of 6th week (**Fig. 5.26** and Table 5.6).

Efficacy parameters like PTC, PTG, LDL_C, HDL_C and glucose levels clearly indicated that the AERSNs containing half of ATR than the ATR suspension were as equally efficient as ATR suspension. Enhancement in efficacy of AERSNs might be resulted due to considerable improvement in the ATR bioavailability by virtue of their nano size as well as bio-adhesiveness imparted by positive surface charge. After six weeks, the treatment was stopped, which showed that the decreased levels of lipid as well as glucose parameters gradually increased by time and reached the HFD control levels at the end of the 8th week. Elevation trend of lipid parameters in HFAET and HFAST groups were almost similar during 6th-8th week. There was no significance difference between the trend of lipid parameters of HFPET and HFC groups, which demonstrated no any effect of placebo nanoparticles itself. The salient finding of the study thus, proved the efficacy of AERSNs at 50% reduced dose of ATR as AERSNs in comparison to ATR suspension.

5.2.1.8.3 Safety study

Statins therapy often imparts several skeleton muscle toxicities such as mild myalgia, myopathy and myositis to rhabdomyolysis. Owing to higher incidence of severe muscle myopathies, Cerivastatin was promptly withdrawn from market in 2001. The reports of ATR associated complications are increasing day by day due to its accumulation in non-hepatic tissues. Several biomarkers like CK, LDH, creatinine and BUN has been used for diagnosis of rhabdomyolysis. Elevated level of CK (>10 times than upper limits of normal level) with renal

impairment clearly indicate the pathology of rhabdomyolysis. Elevated levels of LDH, creatinine, AST and BUN provide the indication of membrane damage.

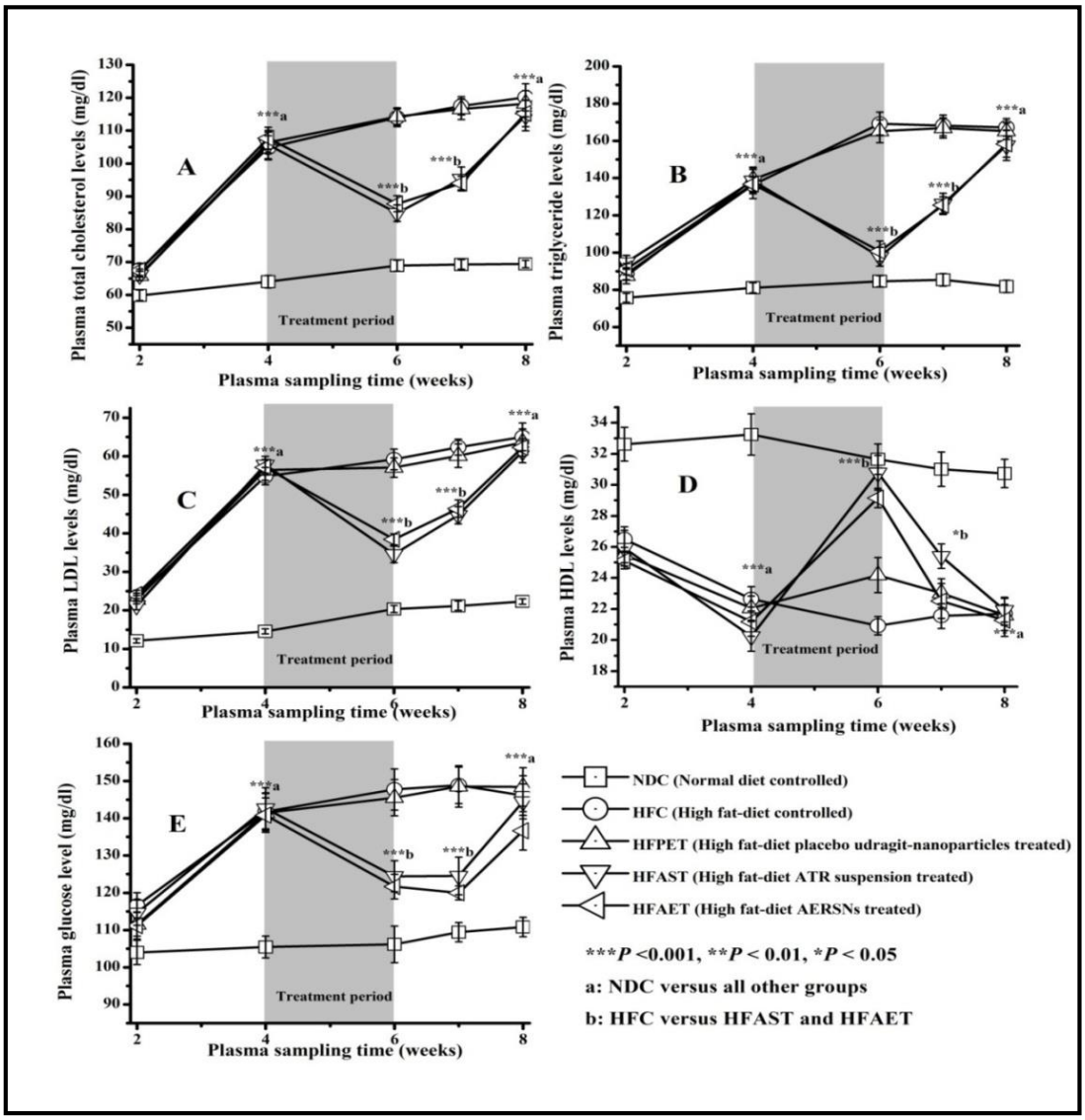

Fig. 5.26 Exhibiting (A) Plasma total cholesterol levels (B) Plasma triglyceride levels (C) Plasma low density lipoprotein-cholesterol (LDL_C) levels (D) Plasma high density lipoprotein (HDL_C) levels and (E) Plasma glucose levels versus time profile of different treated groups

The safety profile of AERSNs was determined by measuring the CK, LDH, creatinine, AST and BUN level in plasma with the aid of UV-visible spectrophotometer (Shimadzu-1800, Japan), using span diagnostic kits. Plasma samples at the end of 4th, 6th and 8th week of different groups were evaluated for safety profile. CK levels were found to be normal in all the groups whereas creatinine, LDH, AST and BUN levels were significantly elevated in HFAST group

than that of HFAET group as evidenced in **Fig. 5.27**. Table 5.6 exhibits that all the safety profile levels of HFAET group are significantly better than that of HFAST group, which might be attributed to the following plausible reasons: (a) 50% reduction of ATR dose could have resulted into significant decrease in associated toxicity, (b) AERSNs could have protected drug from degradation and instant metabolism and have released the drug in sustained manner which contributed not only in efficacy but also in reduced toxicity (c) AERSNs could have altered the tissue distribution which might be entirely different from the pure drug. Liver histology depicted in **Fig. 5.28** indicated normal sanguine cell in all the treated groups which confirmed no toxic effect of drug and AERSNs on liver cell.

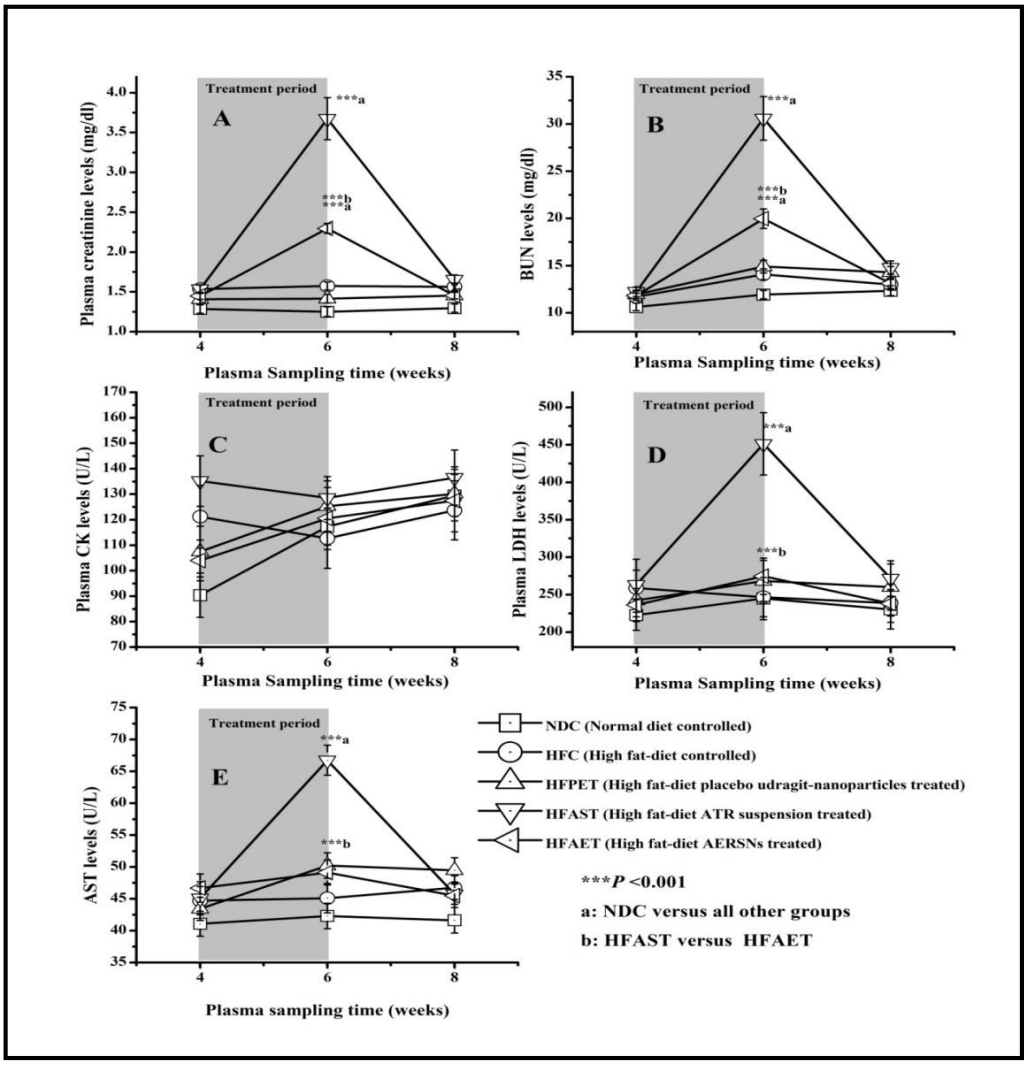

Fig. 5.27 Depicting (A) Plasma creatinine levels (B) Blood urea nitrogen (BUN) levels (C) Plasma creatinine kinase (CK) levels, (D) Plasma lactate dehydrogenase (LDH) levels and (E) Aspartate amino transferase (AST) levels versus time profile of various treated groups

Table 5.6 Plasma efficacy and safety related biochemical parameters in different groups of rats at the end of 6th week

S. No.	Biochemical Parameters	NDC	HFD	HFPET	HFAST	HFAET
1	PTC (mg/dl)	68.9±1.7	114.0±2.7^{***a}	114.3±2.7^{***a}	84.9±2.5^{***b}	87.7±2.4^{***b}
2	PTG (mg/dl)	84.6±3.0	169.2±6.2^{***a}	165.2±6.1^{***a}	97.7.0±5.0^{***b}	100.7±5.5^{***b}
3	$VLDL_C$ (mg/dl)	16.9±0.6	33.9±1.2^{***a}	33.0±1.2^{***a}	19.5±1.0^{***b}	20.1±1.1^{***b}
4	HDL_C (mg/dl)	31.7±1.0	20.9±1.0^{***a}	24.2±1.1^{***a}	30.8±1.1^{***b}	29.2±0.6^{**b}
5	LDL_C (mg/dl)	20.3±0.9	59.2±2.7^{***a}	57.1±2.5^{***a}	34.6±2.1^{***b}	38.4±1.4^{***b}
6	PG (mg/dl)	106.2±4.9	147.8±5.5^{***a}	145.5±4.9^{***a}	124.4±4.2^{**b}	121.6±3.3^{***b}
7	PC level (mg/dl)	1.25±0.06	1.57±0.05	1.41±0.05	3.67±0.26^{***c}	2.23±0.06^{*c***d}
8	BUN (mg/dl)	13.9±0.6	14.1±0.6	14.9±0.7	30.6±2.3^{***c}	20.0±1.0^{*c***d}
9	CK (U/L)	117.3±7.3	112.7±11.7	125.3±9.9	128.5±8.4	120.5±12.1
10	LDH (U/L)	244.8±28.1	246.7±26.3	268.3±27.3	451.2±41.5^{***c}	274.7±24.3^{**d}
11	AST (U/L)	42.3±2.0	45.1±2.3	50.2±2.1	66.8±2.4^{***c}	49.1±2.0^{***d}

PTC: plasma total cholesterol, PTG: plasma triglyceride, $VLDL_C$: very low density lipoprotein cholesterol, HDL_C: high density lipoprotein cholesterol, LDL_C: low density lipoprotein cholesterol, PG: plasma glucose, PC: plasma creatinine, BUN: blood urea nitrogen, CK: creatinine kinase, LDH: lactate dehydrogenase, AST: aspartate aminotranferase, NDC: normal diet controlled, HFC: high fat-diet controlled, HFPET: high fat-diet placebo-eudragit RSPO-nanoparticle treated, HFAST: high fat-diet ATR calcium suspension treated, HFAET: high fat-diet AERSNs treated. All values are expressed in mean±SEM (n=6); ***P < .001, **P <.01 and *P <.05 [a] versus NDC, [b] versus HFC and HFPET, [c] versus NDC, HFC and HFPET, [d] versus HFAST

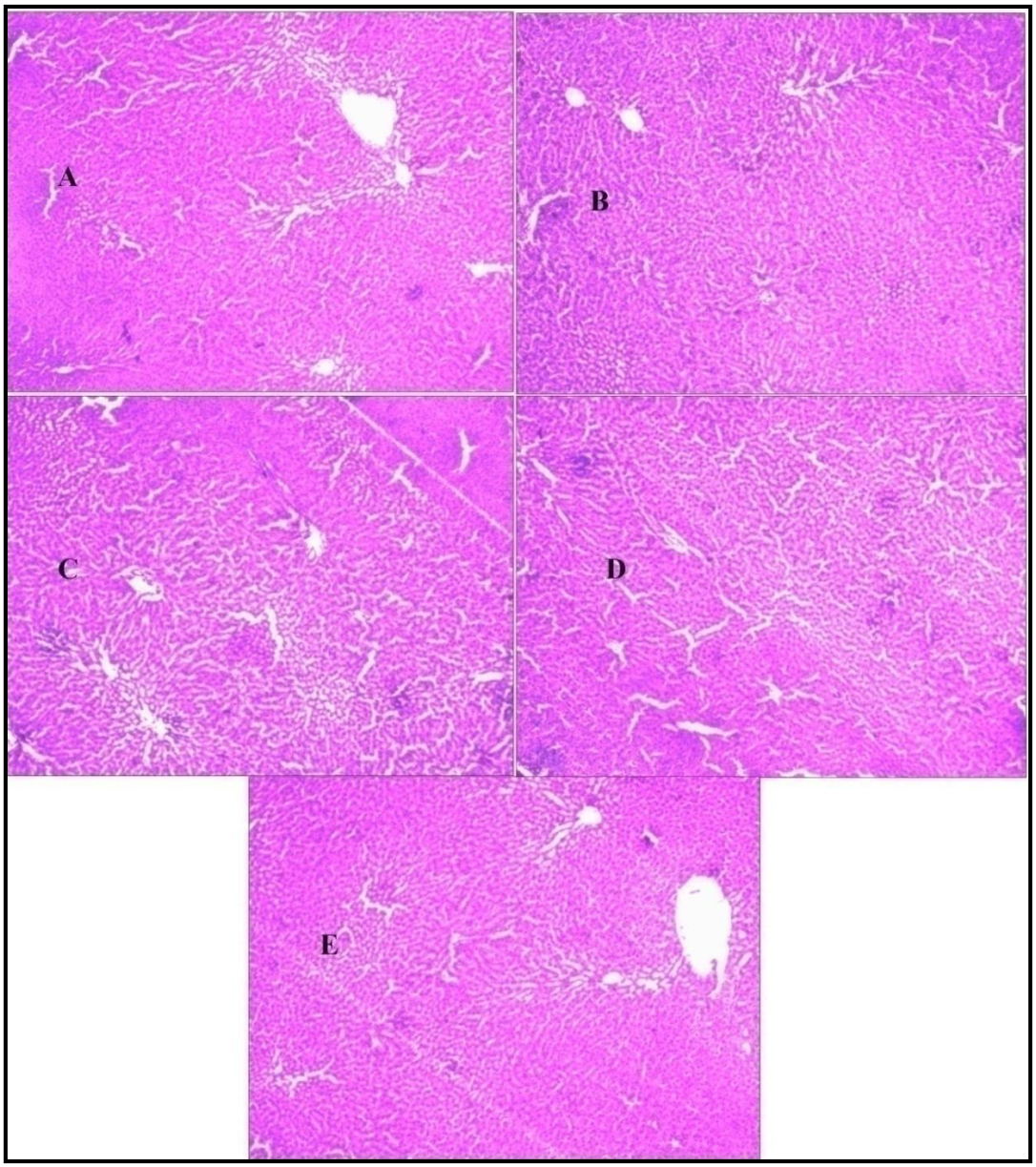

Fig. 5.28 Histomicrograph of stained liver tissue of various groups (A) Normal control, (B) High fat-diet control (C) Placebo nanopaticle treated, (D) Drug suspension treated and (E) AERSNs treated

5.2.2 Preparation, *in vitro* and *in vivo* characterization of APLNs

5.2.2.1 APLNs preparation and optimization using CCD experimental design

Nanoprecipitation is a simple, fast, reproducible method and widely used for the preparation of PNs. The nanoparticle formation is instantaneous and one step process. Nanoprecipitation technique often produces small PNs (100–300 nm) having largest possible zeta potential with narrow unimodal distribution and for this a wide range of polymers can be used (Mora-Huertas et al., 2012).

The basic principle of this technique is based on the interfacial deposition of a polymer after displacement of a semi-polar solvent, miscible with water forming a lipophilic solution. Rapid diffusion of the solvent into non-solvent phase results in the decrease of interfacial tension between the two phases, which increases the surface area and leads to the formation of small droplets of organic solvent. Nanoprecipitation system consists of three basic components: the polymer, the polymer solvent and the non-solvent of the polymer. Acetone (ICH class 3 solvent) was selected for the preparation of organic phase as it is less toxic solvent according as ICH Q3C (R4) guideline, both the PLGA and ATR easily soluble, does not form azeotropic mixture with water and easily get evaporated. TPGS was chosen as stabilizer due to its antioxidant nature and it enhances the nanoparticle absorption (Zhang et al., 2012).

Prepared PNs were found to be a translucent milky in appearance without any visible sign of particles. APLNs were prepared according to CCD as shown in Table 4.8 (Chapter 4.2.2.2). Mean diameter PS, %EE and polydispersity index were also shown in Table 4.8 (Chapter 4.2.2.2). Two selected dependent variables R_1 and R_2 values were found to be in the range of 140 to 345 nm and 56.4 to 95.3%, respectively. Mathematical relationships were established among dependent and independent variables by response surface regression analysis using Design- Expert 7.0 software and obtained as follow:

$$R_1 \text{ (Mean diameter PS)} = 195.50 + 50.33X_1 - 16.92X_2 - 20.42X_3 - 16.33X_4 + 10.50X_1X_2 + 17.88X_1^2 + 9.13X_2^2 + 11.75X_3^2 \quad \text{equation (5.3)}$$

$$R_2 \text{ (EE)} = 80.47 + 10.19X_1 - 5.08X_2 - 2.99X_3 - 2.42X_4 \quad \text{equation (5.4)}$$

Equation (5.3) showed the linear terms: X_1, X_2, X_3 and X_4; interaction term: X_1X_2 and quadratic terms: X_1^2, X_2^2 and X_3^2 were significant in mean PS determination. All other terms were insignificant (p>.05). A (polymer content) was a major factor influencing the mean PS of PNs. Negative coefficient of X_2, X_3 and X_4 pointed that the PS decrease with the increase in surfactant concentration, volume of organic phase and stirring speed.

Equation (5.4) showed the linear terms X_1, X_2, X_3 and X_4 were significant in the determination of EE of prepared PNs. All other terms were insignificant (p>.05). Again polymer content was a major factor with higher coefficient on EE of prepared PNs. Negative coefficient of X_2, X_3 and X_4 indicated that the EE decrease with the increase in surfactant concentration, volume of organic phase and stirring speed. The correlation coefficients (R^2) of polynomial model R_1 and R_2 were found to be 0.949 and 0.951, respectively.

The three dimensional response surface plots for significant independent variables on the dependent variables are shown in **Fig. 5.29**. **Fig. 5.29A & B** part showed the effect of independent variables on the mean particle size of prepared PNs. As depicted in **Fig. 5.29A** there is an increment in mean PS with the increase of polymer content and decrement in PS with the increase of surfactant concentration. As depicted in **Fig. 5.29B**, there is a decrement in mean PS with the increment in volume of organic solvent and the stirring speed. **Fig. 5.29C & D** showed the effect of independent variables on EE of ATR in PNs. Polymer content influenced substantially on EE of PNs as shown in **Fig. 5.29C**. As polymer content increases there is an increase in drug EE of PNs. All other independent variables also influenced the EE. As surfactant concentration, stirring speed and the volume of organic phase increased there was a decrement in EE and *vice versa*.

After selecting constraints of desirability within the range, the optimum level of polymer content, surfactant concentration, volume of organic phase and stirring speed were found to be 125 mg, 0.31 % (w/v), 8.0 ml and 1250 rpm, respectively. At these levels of independent variables, the predicted value of dependent variables mean particle size and the entrapment efficiency were generated to be 204 nm and 82.7 %, respectively having desirability of 0.681. To validate the experimental model, the optimized batch of APLNs was prepared using optimal level of independent variables and matched the responses mean PS and EE with the predicted values. The predicted responses well closely matched with the experimental responses (mean PS 207 and EE 81.3) with less than 1.7 % of bias which suggested that the predicted optimized formulation was reliable and reasonable.

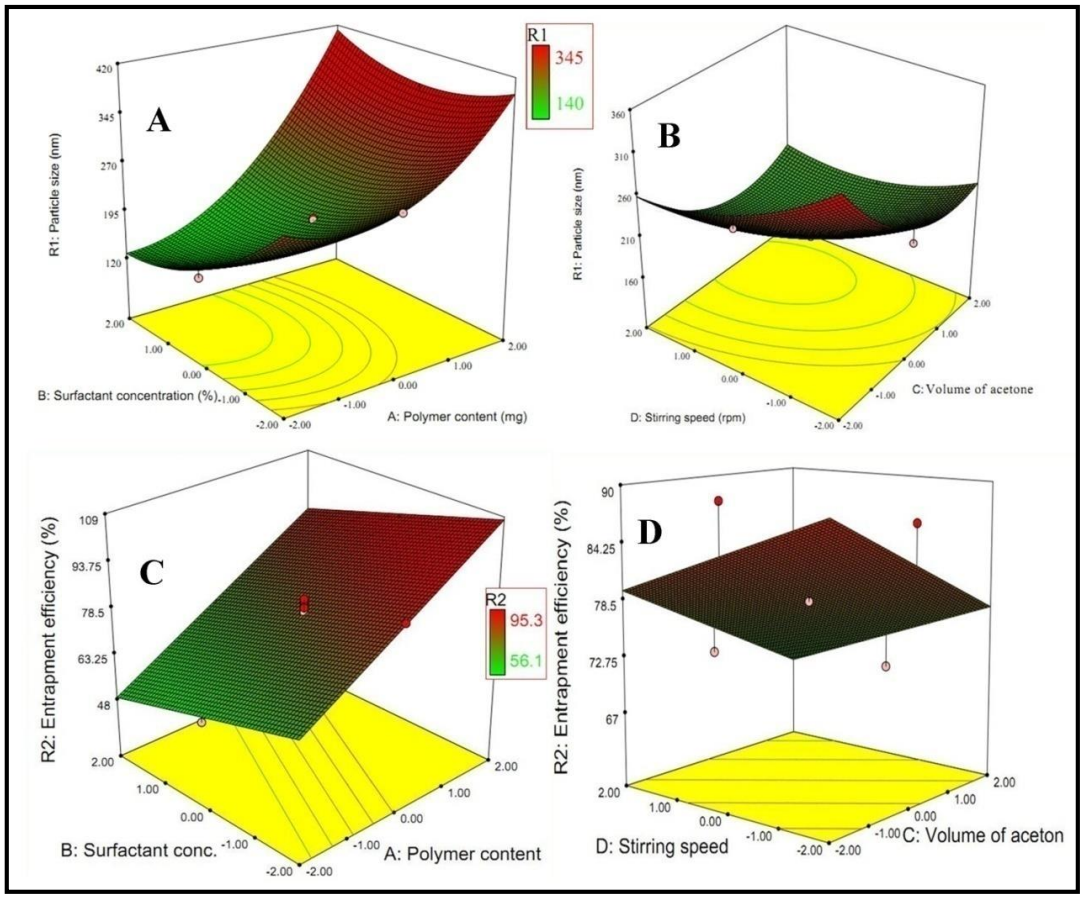

Fig. 5.29 Three-dimensional surface response plot showing the effect of polymer content, surfactant concentration, volume of organic solvent and stirring speed on (A & B) Mean diameter PS and (C & D) Mean EE of APLNs

5.2.2.2. Determination of particle size, polydispersity index, zeta Potential

The mean diameter PS of prepared PNs was found to be in the range of 140–345 nm (Table 4.8, Chapter 4.2.2.2). As discussed in above optimization section; the polymer content, surfactant concentration, volume of organic phase and stirring speed were significantly influenced the mean PS. Increase in polymer content attributed the increase in viscosity of organic phase which led to reduced shear stress and promote the larger size droplet formation. It also hindered rapid dispersion of PLGA solution into the aqueous phase, resulting in larger droplets which formed larger nanoparticles after diffusion and evaporation of the organic solvent (Song et al., 2008). The surfactant was used as a stabilizer in PNs formulation. As surfactants formed an adsorbed layer around the nanoparticles and prevent it to impinge with other nanoparticle led to non-aggregation of particles (Galindo-Rodriguez et al., 2004). Increased volume of

acetone resulted in reduction of mean PS due to decreased viscosity of organic phase and more dilution of polymer. Stirring speed provide the shear force to reduce the particle size and facilitate rapid diffusion of organic solvent into the aqueous phase which facilitate higher degree of nucleation. Consequently, higher stirring speed resulted in reduction in mean PS of PNs.

Polydispersity index (PDI) and zeta potential (ZP) are crucial characteristic parameters for PNs formulation. PDI indicates the degree of particle size distribution. A minimum PDI is desired in PNs formulation for better stability. PDI was observed in the range of 0.175-0.567. The optimized formulation showed a good PDI 0.225. A narrow range of particle size distribution is essential to prevent the particle growth due to Ostwald ripening (Muller & Jacobs, 2002). ZP, the electric potential at the plane of shear, is an important indicator of physical stability of colloidal nanoparticles system. Higher ZP showed higher charges on the surface of nanoparticles thus repulsion forces overcome the particle aggregation. ZP of the prepared PNs was observed in the range of -18 to -22 mV which indicated a stable formulation. Negative potential was due to the polymer and drug anionic nature.

Polymer content, surfactant concentration, volume of organic solvent and stirring speed were significant in determining the %EE of PNs as depicted in equation (5.4). Enhanced polymer content increases the organic phase viscosity which consequently hinders the diffusion of drug from the organic phase to aqueous phase and enhances the EE. Raised concentration of surfactant causes the increase in micelle formation of drug with surfactant leading to lesser EE. Raised volume of acetone decreases the organic phase viscosity consequently, facilitates the drug diffusion from the organic phase and resulted in lesser EE. Higher stirring speed also facilitates drug diffusion from organic phase to aqueous phase resulting in lower EE.

5.2.2.3 Solid state characterizations of ALPNs by FT-IR, DSC and PXRD

FT-IR spectra of placebo nanoparticles, ATR, physical mixture (PM) of ATR with PLGA and freeze dried optimized batch of APLNs are shown in **Fig.**

5.30. ATR retained all their characteristic peaks in PM and APLNs. The significant peaks (3000-3700 cm^{-1}) were retained in PM and APLNs. Peak at 3670 cm^{-1} (free -O-H stretching) was prominent in PM but almost absent in APLNs due to amorphous nature of ATR incorporated in PNs (Kim et al., 2008). Peaks at 3367 (N-H stretching) and 3055 (symmetric O-H stretching) were prominent in ATR along with PM and ALPNs. In finger prints region of ATR the characteristic peaks at 1649 (asymmetric C=O stretching) 1578 (symmetric C=O stretching), 1550–1468 (C–C ring stretching), 1317 (CH_3/CH_2 deformation), 1243 (C–N stretching) and 1213 cm^{-1} (C–N stretching/C–O stretching) were retained in PM and ALPNs. On the basis of FT-IR spectra investigation, no chemical interactions were observed between drug and polymer.

DSC thermograms of ATR, placebo nanoparticles, PM and freeze dried batch APLNs are shown in **Fig. 5.31**. Thermogram of ATR exhibited its crystalline nature with sharp melting point at 165°C. ATR maintained its crystalline characteristics in PM but became amorphous in ALPNs. The amorphous nature of ATR in freeze dried batch APLNs of PNs was possibly due to particle size reduction and dispersion of ATR in nanoparticles polymer matrix.

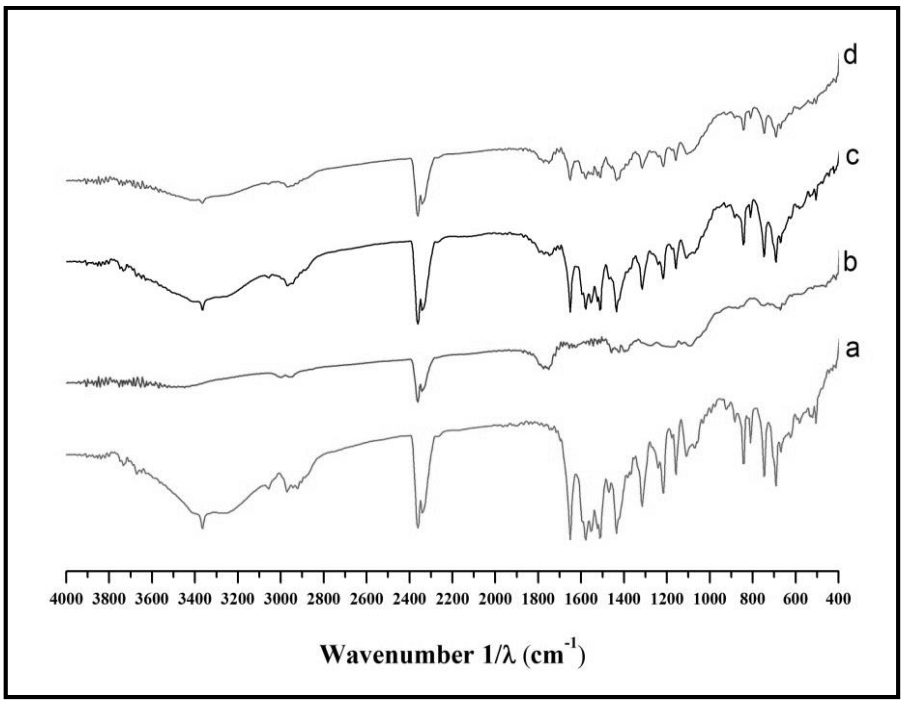

Fig. 5.30 FT-IR spectra of (a) ATR, (b) Placebo nanoparticles, (c) Physical mixture of ATR and PLGA and (d) Optimized formulation APLNs

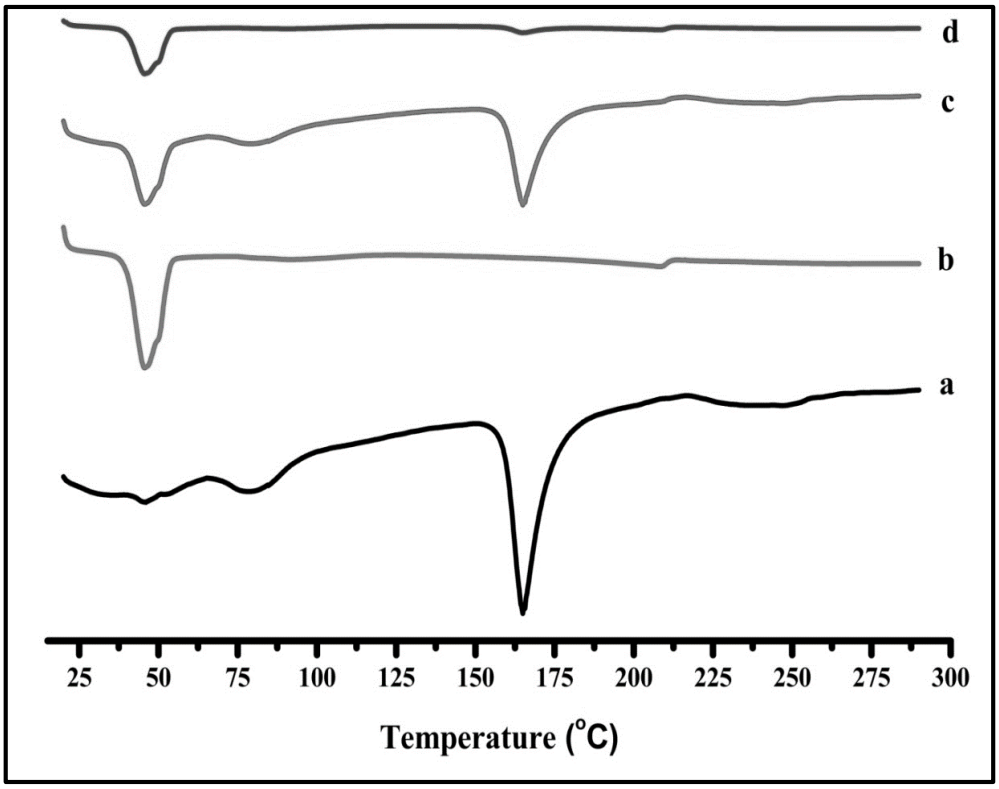

Fig. 5.31 DSC thermograms of (a) ATR, (b) Placebo nanoparticles, (c) Physical mixture of ATR and PLGA and (d) optimized formulation batch APLNs

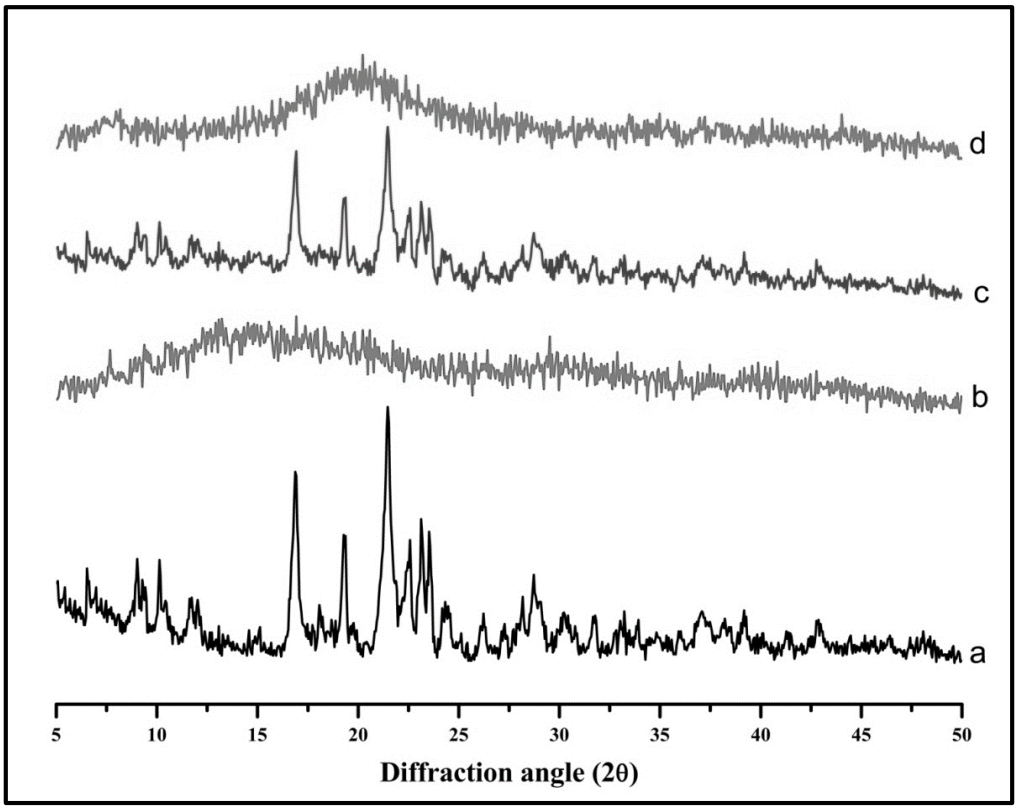

Fig. 5.32 PXRD diffractograms of (a) ATR, (b) Placebo nanoparticles, (c) Physical mixture and (d) Optimized batch of APLNs

PXRD diffraction pattern of ATR, placebo nanoparticles, PM and batch APLNs are shown in **Fig. 5.32**. Prominent diffraction peaks at 2θ = 6.52, 9.02, 9.27, 10.12, 10.42, 11.62, 12.06, 16.87, 19.27, 21.47, 22.57, 23.12 and 23.52° were observed for pure ATR which retained in PM.[34] The diffraction pattern of freeze dried APLNs did not exhibit any characteristic peak of ATR and confirmed the amorphous nature of ATR in PNs.

5.2.2.4 Morphological study of APLNs

AFM micrograph of optimized batch of APLNs is shown in **Fig. 5.33a**. The photomicrographs of AFM supported their comparable hydrodynamic particle size measured by particle size analyzer and uniformity of particle size distribution.

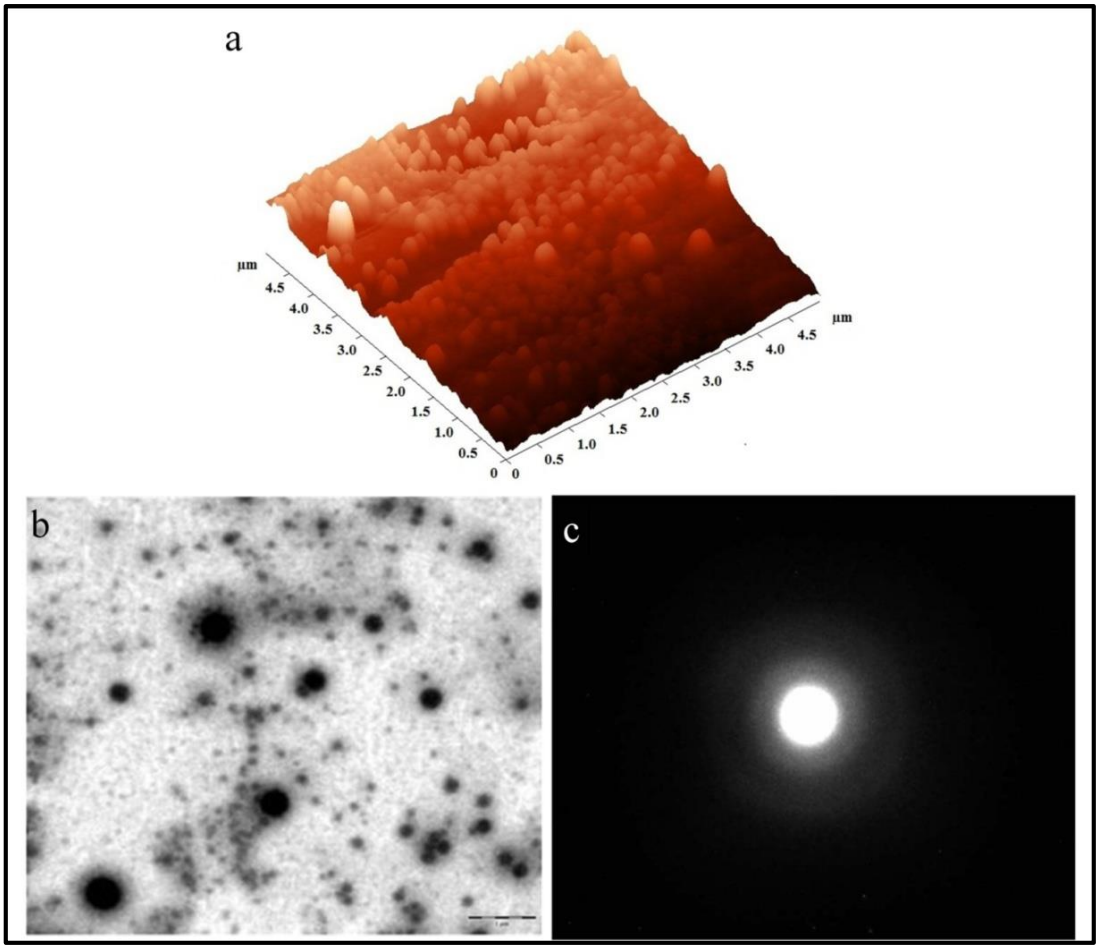

Fig. 5.33 (a) AFM image, (b) TEM micrograph image and (c) Electron diffusion ring pattern of optimized batch of APLNs

Morphological characteristic of optimized batch APLNs was observed by TEM. **Fig. 5.33b** shows the TEM micrograph image of APLNs. Image showed nearly spherical shape of nanoparticles in optimized batch of formulation with uniform distribution. Here particle size was observed to be around 200 nm. Electron diffraction ring pattern of the optimized formulation APLNs is shown in **Fig. 5.33c** and found to be smooth small ring confirming the amorphous nature of APLNs (Rawat et al., 2011).

5.2.2.5. In vitro release study

Fig. 5.34 shows the *in vitro* drug release profile of ATR from APLNs. The initial burst release was observed followed by controlled release. 50 % of the drug was released in 23 h. Several release kinetic models (zero order, first order, Higuchi, Korsmeyer-Peppas and Hixson-Crowell models) were fitted with the release data and analyzed for release mechanism. Table 5.7 enlists the different model correlation coefficient (R^2), rate constant (K) and release exponent (n). Based on higher R^2 value the release kinetic best suited in zero order release kinetics which supported surface erosion based release mechanism. Generally the BCS class II drug incorporated in PLGA nanoparticles follow the zero order release kinetic facilitated through surface erosion mechanism (Mittal et al., 2007).

Table 5.7 Drug release kinetic models of Optimized batch

Release kinetic model of batch APLNs										
Zero order		**First order**		**Higuchi model**		**Korsmeyer-Peppas model**			**Hixson-Crowell model**	
R^2	K_0 (%/h)	R^2	K_1 (h^{-1})	R^2	K_H ($\%h^{-1/2}$)	R^2	K_{kp}	n	R^2	K_{HC} ($\%^{1/3}h^{-1}$)
0.987	0.964	0.917	0.008	0.978	9.325	0.950	22.05	0.297	0.872	0.036

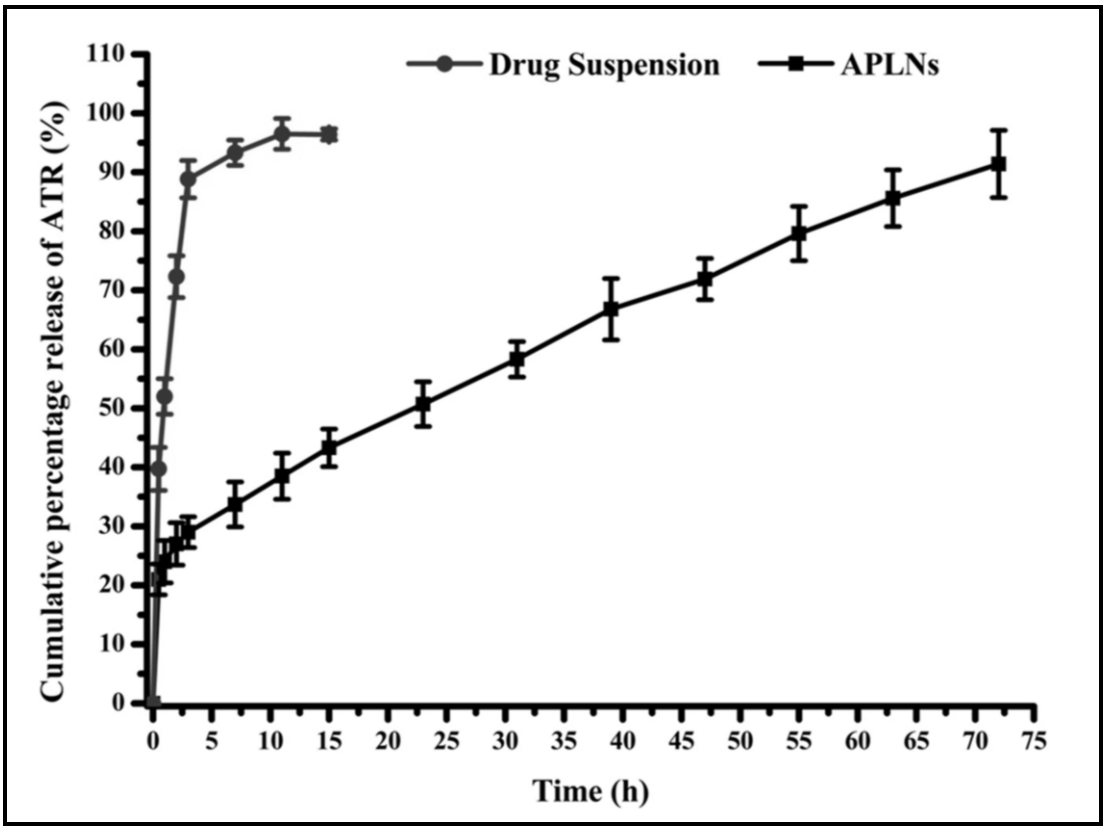

Fig. 5.34 *In vitro* drug release profile of APLNs and drug suspension in phosphate buffer pH 7.4 (vertical bars represent the standard deviation)

5.2.2.6 Storage stability study:

The stability study of APLNs under various storage conditions are demonstrated in **Fig. 5.35**. Under different storage condition, refrigerated condition was best suited for storage of APLNs. Formulation associated properties (PS, EE and PDI) did not change significantly subjected under refrigerated condition (4±1°C) during study period of six months. Under room temperature condition (25±2°C/60±5% RH), noticeable change in EE observed. Under accelerated condition (40±2°C/75±5 RH), significant change in PS, EE and PDI was observed possibly attributed to instability of drug and formulation at harsh conditions of storage.

5.2.2.7 Trace organic solvent (acetone) estimation in formulation

Under gas chromatography condition as stated in previous chapter 4.2.2.8, standard chromatograms of acetone (1000 ppm) with 1-propanol (1500 ppm) as

internal standard (IS) was injected to develop the chromatogram. This standard chromatogram is shown in **Fig. 5.36a**. Chromatogram of freshly prepared APLNs sample spiked with IS (1500 ppm) was developed by injecting in GC system. APLNs chromatogram did not exhibit any signal peak of acetone confirming either absence of acetone in APLNs or present below detectable limit (30 ppm) (**Fig. 5.36b**). Henceforth, the APLNs formulation was safe for oral intake as permissible limit of acetone is reported to be 5000 ppm which is far above than that might be present in APLNs.

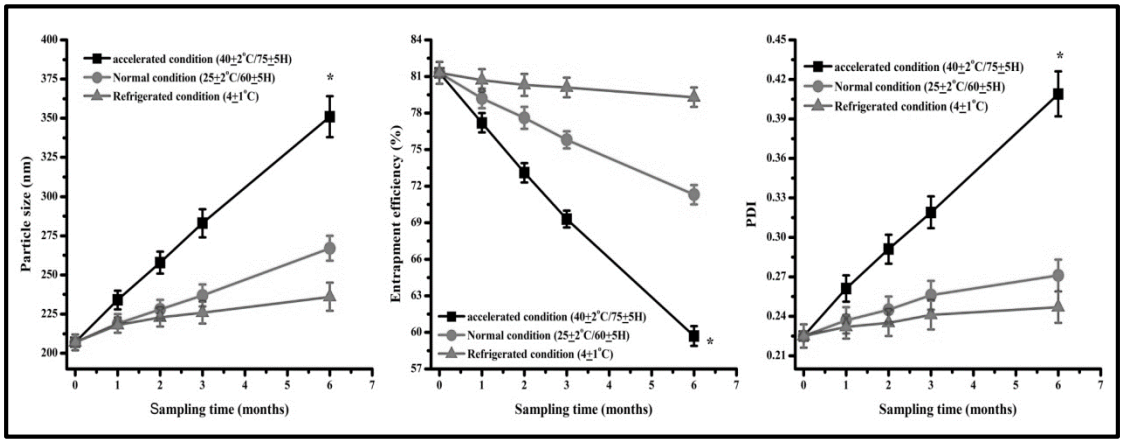

Fig. 5.35 The particle size, entrapment efficiency and polydispersity index of optimized APLNs during stability study of 6 months under different environmental conditions [* represents a significant change (p<0.05) compared to properties of APLNs on 0 days]

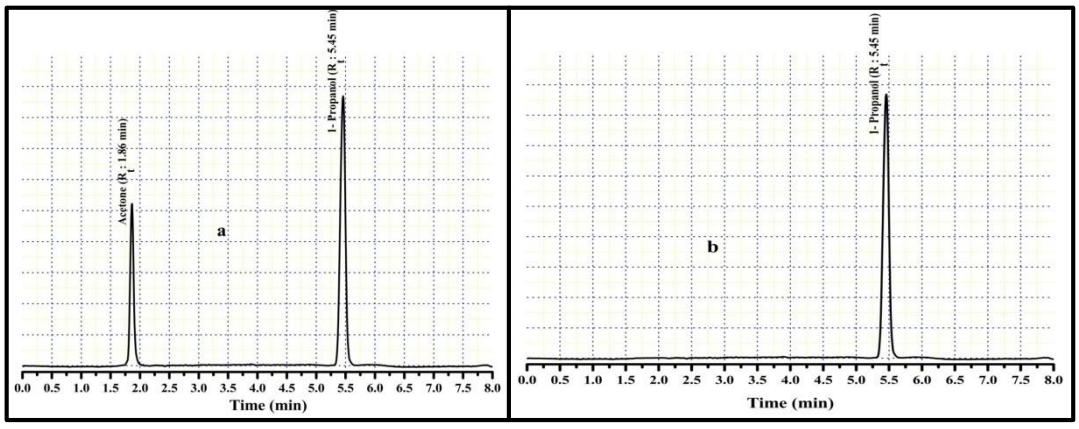

Fig. 5.36 Gas chromatogram of (a) Standard acetone (1000 ppm) and internal standard 1-propanol (1500 ppm) in deionized water (b) Aqueous sample of APLNs with internal standard 1-propanol (1500 ppm)

5.2.2.8 In vivo study

5.2.2.8.1 Pharmacokinetic study

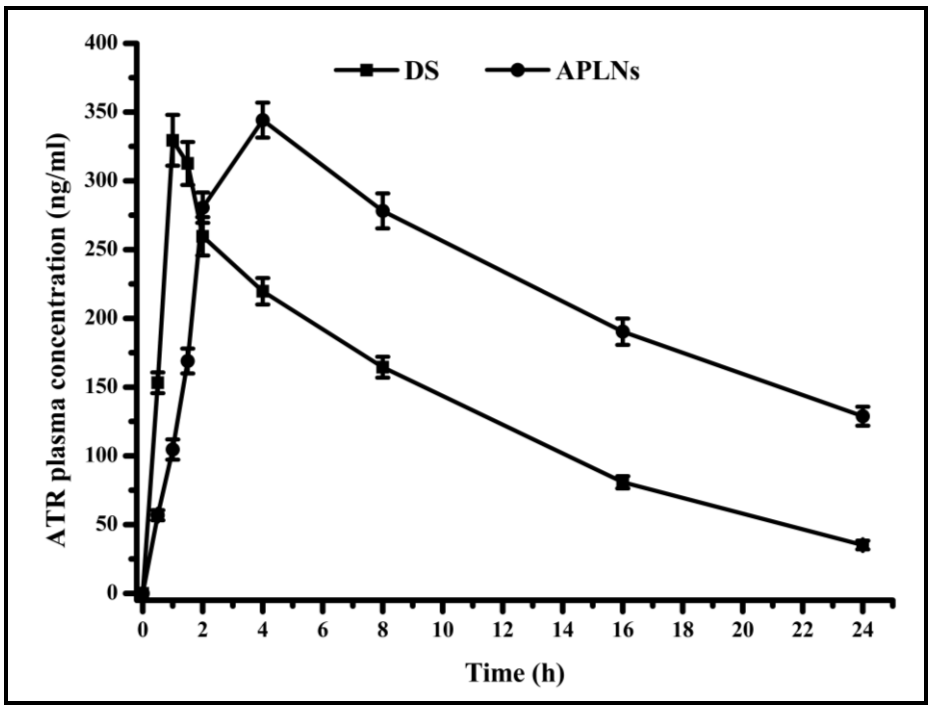

Fig. 5.37 Pharmacokinetic profiles of APLNs and drug suspension (DS) (vertical bars represent the standard deviation and dose is equivalent to 20 mg/kg of ATR)

For pharmacokinetic study, the plasma drug concentration time profile has been shown in **Fig. 5.37**. Pharmacokinetic parameters of APLNs and drug suspension (Astin, Microlab Ltd.) were calculated and compared statistically by using Kinetica and Graphpad Prism, respectively (Table 5.8). There was no significant change in C_{max} (p>0.05) between APLNs and ATR suspension as observed. T_{max} (p<0.05) was significantly increased in APLNs than the drug suspension due to slow release of drug from PNs. Area under curve in 24 h ($AUC_{0\text{-}24h}$) and observed area under curve in infinite time ($AUC_{0\text{-}\infty}$) for the APLNS were found to be significantly (p<0.05) higher than pure drug suspension. The $AUC_{0\text{-}24h}$ and $AUC_{0\text{-}\infty}$ of APLNs were found to be 1.66 and 2.23 times higher than that of pure drug suspension. The relative bioavailability of APLNS formulation was observed to be 2.23 with respect to pure drug suspension. Enhancement in AUC contributed by enhanced systemic absorption of PNs from GIT due to nano range particle size, PLGA bio-adhesive properties and TPGS (Shaikh et al., 2009;

He at al., 2007). Mean residence time (MRT) of APLNS was significantly higher (p<0.05) than drug suspension. Surface absorbed hydrophilic TPGS on PNs might have enhanced its systemic residence time due to intact poly ethylene glycol in TPGS (Storm et al., 1995). Further; it was observed that the APLNS maintained the higher plasma drug level than the pure drug suspension after 4 h of oral intake.

Table 5.8 Pharmacokinetic parameters of APLNs and drug suspension after single dose administration (n=6 and does: 20 mg/kg)

Pharmacokinetic Parameter	**APLNs**	**Drug suspension**
$AUC_{0\text{-}24h}$ (ng h ml^{-1})	5255±227*	3156±83
$AUC_{0\text{-}\infty}$ (ng h ml^{-1})	7900±292*	3543±94
T_{max} (h)	4.0000	1.1600±0.1053
C_{max}(ng ml^{-1})	344.17±10.39	329.5±11.1
F_{rel}	2.23±0.09	1.0
MRT observed (h)	21.85±0.90*	10.95±0.32

*P < 0.05 significant change as compared to drug suspension

5.2.1.8.2 Efficacy study

At the end of fourth week, HFD fed rats exhibited significant elevation in plasma levels of different biochemical parameters such as PTC, PTG, LDL_C, glucose and $VLDL_C$, whereas decrease in HDL_C level than the NDC group (**Fig. 5.38**). HFPPLT, HFAST and HFAPT groups were treated as aforementioned, during 4^{th}-6^{th} weeks (Table 10, Chapter 4.2.2.9.3). A significant decrement in elevated levels of PTC, PTG, LDL_C and PGL whereas, considerable enhancement in HDL_C level were observed in HFAST and HFAET groups than HFC and HFPET groups at the end of 6th week (**Fig. 5.38** and Table 5.9).

PTC, PTG, LDL_C, HDL_C and glucose levels clearly indicated that the APLNs containing half dose of ATR than the ATR suspension were equally efficient as ATR suspension. Enhancement in efficacy of APLNs possibly attributed to considerable improvement in the ATR bioavailability by virtue of their nano size

as well as TPGS bioavailability enhancing property. During washout period, treatment was stopped and at the end of eighth week all treatment group again attained comparable elevated lipid and glucose profile. Elevation trend of lipid parameters in HFAST groups were found to be steeper than HFAPT group during 6^{th}-8^{th} week due to sustained release effect of APLNs. There was no any significant difference in lipid/glucose profile trend of HFC and HFPPLC group was found which discard out any effect of placebo nanoparticles on efficacy profile. The prominent outcome of the study thus, proved the efficacy of APLNs at half dose of ATR as APLNs in comparison to ATR suspension.

5.2.1.8.3 Safety study

Statins therapy often leads to several skeleton muscle toxicities such as mild myalgia to severe rhabdomyolysis. Several biomarkers like CK, LDH, creatinine, BUN and AST have been used for diagnosis of rhabdomyolysis. These biochemical parameters were assessed in collected plasma sample of different treated group at the end of 4^{th}, 6^{th} and 8^{th} week to study the possible muscle toxicity of ATR and APLNs. Creatinine, LDH, AST and BUN levels were significantly raised in HFAST group than that of HFAPT group as depicted in **Fig. 5.39**. Safety profiles of all the groups are enlisted in Table 5.9 (sixth week only). CK levels were found to be normal in all the groups during eight week study. Safety profile of HFAPT groups were found to be significantly ameliorated than HFAST group and this may possibly attributed to dose reduction of ATR; protection of ATR from degradation and metabolism; sustained drug release effect of ALPNs and localization of APLNs in highly perfused organ. Liver tissue of all the groups indicated rubicund and healthy one as depicted in **Fig. 5.40**. Liver tissue maintained its integrity and salubriousness at this ATR dose.

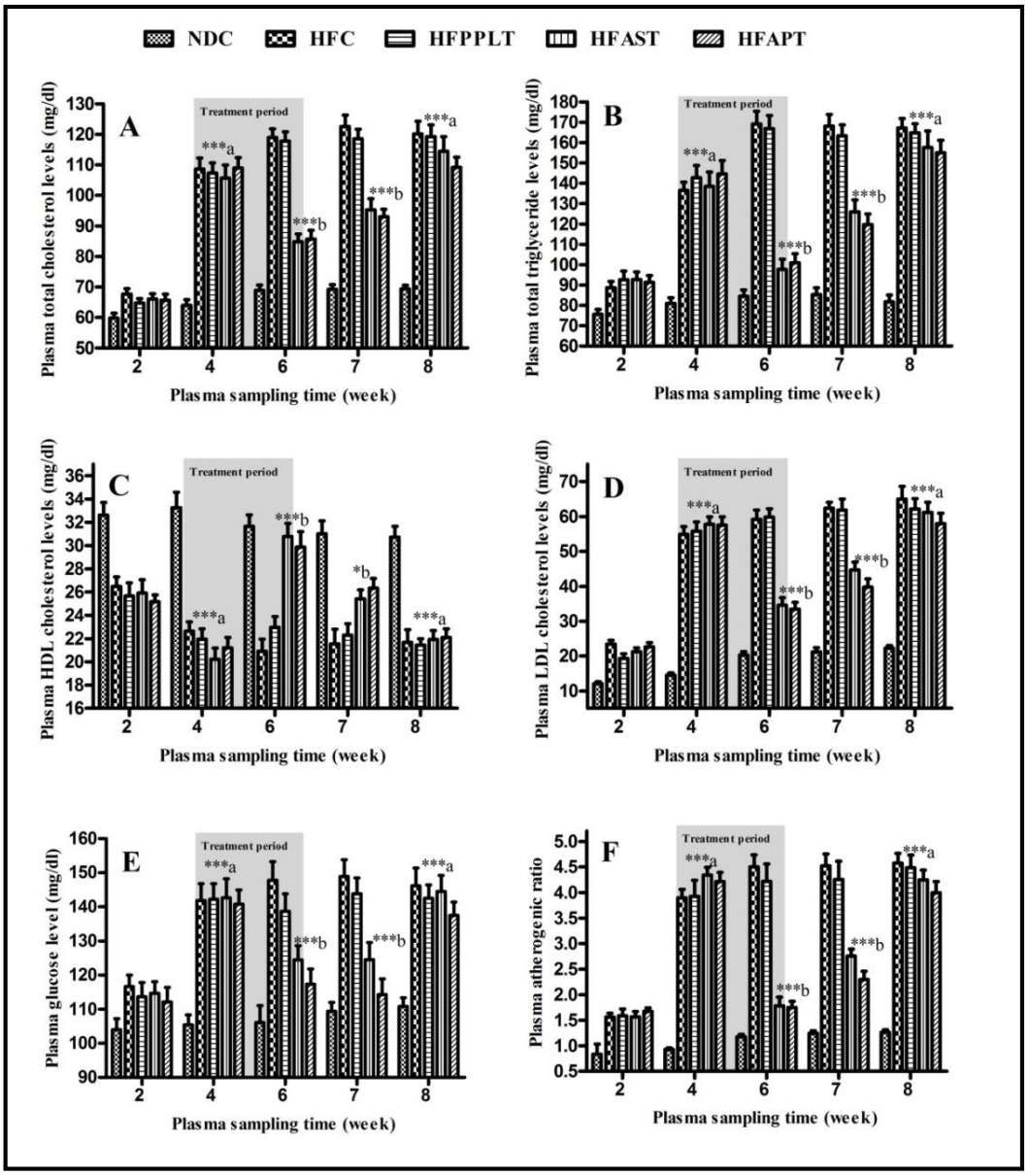

Fig. 5.38 (A-F) Showing the plasma (A) Total cholesterol, (B) Triglyceride, (C) HDL cholesterol, (D) LDL cholesterol, (E) Glucose and (F) Atherogenic ratio level time profile of different groups (vertical bars showing S.E.M. and Bonferroni post-test two way ANOVA statistics applied)

NDC: normal diet control, HFC: high fat diet control, HFPPLT: high fat-diet PLGA-placebo-nanoparticles treated, HFAST: high fat-diet ATR suspension treated, HFAPT: high fat-diet APLNs treated, HDL: high density lipoprotein, LDL: low density lipoprotein and AI: atherogenic index

***p<0.001, *p<0.05

a: statistically significant versus NDC, b: statistically significant versus HFC and HFPPT within same week. (Dose: 3mg/kg/day ATR to HFAST group & 1.5mg/kg/day of ATR present in formulation to HFAPLT group)

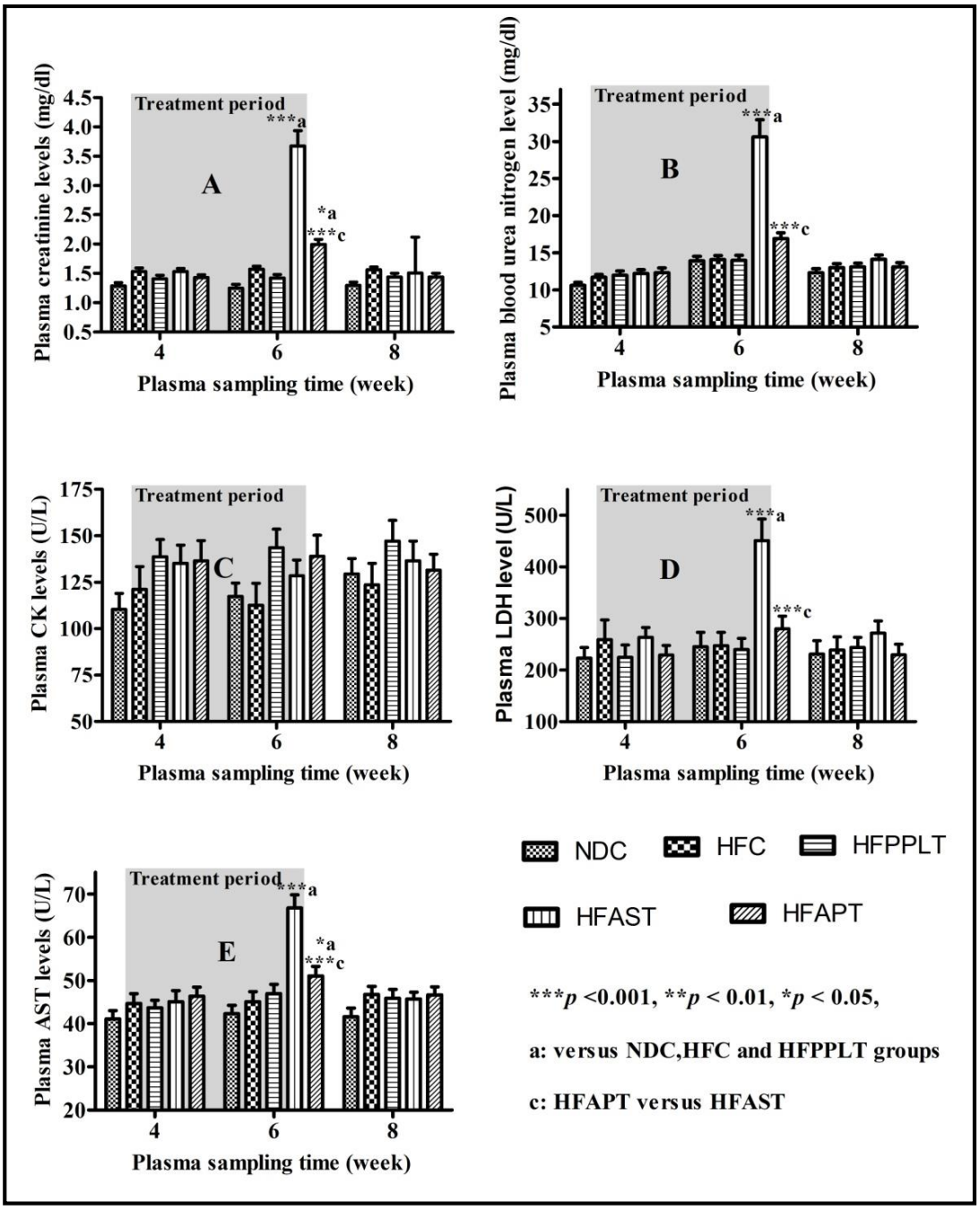

Fig. 5.39 Depicting (A) Plasma creatinine levels (B) Blood urea nitrogen (BUN) levels (C) Plasma creatinine kinase (CK) levels, (D) Plasma lactate dehydrogenase (LDH) levels and (E) Aspartate amino transferase (AST) levels versus time profile of various treated groups

NDC: normal diet control, HFC: high fat diet control, HFPPLT: high fat-diet PLGA-placebo-nanoparticles treated, HFAST: high fat-diet ATR suspension treated, HFAPT: high fat-diet APLNs treated, HDL: high density lipoprotein and LDL: low density lipoprotein

Table 5.9 Plasma efficacy and safety related biochemical parameters in different groups of rats at the end of 6th week

S. No	Biochemical Parameters	NDC	HFC	HFPPLT	HFAST	HFAPT
1	PTC (mg/dl)	68.9±1.7	114.0±2.7^{***a}	117.8±3.0^{***a}	84.9±2.5^{***b}	85.7±3^{***b}
2	PTG (mg/dl)	84.6±3.0	169.2±6.2^{***a}	166.9±6.4^{***a}	97.7.0±5.0^{***b}	100.9±4.5^{***b}
3	$VLDL_C$ (mg/dl)	16.9±0.6	33.9±1.2^{***a}	33.4±1.2^{***a}	19.5±1.0^{***b}	20.2±1.1^{***b}
4	HDL_C (mg/dl)	31.7±1.0	20.9±1.0^{***a}	23.0± 0.9^{***a}	30.8±1.1^{***b}	29.9±1.3^{**b}
5	LDL_C (mg/dl)	20.3±0.9	59.2±2.7^{***a}	61.4±2.4^{***a}	34.6±2.1^{***b}	35.6±2.0^{***b}
6	PG (mg/dl)	106.2±4.9	147.8±5.5^{***a}	138.7±5.1^{***a}	124.4±4.2^{**b}	117.3±4.5^{***b}
7	AI	1.18±0.04	4.50±0.23^{***a}	4.19±0.24^{***a}	1.78±0.17^{***b}	1.89±0.15^{***b}
8	PC (mg/dl)	1.25±0.06	1.57±0.05	1.42±0.06	3.67±0.26^{***c}	1.99±0.09^{*c***d}
9	BUN (mg/dl)	13.9±0.6	14.1±0.6	14.0±0.7	30.6±2.3^{***c}	16.9±0.8^{*c***d}
10	CK (U/L)	117.3±7.3	112.7±11.7	143.7±9.9	128.5±8.4	139.0±11.4
11	LDH (U/L)	244.8±28.1	246.7±26.3	239.8±21.4	451.2±41.5^{***c}	279.7±24.4^{**d}
12	AST (U/L)	42.3±2.0	45.1±2.3	46.9±2.2	66.8±2.4^{***c}	51.1±2.2^{***d}

PTC: plasma total cholesterol; PTG: plasma triglyceride; $VLDL_C$: very low density lipoprotein cholesterol; HDL_C: high density lipoprotein cholesterol; LDL_C: low density lipoprotein cholesterol; PG: plasma glucose; AI: plasma atherogenic index; BUN blood urea nitrogen; CK: creatinine kinase; LDH: lactate dehydrogenase; AST: aspartate transaminase; NDC: normal diet controlled; HFC: high fat-diet controlled; (n=6) HFPPLT: high fat-diet placebo-PLGA-nanoparticles treated; HFAST: High fat-diet ATR calcium suspension treated; HFAPT, High fat-diet APLNs treated;

All values are expressed in mean±SEM; ***p<0.001, **p<0.01 and *p<0.05; [a] statistically significant versus NDC; [b] statistically significant versus HFC; [c] statistically significant versus NDC, HFC and HFPPLT; [d] statistically significant versus HFAST

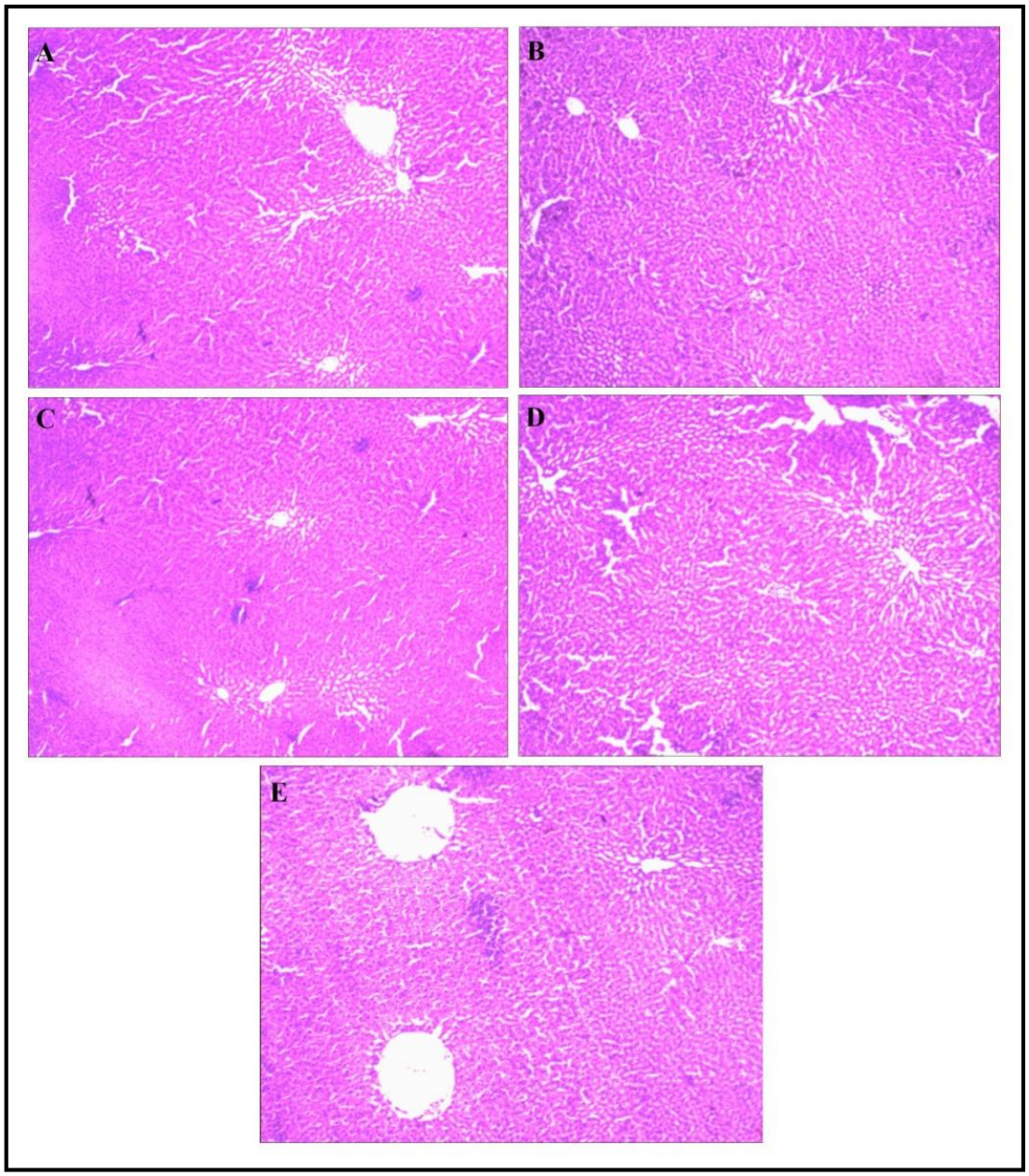

Fig. 5.40 Histomicrographs of stained liver tissue of (A) NDC, (B) HFC (C) HFPPLT, (D) HFAST and (E) HFAPT groups

5.2.3 Preparation, *in vitro* and *in vivo* characterization of ALPNs

5.2.3.1 ALPNs preparation using CCD experimental design

30 batches of ALPNs (Table 4.9, Chapter 4.2.2.2) were prepared by employing CCD RSM. Results indicated that all selected independent variables significantly determined PS and EE of ALPNs. The adjusted mathematical expression with R^2 value of response variables as a function of independent variables are as follow

Mean diameter hydrodynamic particle size (R_1) = $201.7 + 33.7X_1 - 16.1X_2 – 15.2X_3 - 16.7X_4 + 4.7X_1X_2 – 4.5X_1X_4 + 13.6X_1^2 + 6.7X_3^2$ equation (5.5) ($R^2 = 0.98$)

Mean entrapment efficiency (R_2) = $75.0 + 9.4X_1 - 2.9X_2 - 3.7X_3 - 2.5X_4 + 2.9X_1X_3 + 1.8X_1^2$ equation (5.6) ($R^2 = 0.92$)

Higher R^2 value and insignificant ($p>0.05$) lack of fit showed good fit of regression model. PS, EE and PDI were obtained in the range of 146–324 nm, 57.3–95.7% and 0.163–0.394, respectively. Polymer content was found to be the dominating factor amongst all significant independent variables as evidenced by higher positive coefficient in regression analysis equations.

Equation (5.5) explains the influence of different independent variables on PS of ALPNs which is depicted in **Fig. 5.41A** and **Fig. 5.41B**. Higher polymer content led to higher viscosity of organic phase which favored larger PS of ALPNs (Galindo-Rodriguez et al., 2004). TPGS concentration, volume of acetone and stirring speed possessed negative coefficient, indicating that an increment in these independent variables favor smaller PS. Increased TPGS concentration fortified boundary layer around particles, which limits the particles impingement and aggregation, resulting into mono dispersed nanoparticles with smaller PS (Wang et al., 2013). Increased volume of acetone lowered the viscosity of organic phase and favored smaller PS. Higher stirring speed favored smaller PS, as stirring provided shear force to break down the organic phase droplets.

Equation (5.6) as well as **Fig. 5.41C** and **Fig. 5.41D** demonstrate the effect of selected independent variables on EE of ALPNs. Raised polymer content favored enhancement of EE due to higher viscosity of organic phase, which have limited the drug diffusion from the organic phase subsequently (Chorni et al., 2002; Patel et al., 2015). Negative coefficient of other variables indicated that an increase in these variables favor lowering of EE. An increment in TPGS concentration have increased the drug solubility in aqueous medium due to micelles formations and thus, reduced EE. Raised volume of acetone caused a reduction in organic phase viscosity, which led to lowering of EE. Higher stirring

speed provided higher dispersing force, which led to facilitated diffusion of drug from organic phase to aqueous phase and resulted into lower EE.

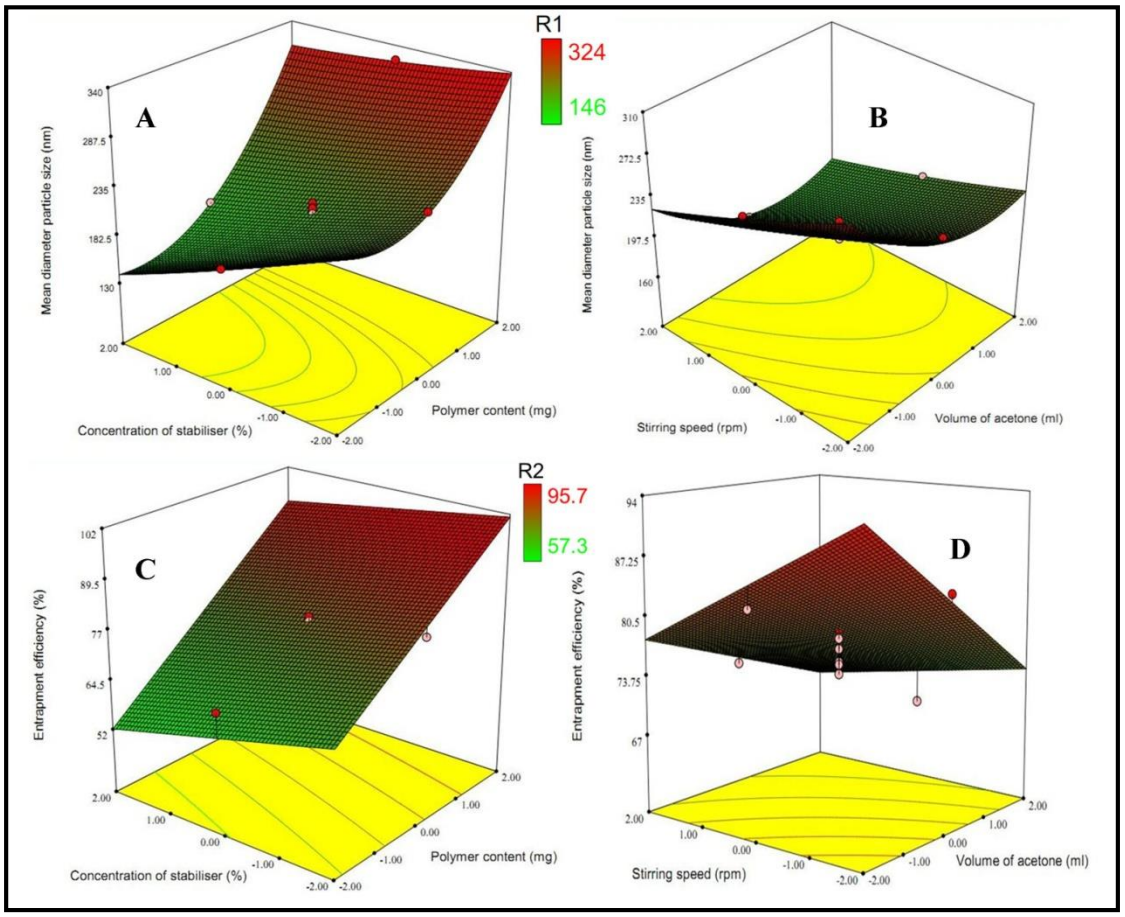

Fig. 5.41 Three-dimensional surface response plot showing the effect of polymer content, surfactant concentration, volume of organic solvent and stirring speed on (A & B) Mean diameter particle size, and (C & D) Mean entrapment efficiency of PNs

Zeta potential (ZP) of ALPNs was found to be in the range of -18 to -29 mV. Negative potential was attributed to anionic nature of polymer and drug. Optimal values of independent formulation parameters were obtained as X_1: 115 mg, X_2: 0.8%, X_3: 9 ml and X_4: 1250 rpm with predicted response variables R_1: 188 nm and R_2: 78% by setting the constraint minimum to PS and maximum to EE simultaneously in an optimization tool. Optimized batch of ALPNs was prepared by using the optimal formulation parameters and the observed response variables were 197±5 nm PS, 75.6±3.2% EE, 0.213±0.012 PDI and

(24.4±1.9) mV ZP, which were close to the predicted response variables. The optimized batch was subjected for further evaluation.

5.2.3.2 Solid state characterization of ALPNs by FT-IR, DSC and PXRD

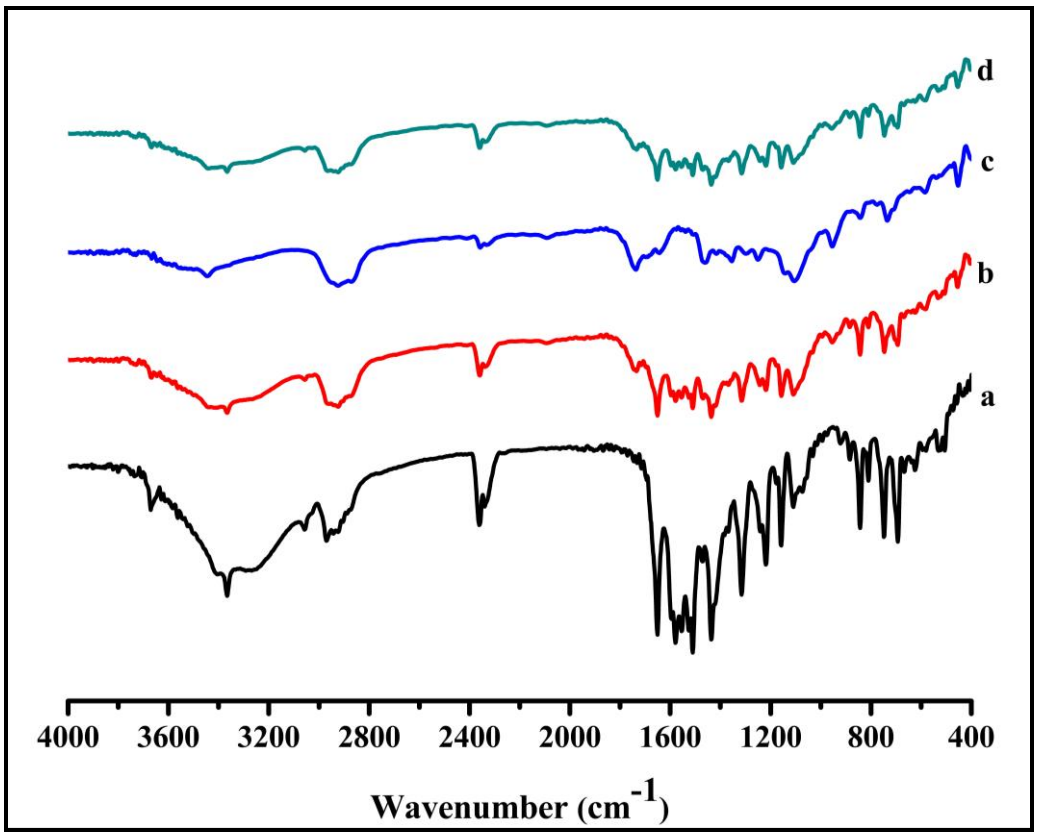

Fig. 5.42 FT-IR spectra of (a) ATR, (b) Physical mixture, (c) Placebo nanoparticles and (d) Optimized formulation ALPNs

Fig. 5.42 illustrates FT-IR spectra of ATR with characteristic peaks at 3670 cm^{-1} (free O-H stretching of trihydrate), 3367 cm^{-1} (N-H stretching), 3222 cm^{-1} (asymmetric O-H stretching), 3055 cm^{-1} (symmetric O-H stretching), 1649 cm^{-1} (asymmetric C=O stretching), 1578 cm^{-1} (symmetric C=O stretching), 1550–1468 cm^{-1} (C–C ring stretching), 1317 cm^{-1} (CH_3/CH_2 deformation) and 1243 cm^{-1} (C–N stretching); which were retained in physical mixture as well as ALPNs (Zhang et al., 2009). The carbonyl peak of PCL was shifted from 1735 to 1737 cm^{-1} in placebo nanoparticles and ALPNs possibly due to overlapping of TPGS carbonyl peak (1739 cm^{-1}). The characteristics C-O-C stretching vibration of repeated –OCH_2CH_2 chain of TPGS from 1101 cm^{-1} to 1263 cm^{-1} were observed in ALPNs and placebo nanoparticles spectra, which suggest the presence of TPGS

absorbed on the nanoparticles surface (Zheng et al., 2013). Prominent peaks of placebo nanoparticles were also preserved in ALPNs. No any other peaks were observed apart from ATR and placebo nanoparticles in ALPNs spectra which accorded good chemical compatibility of ATR in ALPNs.

Fig. 5.43 shows the DSC thermogram patterns of ATR, PM, PN and ALPNs. A broad endotherm ranging from 70–130°C (could be attributed to loss of trihydrate) and a sharp endotherm at 165°C (corresponded to melting point of ATR) was observed in ATR thermograph. These endotherms were also present in PM, which indicated good physical compatibility of drug with polymer. An endotherm in the region of 56-63°C was noticed in each of PM, PNs and ALPNs which attributed to melting point of PCL. ATR loaded in ALPNs did not exhibit any endotherm at melting point conferred amorphous character of ATR distributed in ALPNs.

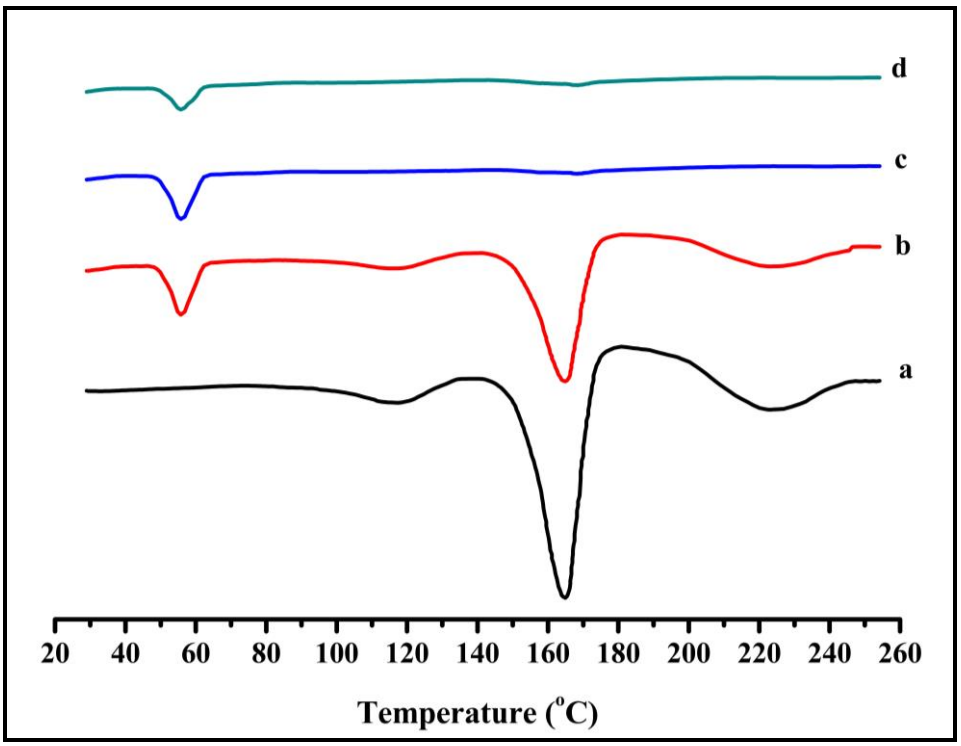

Fig. 5.43 DSC spectra of (a) ATR, (b) Physical mixture, (c) Placebo nanoparticles and (d) Optimized formulation ALPNs

PXRD patterns of ATR, PM, PN and ALPNs are demonstrated in **Fig. 5.44**. Many salient sharp diffraction peaks of ATR at 6.02, 9.06, 9.36, 10.16, 10.44, 11.76, 12.08, 16.92, 19.32, 21.50, 22.58, 23.18 and 23.56° of 2θ were observed

and also remained in PM, which corroborated good physical compatibility of drug with polymer. No any prominent sharp peaks were noticed in PNs and ALPNs, which correspond to their amorphous character. ATR lost crystalline character in ALPNs probably due to smaller particle size and its dispersion into polymer matrix.

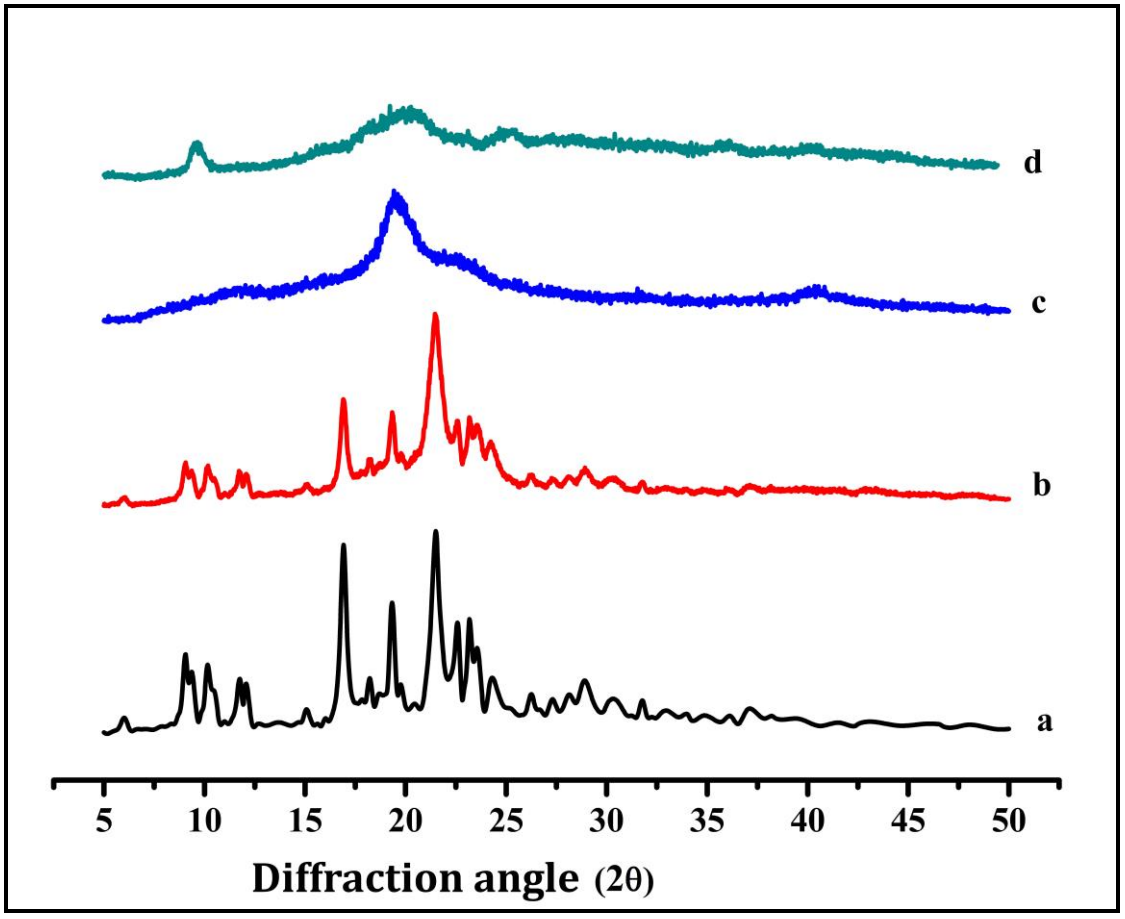

Fig. 5.44 PXRD diffractograms of (a) ATR, (b) Physical mixture, (c) Placebo nanoparticles and (d) Optimized formulation ALPNs

5.2.3.3 Morphological study of ALPNs

Fig. 5.45A and **Fig. 5.45B** show AFM and TEM image of ALPNs, respectively. AFM image exhibited the discrete spherical shape with smooth surface of ALPNs and size is comparable to hydrodynamic PS. TEM micrograph also exhibited comparable PS of ALPNs to that of hydrodynamic PS. ED pattern of ALPNs, as shown in **Fig. 5.45C**, exhibited diffuse elastic scattered ring without

any spotty diffraction patterns, confirming the amorphous character of ALPNs (Stormer et al., 2007).

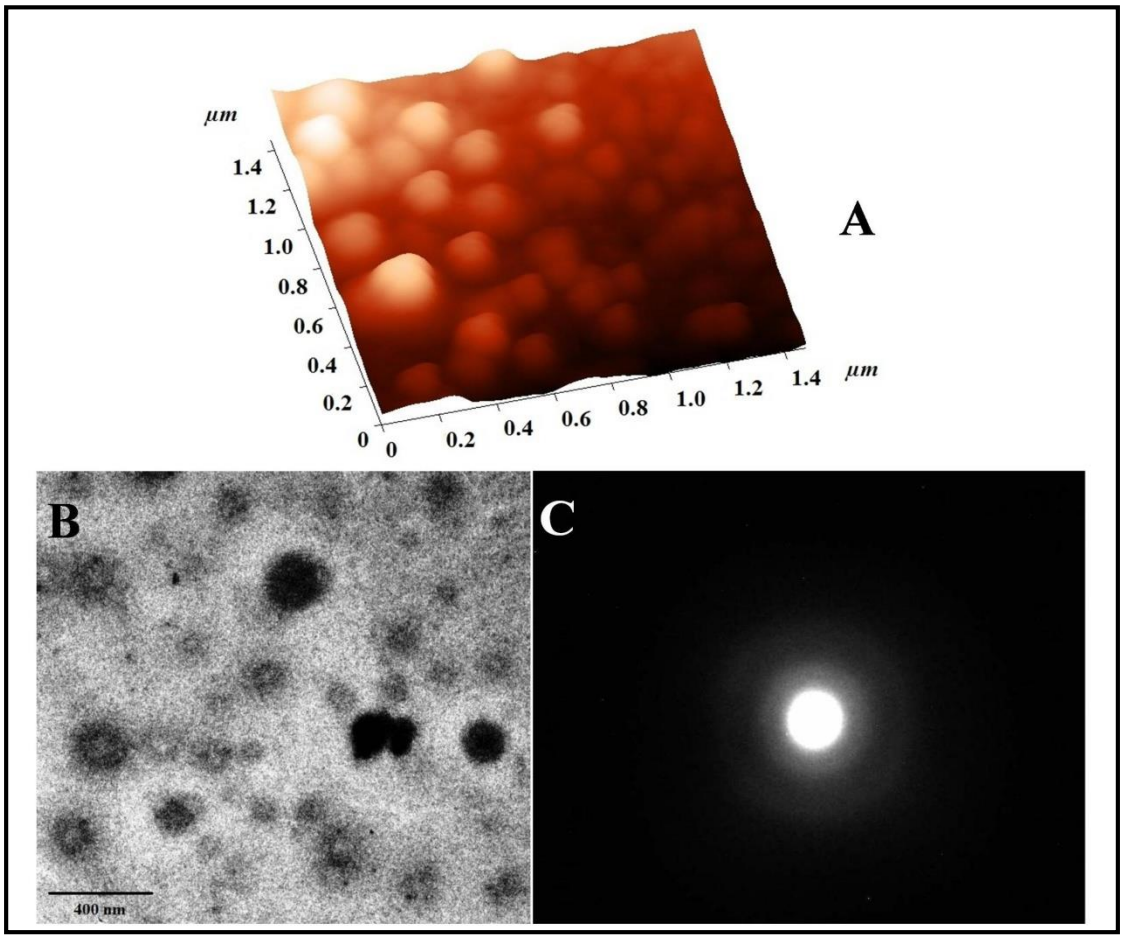

Fig. 5.45 (A) AFM image, (B) TEM image and (C) Electron diffusion ring pattern of optimized batch of APLNs

5.2.3.4 In vitro release study of ALPNs

ATR release profile from the ALPNs illustrated initial burst release followed by subsequent sustained release (**Fig. 5.46**). 50% of drug was released in initial 2 h and completely released in 10 h from pure drug suspension. ALPNs released 50% of drug in 16 h while, rest in 96 h. Kinetic release parameters of various models are shown in Table 5.10. Release data of ALPNs were best fitted into KP model on the basis of higher correlation coefficient. The n value (<0.45) corresponded to Fickian diffusion controlled release mechanism (Fan et al., 2013). ALPNs exhibited 96 h sustained release profile of ATR with diffusion controlled mechanism.

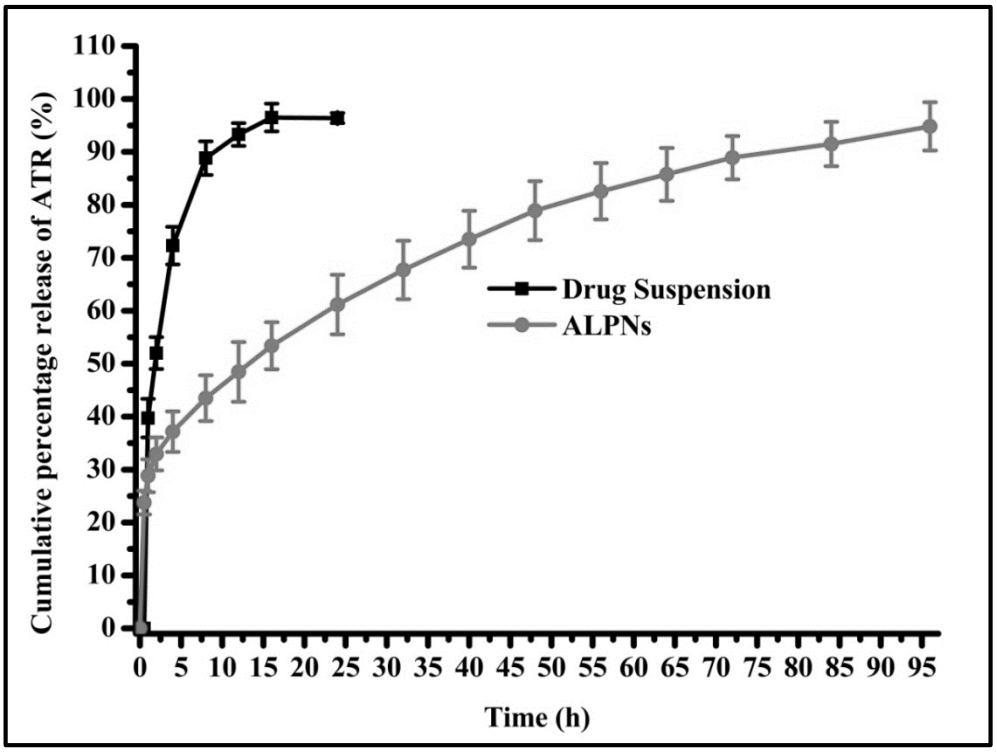

Fig. 5.46 Representing the *in vitro* drug release profile of optimized batch of APLNs and drug suspension in phosphate buffer pH 7.4 (vertical bars represent the standard deviation)

Table 5.10 Drug release kinetic models of Optimized batch of ALPNs

Release kinetic model of ALPNs										
Zero order		**First order**		**Higuchi model**		**Korsmeyer-Peppas model**			**Hixson-Crowell model**	
R^2	K_0 (%/h)	R^2	K_1 (h^{-1})	R^2	K_H (%$h^{-1/2}$)	R^2	K_{kp}	n	R^2	K_{HC} (%$^{1/3}h^{-1}$)
0.844	0.801	0.807	0.005	0.966	8.573	0.987	26.99	0.269	0.967	0.026

5.2.3.5 Stability study of ALPNs

Storage stability study was conducted to assess the potential of ALPNs to withstand the environmental changes. Physical appearance of ALPNs did not change in different environmental conditions. The properties of ALPNs stored under different environmental conditions have been depicted in **Fig. 5.47.** A significant change (p<0.05) in ALPNs properties (PS, EE and PDI) was observed after storage under accelerated condition (40±2°C/75±5% RH) which was attributed to instability of ALPNs due to agglomeration of nanoparticles and

degradation of polymer along with drug. However, insignificant change (p>0.05) in ALPNs properties was observed after storage under normal condition (25±2°C/60±5% RH) and refrigerated condition (4±1°C). Thus, ALPNS should be stored below room temperature (<25°C), preferably at refrigerated condition for long term use.

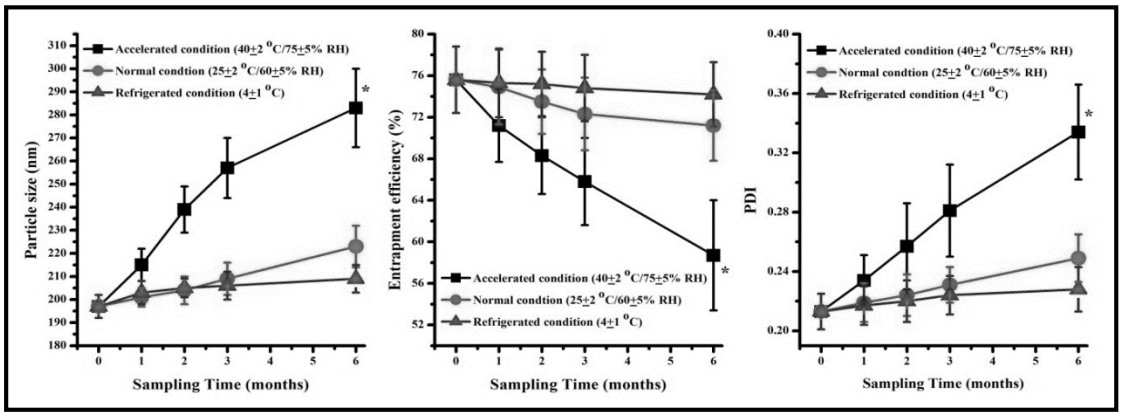

Fig. 5.47 The particle size, entrapment efficiency and polydispersity index (PDI) of optimized ALPNs during stability study of 6 months under different environmental conditions [* represents a significant change (p<0.05) compared to properties of ALPNs on 0 days]

5.2.3.6 Estimation of residual acetone in ALPNs colloidal system

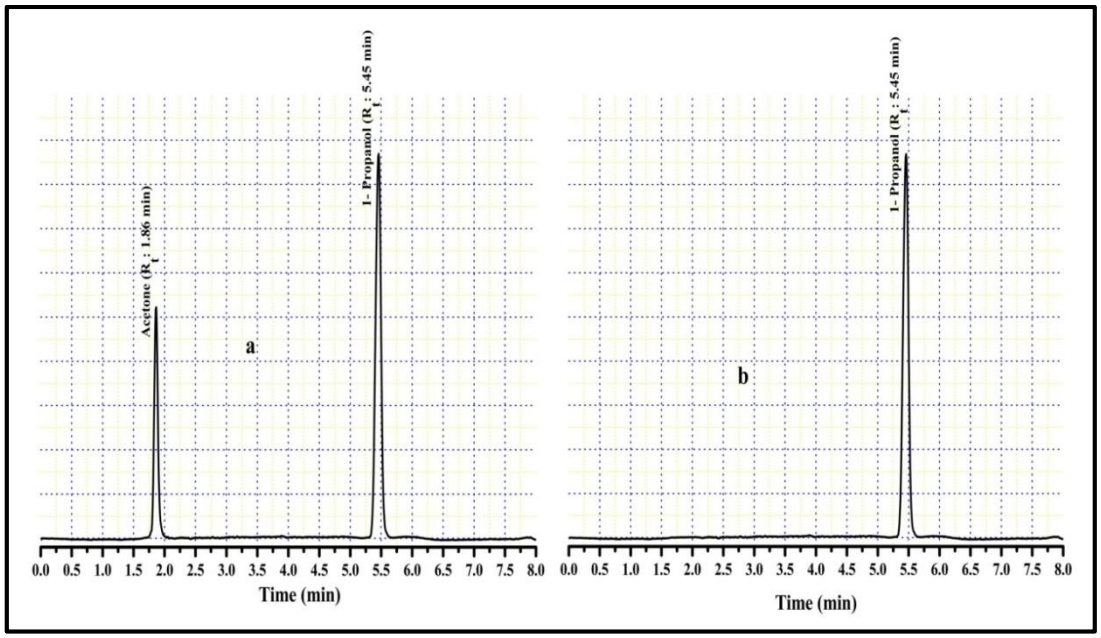

Fig. 5.48 Gas chromatogram of (a) Standard acetone (1000 ppm) and internal standard 1-propanol (1500 ppm) in deionized water (b) Aqueous sample of ALPNs with internal standard 1-propanol (1500 ppm).

Gas chromatography study had been performed to estimate the residual acetone present in ALPNs formulation with 1-propanol as internal standard (IS) as mentioned earlier in previous chapter. Chromatogram of ALPNs shown in **Fig. 5.48b** indicates either absence or below detectable limit of acetone (LOD: 30 ppm). The possible below 30 ppm presence of acetone allow it for use this ALPNs formulation as the permissible limit of acetone is 5000 ppm.

5.2.3.7 In vivo study

5.2.3.7.1 Pharmacokinetic study of ALPNs

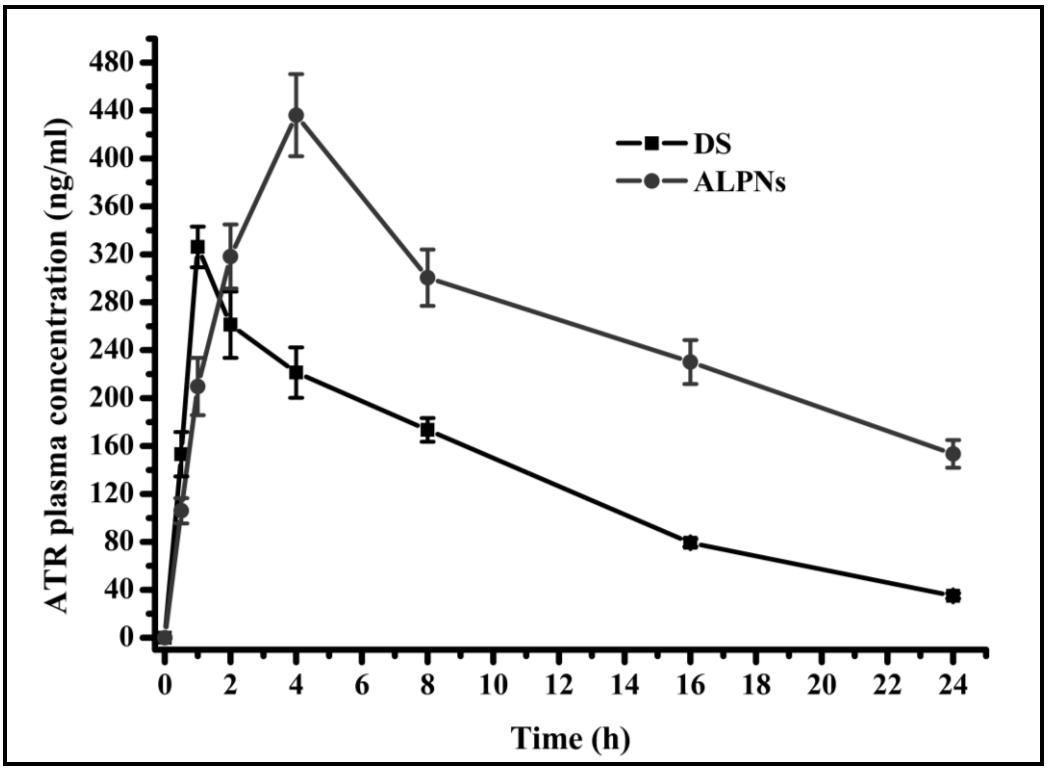

Fig. 5.49 Pharmacokinetic profile of ALPNs and drug suspension (DS) (vertical bars represent the standard deviation and dose was equivalent to 20 mg/kg of ATR)

Rat plasma ATR concentration time profiles after single oral dose administration of DS and ALPNs are shown in **Fig. 5.49**. Different pharmacokinetic parameters of DS and ALPNs are summarized in Table 5.11. Two times enhancement in $AUC_{0\text{-}24h}$ and 2.8 times in $AUC_{0\text{-}\infty}$ were noticed in ALPNs group in comparison to DS group. The significant enhancement in bioavailability attributed to enhanced absorption of ATR incorporated in ALPNs,

which might be due to smaller particle size, higher uptake of nanoparticles via Payer's patches and TPGS' bioavailability enhancing properties (Zhang et al., 2012; Pérez-Herrero & Fernández-Medarde, 2015). A significant enhancement (1.34 times) in maximum plasma concentration (C_{max}) was observed in ALPNs due to higher absorption of ALPNs from GIT. T_{max} was observed to be higher in ALPNs (4 h) than the DS (1 h), which might be attributed to sustained drug release features of ALPNs. Mean residence time (MRT) of ATR was detected significantly higher in ALPNs, probably due to sustained drug release behaviour and surface absorbed TPGS of ALPNs, which might have improved the residence period, possibly by providing hydrophilic surface (PEG of TPGS) to nanoparticles (Vuddanda et al., 2014). Hence, ALPNs provided a superior nanoparticles platform in order to enhance the oral bioavailability.

Table 5.11 Pharmacokinetic parameters of ATR after single dose oral administration of ALPNs and ATR suspension (n=6 and dose: 20 m/kg of ATR)

Pharmacokinetic Parameter	**ALPNs**	**ATR suspension**
$AUC_{0\text{-}24h}$ (ng.h.ml^{-1})	6204.0±205.2**	3113.0±55.8
$AUC_{0\text{-}\infty}$ (ng.h.ml^{-1})	9754.7±309.2**	3470.9±58.7
C_{max} (ng.ml^{-1})	436.2±15.3*	326.2±6.9
T_{max} (h)	4.0	1.0
F_{rel}	2.81±0.12	1.0
MRT (h)	23.88±0.85 ***	11.06±0.15

Data are represented as mean±SEM. Statistical significance compared with ATR suspension. *p<0.05, **p<0.01 and ***p<0.001. ALPNs: ATR loaded PCL nanoparticles.

5.2.3.7.2 Efficacy and safety study

A significant elevation in plasma total cholesterol (75-81%), triglyceride (75-84%), low density lipoprotein-cholesterol (200-300%), glucose level (32-39%) and atherogenic index (318-367%) while a significant reduction in high density lipoprotein-cholesterol (27-33%) were noticed in high fat-diet rat groups than the NDC group, at the end of 4th week (hyperlipidemia induction period) (**Fig. 5.50**). Different groups were treated with different regimen as mentioned in Table 4.10 (Chapter-4.2.2.9.3) during treatment period (4th–6th

week). Dose size of ALPNs to HFALT group was chosen half of equivalent weight of pure ATR administered to HFAST group on the basis of pharmacokinetic output. The shaded region in **Fig. 5.50** indicates the treatment period during fourth to sixth week. At the end of sixth week, a significant reduction in elevated level of PTC, PTG, LDL_C, $VLDL_C$ and glucose were noticed in HFAST and HFALT groups (**Fig. 5.50** and Table 5.12). Plasma HDL_C level was found to be significantly improved in ATR and ALPNs treated groups at the end of sixth week. The plasma AI was found to be significantly decreased in HFALT and HFAST group than HFC and HFPPCT groups. The pattern of elevation or reduction in plasma lipid profile was approximately similar in HFALT and HFAST group during treatment period. During 6^{th} to 7^{th} week, the plasma lipid elevation rates were observed to be slightly slower in HFAPT group than the HFAST group, which might be attributed to sustained release of drug from ALPNs. No significant difference was observed between plasma lipid and glucose profile of HFC and HFPPCT group, concluding insignificant effect of placebo nanoparticles itself on efficacy profile. At the end of 8^{th} week, all the high fat diet groups exhibited similar plasma lipid and glucose profile, indicating drug washed out completely during 6^{th} to 8^{th} week. Efficacy study exhibited similar profile during treatment (4^{th}–6^{th} week) and drug wash out (6^{th}–8^{th} week) period in both the HFAST and HFALT group, which showed dosage regimen of ALPNs containing 1.5 mg of ATR was equally efficacious to that of ATR suspension containing 3 mg of ATR. The prominent outcome of this study was that ALPNs at half dose of ATR were equally effective as to ATR suspension.

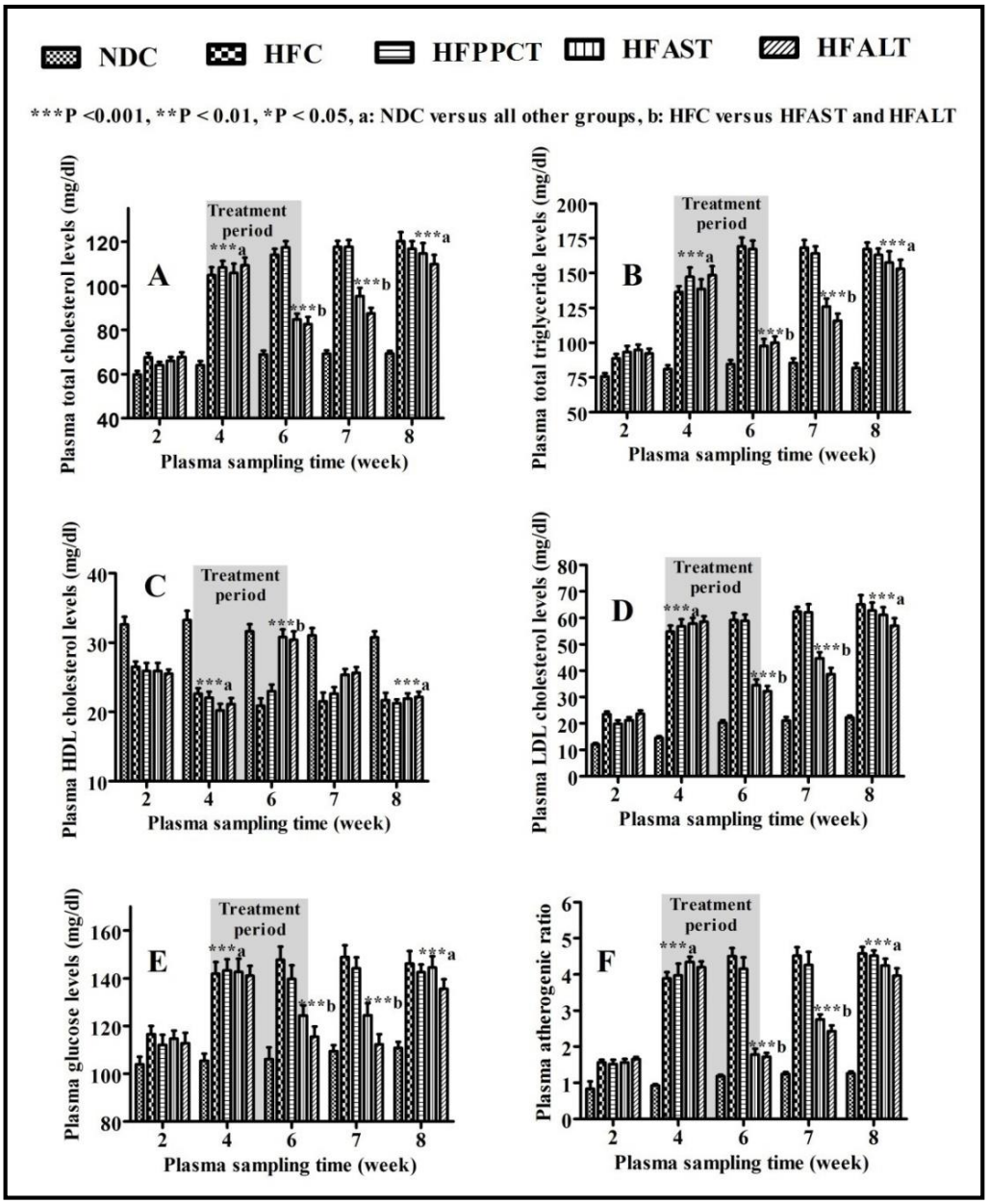

Fig. 5.50 (A-F) Showing the plasma (A) Total cholesterol, (B) Triglyceride, (C) HDL cholesterol, (D) LDL cholesterol, (E) Glucose and (F) Atherogenic ratio level time profile of different groups (vertical bars showing S.E.M. and Bonferroni post-test two way ANOVA statistics applied)

NDC: normal diet control, HFC: high fat diet control, HFPPCT: high fat-diet PCL-placebo-nanoparticles treated, HFAST: high fat-diet ATR suspension treated, HFALT: high fat-diet ALPNs treated, HDL: high density lipoprotein, LDL: low density lipoprotein and AI: atherogenic index

***p<0.001,

a: statistically significant versus NDC, b: statistically significant versus HFC and HFPPT within same week. (Dose: 3mg/kg/day ATR to HFAST group & 1.5mg/kg/day of ATR present in formulation to HFAPT group)

Long term therapy of escalated dose of statins may cause severe skeleton muscle toxicity like rhabdomyolysis (Cziraky et al., 2013). Rhabdomyolysis can be diagnosed by examining plasma CK profile and creatinine level. Plasma CK level greater than ten times of upper limit of normal CK level with elevated creatinine level can clearly indicate the pathogenesis of rhabdomyolysis (Holbrook et al., 2011). Elevated BUN, LDH and AST level apparently show manifestation of membrane damage (Giannoglou et al., 2007). Safety study of ATR and ALPNs were assessed by determining the plasma biochemical parameters (creatinine, BUN, CK, LDH and AST levels) of collected plasma samples at 4^{th}, 6^{th} and 8^{th} week. Muscle toxicity can be detected and diagnosed by assessing above mentioned parameters. Plasma CK data of all the animal groups were found within normal range. Plasma creatinine, BUN, LDH and AST levels of HFAST group were diagnosed significantly higher than other groups at the end of 6^{th} week, which clearly indicated mild muscle toxicity and absence of rhabdomyolysis (Table 5.12). These four biochemical parameters of HFALT group were observed to be similar or slightly elevated than the NDC, HFC and HFPPCT; which concluded that ALPNs elicited negligible muscle toxicity (**Fig. 5.51** and Table 5.12). ALPNs treated group exhibited a significant improvement in safety parameters than the pure ATR treated group. The reduced toxicity of ALPNs might be attributed to reduced dose size of ATR, sustained drug delivery action, protection of drug from degradation in GIT milieu, constrained drug in vascular system and limited exposure of drug to muscular system. Histology of liver tissue of different groups exhibited normal rubicund cells which inferred no toxic effect of ATR and ALPNs on liver (**Fig. 5.52**).

Table 5.12 Plasma efficacy and safety related biochemical parameters in different groups of rats at the end of 6th week

S. No	Biochemical Parameters	NDC	HFC	HFPPCT	HFAST	HFALT
1	PTC (mg/dl)	68.9±1.7	114.0±2.7^{***a}	117.3±2.9^{***a}	84.9±2.5^{***b}	82.6±3.2^{***b}
2	PTG (mg/dl)	84.6±3.0	169.2±6.2^{***a}	167.2±6.1^{***a}	97.7.0±5.0^{***b}	99.9±4.6^{***b}
3	$VLDL_C$ (mg/dl)	16.9±0.6	33.9±1.2^{***a}	33.7±1.2^{***a}	19.5±1.0^{***b}	20.0±0.9^{***b}
4	HDL_C (mg/dl)	31.7±1.0	20.9±1.0^{***a}	23.0±0.91^{***a}	30.8±1.1^{***b}	30.4±1.2^{***b}
5	LDL_C (mg/dl)	20.3±0.9	59.2±2.7^{***a}	58.8±2.4^{***a}	34.6±2.1^{***b}	32.2±2.0^{***b}
6	PG (mg/dl)	106.2±4.9	147.8±5.5^{***a}	139.7±5.7^{***a}	124.4±4.2^{**b}	115.5±4.3^{***b}
7	AI	1.18±0.04	4.50±0.23^{***a}	4.16±0.32^{***a}	1.78±0.17^{***b}	1.73±0.1
8	PC (mg/dl)	1.25±0.06	1.57±0.05	1.44±0.06	3.67±0.26^{***c}	1.82±0.08^{***d}
9	BUN (mg/dl)	13.9±0.6	14.1±0.6	14.6±0.7	30.6±2.3^{***c}	16.2±.74^{***d}
10	CK (U/L)	117.3±7.3	112.7±11.7	139.7±9.7	128.5±8.4	131.5±10.6
11	LDH (U/L)	244.8±28.1	246.7±26.3	235.8±16.1	451.2±41.5^{***c}	270.7±19.0^{***d}
12	AST (U/L)	42.3±2.0	45.1±2.3	50.7±2.6	66.8±2.4^{***c}	48.2±2.0^{***d}

PTC: plasma total cholesterol; PTG: plasma triglyceride; $VLDL_C$: very low density lipoprotein cholesterol; HDL_C: high density lipoprotein cholesterol; LDL_C: low density lipoprotein cholesterol; PG: plasma glucose; AI: plasma atherogenic index; BUN blood urea nitrogen; CK: creatinine kinase; LDH: lactate dehydrogenase; AST: aspartate transaminase; NDC: normal diet controlled; HFC: high fat-diet controlled; HFPPCT: high fat-diet placebo-PCL-nanoparticles treated; HFAST: High fat-diet ATR suspension treated; HFALT: High fat-diet ALPNs treated;

All values are expressed in mean±SEM (n=6); ***p<0.001, **p<0.01 and *p<0.05;

[a] statistically significant versus NDC; [b] statistically significant versus HFC; [c] statistically significant versus NDC, HFC and HFPPCT; [d] statistically significant versus HFAST

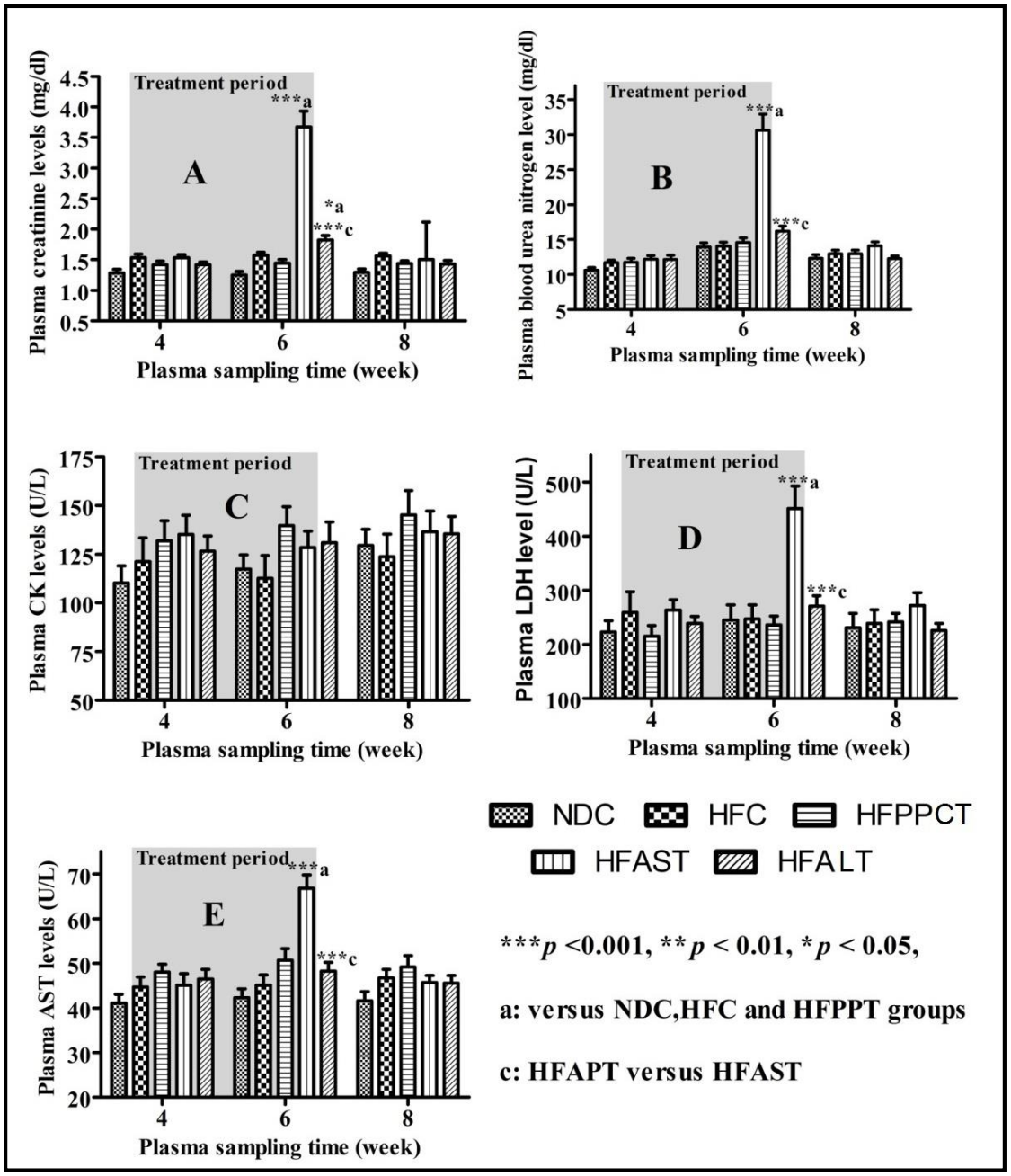

Fig. 5.51 Showing plasma (A) Creatinine levels (B) Blood urea nitrogen (BUN) levels (C) Creatinine kinase (CK) levels, (D) Plasma lactate dehydrogenase (LDH) levels and (E) Aspartate amino transferase (AST) levels versus time profile in different groups (vertical bars represent S.E.M. and Bonferroni post-test two way ANOVA statistics has been applied)

NDC: normal diet control, HFC: high fat diet control, HFPPCT: high fat-diet PCL-placebo-nanoparticles treated, HFAST: high fat-diet ATR suspension treated, HFALT: high fat-diet ALPNs treated

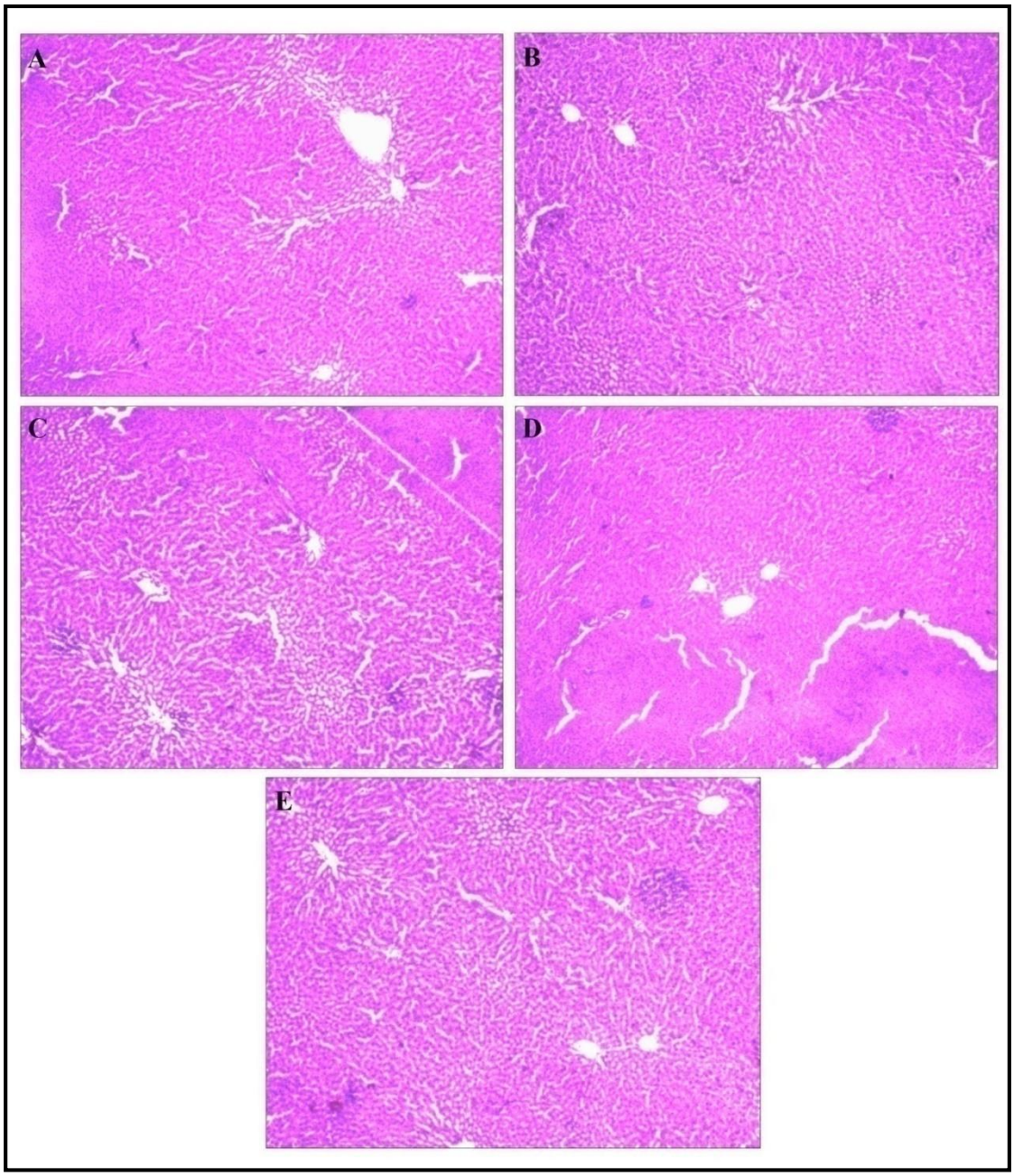

Fig. 5.52 Histomicrograph of stained liver tissue of (A) Normal diet control, (B) High fat-diet control (C) Placebo nanopaticle treated, (D) ATR suspension treated and (E) ALPNs treated groups